

# Accepted Manuscript

## Early Cambrian chronostratigraphy and geochronology of South Australia

Marissa J. Betts, John R. Paterson, Sarah M. Jacquet, Anita S. Andrew, Philip A. Hall, James B. Jago, Elizabeth A. Jagodzinski, Wolfgang V. Preiss, James L. Crowley, Tom Brougham, Ciaran P. Mathewson, Diego C. García-Bellido, Timothy P. Topper, Christian B. Skovsted, Glenn A. Brock



PII: S0012-8252(18)30122-3  
DOI: doi:[10.1016/j.earscirev.2018.06.005](https://doi.org/10.1016/j.earscirev.2018.06.005)  
Reference: EARTH 2644  
To appear in: *Earth-Science Reviews*  
Received date: 2 March 2018  
Revised date: 7 June 2018  
Accepted date: 7 June 2018

Please cite this article as: Marissa J. Betts, John R. Paterson, Sarah M. Jacquet, Anita S. Andrew, Philip A. Hall, James B. Jago, Elizabeth A. Jagodzinski, Wolfgang V. Preiss, James L. Crowley, Tom Brougham, Ciaran P. Mathewson, Diego C. García-Bellido, Timothy P. Topper, Christian B. Skovsted, Glenn A. Brock , Early Cambrian chronostratigraphy and geochronology of South Australia. *Earth* (2017), doi:[10.1016/j.earscirev.2018.06.005](https://doi.org/10.1016/j.earscirev.2018.06.005)

This is a PDF file of an unedited manuscript that has been accepted for publication. As a service to our customers we are providing this early version of the manuscript. The manuscript will undergo copyediting, typesetting, and review of the resulting proof before it is published in its final form. Please note that during the production process errors may be discovered which could affect the content, and all legal disclaimers that apply to the journal pertain.

## Early Cambrian chronostratigraphy and geochronology of South Australia

Marissa J. Betts<sup>1,2,3,\*</sup>, John R. Paterson<sup>1</sup>, Sarah M. Jacquet<sup>2,4</sup>, Anita S. Andrew<sup>5</sup>, Philip A. Hall<sup>6</sup>, James B. Jago<sup>7</sup>, Elizabeth A. Jagodzinski<sup>8</sup>, Wolfgang V. Preiss<sup>8</sup>, James L. Crowley<sup>9</sup>, Tom Brougham<sup>1</sup>, Ciaran P. Mathewson<sup>2</sup>, Diego C. García-Bellido<sup>10,11</sup>, Timothy P. Topper<sup>3,12,13</sup>, Christian B. Skovsted<sup>13</sup> and Glenn A. Brock<sup>2</sup>

<sup>1</sup>Palaeoscience Research Centre, School of Environmental and Rural Science, University of New England, Armidale, NSW, Australia, 2351. marissa.betts@une.edu.au, jpater20@une.edu.au, tbrougha@myune.edu.au

<sup>2</sup>Department of Biological Sciences, Macquarie University, North Ryde, Sydney, NSW, Australia, 2109. glenn.brock@mq.edu.au, cmath91@gmail.com

<sup>3</sup>Shaanxi Key Laboratory of Early Life and Environments and State Key Laboratory of Continental Dynamics, Department of Geology, Northwest University, Xi'an, China, 710069. timothy.topper@nwu.edu.cn

<sup>4</sup>Department of Geological Sciences, University of Missouri, Columbia, MO 65211, USA. jacquets@missouri.edu

<sup>5</sup>Department of Earth and Planetary Sciences, Macquarie University, North Ryde, Sydney, NSW, Australia, 2109. anita.andrew53@gmail.com

<sup>6</sup>Department of Geology and Geophysics, School of Physical Sciences, University of Adelaide, North Terrace, Adelaide, SA, 5005, Australia. tony.hall@adelaide.edu.au

<sup>7</sup>School of Natural and Built Environments, University of South Australia, Mawson Lakes, Adelaide, SA, Australia, 5005. jim.jago@unisa.edu.au

<sup>8</sup>Geological Survey of South Australia, GPO BOX 320, Adelaide, SA, 5001. liz.jagodzinski@sa.gov.au, wolfgang.preiss@sa.gov.au

<sup>9</sup>Department of Geosciences, Boise State University, Boise, ID 83725, USA.

jimcrowley@boisestate.edu

<sup>10</sup>School of Biological Sciences, University of Adelaide, North Terrace, Adelaide, SA 5005,

Australia. diego.garcia-bellido@adelaide.edu.au

<sup>11</sup>Earth Sciences Section, South Australian Museum, North Terrace, Adelaide, SA 5000,

Australia

<sup>12</sup>Palaeoecosystems Group, Department of Earth Sciences, Durham University, Durham DH1

3LE, UK

<sup>13</sup>Department of Palaeobiology, Swedish Museum of Natural History, Box 50007, SE-104 05

Stockholm, Sweden. christian.skovsted@nrm.se

\*Corresponding author

*Abstract*

The most successful chronostratigraphic correlation methods enlist multiple proxies such as biostratigraphy and chemostratigraphy to constrain the timing of globally important bio- and geo-events. Here we present the first regional, high-resolution shelly fossil biostratigraphy integrated with  $\delta^{13}\text{C}$  chemostratigraphy (and corresponding  $\delta^{18}\text{O}$  data) from the traditional lower Cambrian (Terreneuvian and provisional Cambrian Series 2) of South Australia. The global ZHUCE, SHICE, positive excursions II and III and the CARE are captured in lower Cambrian successions from the Arrowie and Stansbury basins. The South Australian shelly fossil biostratigraphy has a consistent relationship with the  $\delta^{13}\text{C}$  results, bolstering interpretation, identification and correlation of the excursions. Positive excursion II straddles the boundary between the *Kulparina rostrata* and *Micrina etheridgei* zones, and the CARE straddles the boundary between the *M. etheridgei* and *Daliyatia odyssei* zones, peaking in the lower parts of the latter zone. New CA-TIMS zircon dates from the upper Hawker Group and Billy Creek Formation provide geochronologic calibration points for the upper *D. odyssei* Zone and corresponding chemostratigraphic curve, embedding the lower Cambrian successions from South Australia into a global chronostratigraphic context. This multi-proxy investigation demonstrates the power of integrated methods for developing regional biostratigraphic schemes and facilitating robust global correlation of lower Cambrian successions from South Australia (part of East Gondwana) with coeval terranes on other Cambrian palaeocontinents, including South and North China, Siberia, Laurentia, Avalonia and West Gondwana.

*Keywords*

Cambrian; global correlation; geologic timescale; isotope chemostratigraphy; chronostratigraphy; biostratigraphy; South Australia

## 1. Introduction

South Australian lower Cambrian (Terreneuvian and provisional Cambrian Series 2) successions represent a vast archive of the earliest complex ecosystems that evolved during the Cambrian Radiation. This bioevent is the most significant animal radiation to have occurred on Earth, profoundly influencing the evolutionary trajectory of life to the present day (Marshall, 2006; Erwin et al., 2011; Wood and Zhuravlev, 2012; Erwin and Valentine, 2013; Mángano and Buatois, 2017; Bicknell and Paterson, 2018). This extraordinary burst of diversification resulted in the emergence of most bilaterian animal phyla, and the establishment of complex ecosystems, trophic webs, and escalatory ‘arms races’.

The Cambrian Radiation is captured in astonishing clarity in East Gondwana, which straddled the palaeoequator and was a major evolutionary epicentre during this time (Brock et al., 2000). Increasingly refined global chronostratigraphy has clarified the timing and tempo of evolutionary events during the early Cambrian, but correlation of lower Cambrian successions from Australia into this broader chronostratigraphy has remained largely unresolved. Endemism, diachronism and facies dependence plague correlation of fossiliferous lower Cambrian successions, and  $\delta^{13}\text{C}$  chemostratigraphy has become the tool of choice to overcome perceived limitations of biostratigraphic and lithostratigraphic correlation (Landing et al., 2013; Wendler, 2013; Smith, A.G. et al., 2015; Smith, D.G. et al., 2015). However, it is the integration of multiple temporal proxies with the ever-improving precision of radiometric geochronology that is proving most effective at resolving problems of dating and correlation of rock packages in the Cambrian.

In 2004, the International Subcommittee on Cambrian Stratigraphy (ISCS) split the Cambrian period into four series, further subdivided into ten stages. Ideally, the lower boundary of each stage is defined using multi-proxy evidence, principally the First Appearance Datum (FAD) of key fauna in combination with chemostratigraphic data, with

the ultimate aim being the ratification of Global Standard Stratotype-section and Points (GSSPs) at these boundaries (Remane et al., 1996; Babcock et al., 2005, 2015; Babcock and Peng 2007; Peng and Babcock 2011, Peng et al., 2012). Trilobites and agnostoid arthropods are particularly well-studied fossil groups, and are used as index fossils for the biostratigraphical subdivision of Cambrian Series 2, Stage 3 and younger intervals (Peng et al., 2004; Babcock et al., 2007). These arthropods are well-preserved, often abundant, readily identifiable, and include many cosmopolitan taxa with short stratigraphic ranges (Peng and Robison, 2000; Zhu et al., 2004; Babcock et al., 2005, 2007; Peng et al., 2004, 2012; Zhang et al., 2017).

Traditionally, the lower part of the Cambrian System is subdivided (in ascending stratigraphic order) into the Terreneuvian Series and unnamed Series 2. The Terreneuvian Series is subdivided into two stages; the lowermost Fortunian Stage, succeeded by unnamed Stage 2. Cambrian Series 2 is subdivided into the unnamed and undefined Stages 3 and 4. The base of Stage 2 has been particularly difficult to define, due mostly to the absence of trilobites. This has demanded reliance on the detailed description and stratigraphic range determination of a variety of other fossil groups.

In Australia, key (non-trilobite) fossil groups that have been applied to the problem of relative dating and correlating of lower Cambrian deposits include archaeocyaths (Kruse and West, 1980; Debrenne and Gravestock, 1990; Zhuravlev and Gravestock, 1994; Kruse and Shi in Brock et al., 2000), acritarchs (Zang et al., 2007; Jago et al., 2012), and a range of spiralian, including biomineralised animals that were previously lumped together under the umbrella term 'small shelly fossils' or SSFs (Matthews and Missarzhevsky, 1975; Steiner et al., 2004, 2007; Devaere et al., 2013, 2014b). Studies on South Australian shelly fossils, especially the enigmatic tommotiids, over the last decade have clarified the phylogenetic affinities, palaeobiology and palaeoecology of these animals that were previously known only

from isolated skeletal components (e.g. Skovsted et al., 2008, 2009a, 2015a,b; Topper et al., 2013; Larsson et al., 2014 ). Intensive research has also highlighted the biostratigraphic value of various shelly fossil groups, which have been used by Betts et al. (2016, 2017b) to produce a detailed, robust and practical biostratigraphic scheme for the lower Cambrian of South Australia.

Formal ratification of lower Cambrian stages has been stymied, largely due to high levels of endemism and the facies-restricted distribution of taxa (Landing and Geyer, 2012; Landing et al., 2013), as well as taphonomic variability and taxonomic controversies. Species with an intercontinental distribution are the most useful for correlation. For example, the micromollusc *Watsonella crosbyi* is known from Avalonia, Mongolia, Siberia, South China, plus West and East Gondwana (Brasier et al., 1996; Li et al., 2011; Kouchinsky et al., 2012; Devaere et al., 2013; Landing et al., 2013; Jacquet et al., 2017b). Consequently, this taxon has been suggested as the best index fossil to define the lower boundary of Cambrian Stage 2 (Li et al., 2011; Parkhaev and Karlova, 2011; Peng and Babcock, 2011; Peng et al., 2012; Jacquet et al., 2017b; Landing and Kouchinsky, 2016). Another early Cambrian mollusc with an almost global distribution includes the helically-coiled mollusc *Aldanella attleborensis*, which has also been suggested as a potential index fossil to define the base of Cambrian Stage 2 (Parkhaev, 2014).

Although some endemism and facies restriction of taxa is inevitable (Landing and Geyer, 2012; Landing et al., 2013), the fact remains that many shelly fossils (e.g. halkieriids, palaeoscoleceids, hyoliths, and brachiopods) occur across a much wider range of facies than do archaeocyaths and acritarchs, and thus have more potential for correlation (Betts et al., 2017a; Kruse et al., 2017). Whilst there are clearly difficulties in high-resolution correlation using Cambrian fossils, shelly taxa can still provide remarkable precision at a global scale, but are especially useful at the regional scale (e.g. Rozanov et al., 1969; Missarzhevsky and

Mambetov 1981; Brasier et al., 1996; Steiner et al., 2007; Devaere et al. 2013; Betts et al., 2016, 2017b). Importantly, the difficulties associated with global correlation can be minimised when regional biostratigraphic schemes are combined with independent correlative tools such as chemostratigraphy (Kaufman et al., 1996) and/or magnetostratigraphy (Kirschvink et al., 1991).

The application of carbon isotope chemostratigraphy throughout the Cambrian is now well established (e.g. Brasier et al., 1992, 1996; Maloof et al., 2005, 2010a,b and references therein; Cremonese et al., 2014; Ishikawa et al., 2014; Smith, et al., 2016; Chang et al., 2017; Ren et al., 2017; Schmid, 2017). This method is recognised as an effective correlation tool because carbon isotopes are relatively resistant to major diagenetic alteration and provide a global signal that can temporally constrain endemic faunas and regional biostratigraphic schemes, especially in pre-trilobitic lower Cambrian packages. A robust, integrated biostratigraphy and chemostratigraphy for lower Cambrian strata in Australia has been lacking (but see Tucker, 1989; Hall, 2012). New chemostratigraphic data presented herein demonstrate that the shelly fossil biozones established by Betts et al. (2016, 2017b) have consistent, repeatable and predictable relationships to  $\delta^{13}\text{C}$  curves derived from the same stratigraphic sections that yield the shelly fossils. The  $\delta^{13}\text{C}$  and  $\delta^{18}\text{O}$  isotopic curves from the lower Cambrian of South Australia can be confidently correlated with the global standard (Maloof et al., 2005, 2010a, b; Peng et al., 2012) based on stratigraphic position, trends and magnitude of  $\delta^{13}\text{C}$  excursions, in combination with co-occurring shelly fossils (including trilobites in the upper parts of some sections).

These relative dating methods are underpinned by new, high-resolution CA-TIMS radiometric dates from zircons derived from volcanic ash beds at critical intervals in the Arrowie and Stansbury basin successions. This is the first study to integrate a robust shelly fossil scheme with abundant  $\delta^{13}\text{C}$  chemostratigraphic data and highly accurate radiometric



dates to temporally constrain lower Cambrian rocks of South Australia. Integration of these independent chronostratigraphic proxies (biostratigraphy and chemostratigraphy) with reliable radiometric (geochronological) ages demonstrates that the successions from South Australia span an interval from the Terreneuvian Series (upper Fortunian Stage) to undefined Cambrian Series 2, Stages 3–4, embedding these successions in a global context.

### 1.1. South Australian shelly fossil biozones

Three lower Cambrian shelly fossil biozones were formally defined and described by Betts et al. (2016, 2017b) (in ascending order): the *Kulparina rostrata*, *Micrina etheridgei*, and *Dailyatia odyssei* zones. These biozones exploit the robust and repeatable stratigraphic ranges of a variety of key tommotiids, brachiopods, molluscs and bradoriids from the Arrowie and Stansbury basins in South Australia. The oldest zone (*K. rostrata* Zone) is entirely pre-trilobitic. It is characterised by a relatively low-diversity shelly assemblage, typically containing five or six taxa, including eccentrothecimorph and camenellan tommotiids and the paterinid brachiopod *Askepasma saproconcha* Topper, Holmer, Skovsted, Brock, Balthasar, Larsson, Pettersson-Stolk and Harper, 2013.

Most of the succeeding *Micrina etheridgei* Zone is also pre-trilobitic, but its upper parts overlap with the lower boundary of the oldest Australian trilobite zone (*Parabadiella huoi* Zone). The *M. etheridgei* Zone is characterized by a high-diversity shelly fossil assemblage that includes eccentrothecimorph and camenellan tommotiids, helcionelloid molluscs, bradoriid arthropods, and lobopodians (Betts et al., 2016, figs. 13–21). The *Dailyatia odyssei* Zone overlaps the *Pararaia tatei*, *Pararaia bunyeroensis* and lowermost *Pararaia janeae* trilobite zones (Betts et al., 2017b, fig. 21). Key shelly fossils occurring in the *D. odyssei* Zone include tommotiids, stoibostrombids and distinctive brachiopod and bradoriid taxa (Betts et al., 2016, 2017b).

Robust regional correlation of the recently established biostratigraphic scheme is enabled by co-occurrence of characteristic shelly taxa in coeval basins including the Stansbury, Officer, Amadeus and Georgina basins, as well as the Transantarctic Mountains (Betts et al., 2016; 2017b, Claybourn, 2016), all of which were part of the East Gondwanan margin during the early Cambrian. Further, it is becoming increasingly apparent that there are close faunal connections between South Australia and other lower Cambrian successions, notably in North and South China (Li and Xiao, 2004; Steiner et al., 2007; Yang et al., 2015; Yun et al., 2016; Pan et al., 2017, in press) and Laurentia (Landing and Bartowski, 1996; Skovsted, 2004; Skovsted and Peel, 2007; Skovsted et al., 2016), particularly during *D. odyssei* Zone time. Species of *Dailyatia* (see Skovsted et al., 2015a for detailed taxonomy) form the backbone of the latest biostratigraphic scheme, and many key accessory taxa in all three zones are also endemic; hence, additional proxies are required to refine global correlation.

### 1.2. Cambrian chemostratigraphy

Global carbon isotope chemostratigraphy is directly affected by major biological fluxes (Maloof et al., 2010a). Inorganic carbon isotope chemostratigraphy exploits the ratio between  $^{12}\text{C}$  and  $^{13}\text{C}$  isotopes preserved in carbonate rocks and shells. The lighter  $^{12}\text{C}$  isotope is preferentially utilised by primary producers in cellular metabolic activities (Brand and Veiser, 1981). Hence,  $^{12}\text{C}$  becomes depleted in the hydrosphere and atmosphere during times of high primary productivity, thereby increasing the inorganic  $^{13}\text{C}$  values in carbonate sediments formed during those periods. Because the oceans are relatively well mixed, carbon isotope values of seawater are preserved in deposits around the globe contemporaneously (Brasier, 1993). As with biostratigraphic divisions, large positive or negative excursions may be due to key oceanic, geochemical and ultimately evolutionary events, and are often related

to faunal turnover and extinction events. An excellent summary of these processes is provided by Ripperdan (1994).

As an independent chronostratigraphic technique, chemostratigraphy can undoubtedly be very effective (e.g. Maloof et al., 2010a,b; Kouchinsky et al., 2012; Landing et al., 2013), although it is critical that sources of potential diagenesis, such as sub-aerial exposure, shell recrystallisation, organic burial rates, the presence of hardgrounds, and local depositional conditions, such as exposure to contaminated groundwater, are identified and addressed (Kaufmann and Knoll, 1995; Wendler, 2013; Bradbury et al., 2015; Swart, 2015).

Oxygen-isotope chemostratigraphy ( $^{18}\text{O}/^{16}\text{O}$  ratio, or  $\delta^{18}\text{O}$ ) is frequently applied in concert with carbon isotopes. Oxygen isotopes have both the benefit and detriment of being more strongly affected by temperature and diagenesis than carbon isotopes (Marshall, 1992). This susceptibility means they are readily applied to characterisation of palaeotemperature and palaeoclimate (e.g. Fricke et al., 1998; Clarke and Jenkyns, 1999; Johnsen et al., 2001; Weissert and Erba, 2004). Rocks that have undergone strong diagenesis will show unusual oxygen isotope values, relative to carbon isotopes within and across stratigraphic sections. The general trend in modern diagenetically-altered rocks is for the  $\delta^{18}\text{O}$  values to positively spike, whilst the  $\delta^{13}\text{C}$  values become more negative (Melim et al., 2001). Thus, if the carbon and oxygen curves independently exhibit uncharacteristic spikes within the same horizon, it can indicate likely diagenetic alteration overprinting primary signals within samples.

Isotopic composition can be sampled directly from calcareous shell material. However, the vital effect, whereby metabolic pathways fractionate isotopes, must be considered (Weiner and Dove, 2003). However, specific calcareous shells are often difficult to identify and isolate in many lowermost Cambrian carbonate successions, and so bulk rock samples collected from cut and polished carbonate blocks provide the best means for

determining isotopic compositions. If sample preparation protocols are followed to limit the possibility of sampling *ex situ* material (e.g. void infills, allochthonous clasts, veins), original signals and trends of  $\delta^{13}\text{C}$  and  $\delta^{18}\text{O}$  that correspond to true average global values can be obtained.

When correlating  $\delta^{13}\text{C}$  curves, the ability to accurately align positive and negative peaks is only possible for periods of major rapid changes in isotopic ratios. In this regard, the Cambrian System is ideal for applying chemostratigraphic methods (Weissert et al., 2008). Within lower Cambrian Stage 2, the most important carbon isotope excursion events include the positive (up to  $\sim +7.0\%$ ) Zhujiqing Carbon-Isotope Excursion (ZHUCE, Zhu et al., 2006; I' in Siberian sections; 6p in Maloof et al., 2010a; "L4" in Landing et al., 2013), which may consist of a number of smaller excursion events (Landing and Kouchinsky, 2016). The ZHUCE  $\delta^{13}\text{C}$  event is one of the largest positive excursions within the lower Cambrian and coincides with a major radiation of SSFs (Zhu et al., 2006; Landing and Kouchinsky, 2016). The slightly younger (negative [up to  $\sim -6.0\%$ ]) Shiyantou Carbon-Isotope Excursion (SHICE) corresponds to a major extinction of small shelly fossils (Zhu et al., 2006). Positive excursions II ( $\sim +1.5\%$ ) and III ( $\sim +0.2\%$ ) (unnamed in Zhu et al., 2006) also provide a basis for global correlation. The Cambrian Arthropod Radiation Isotope Excursion (CARE; IV in Siberian sections and Maloof et al., 2010a) straddles the Terreneuvian, Stage 2–Series 2, Stage 3 boundary (peaking near the base of Stage 3), and reaches maximum values of  $\sim +3.5\%$  (Zhu et al., 2006). The CARE corresponds to the first major radiation of arthropods (especially trilobites) on a global scale (Zhang et al., 2017). The Mingxinsi Carbon Isotope Excursion (MICE) (excursions V, VI, and VII in Siberian sections) occurs within lower Stage 4 (Zhu et al., 2006). Each of these major excursions contains multiple minor 'peaks', making peak-matching using chemostratigraphy alone fraught with difficulty. However, when

calibrated with well-constrained and robust regional biostratigraphic schemes, constraining isotopic curves becomes increasingly well resolved.

### 1.3. *Reliability of chemostratigraphy*

The reliability and accuracy of carbon isotope chemostratigraphy as a stand-alone proxy for regional and global correlation has been questioned (Holmden et al., 1998; Swart and Eberli, 2005; Fanton and Holmden, 2007; Swart, 2008; Swart and Kennedy, 2012; Steiner and Yang, 2017). These authors suggest that  $\delta^{13}\text{C}$  values in carbonate rocks reflect local environmental changes rather than the global carbon cycle, or are a result of diagenesis (Knauth and Kennedy, 2009; Derry, 2010; Higgins et al., 2018). Carbon isotopes may be influenced by a wide array of processes (Kaufman and Knoll, 1995; Wendler, 2013, fig. 1); yet, the fact remains that robust and repeated global secular trends are commonly widely detected. Wendler (2013) suggests this is related to the larger scale of the global carbon budget that likely dominates local signals. The global manifestation of these early Cambrian events implicates a variety of mechanisms in the early Cambrian marine carbon cycle, for example, fluctuations in oceanic redox, nutrient cycling, and the rate of organic matter burial (Halverson et al., 2009). Additionally, interpretation of carbon isotope curves without robust supporting data can result in controversial age assessments (see Smith et al., 2016, 2017; Landing and Kruse, 2017). Hence, demonstration of the reliability of chemostratigraphic data requires coupling with other robust proxies for time (especially biostratigraphy), or accurate radiometric dates, where possible.

## 2. **Stratigraphic sections and lithostratigraphy**

A preliminary lower Cambrian biostratigraphy for South Australia was first outlined by Daily (1956; see also Jago et al., 2006, 2012; Kruse et al., 2009), who introduced 12 informal 'faunal assemblages' for regional correlation, mainly based on faunas from the Arrowie Basin. The assemblages of Daily (1956) were taxonomically undescribed and largely

unconstrained in terms of stratigraphic ranges until work over the last four decades provided baseline taxonomic and stratigraphic data for lower Cambrian fossils in South Australia (Gravestock, 1984; Bengtson et al., 1990; Debrenne and Gravestock, 1990; Kruse, 1991; Jell et al., 1992; Zhuravlev and Gravestock, 1994; Gravestock et al., 2001; Brock and Paterson 2004; Skovsted et al., 2006, 2009a,b, 2011, 2015a,b; Paterson and Brock, 2007; Topper et al., 2007, 2010, 2013; Betts et al., 2014, 2017b; Larsson et al., 2014; Jacquet and Brock 2016; Jacquet et al., 2017b). Betts et al. (2016, 2017b) have recently compiled shelly fossil range data to produce a new biostratigraphic scheme for the lower Cambrian of South Australia. This scheme is based on stratigraphic occurrences of thousands of shelly fossils sampled from 21 stratigraphic sections and drill cores that span the entire Hawker and Normanville groups, representing more than 5 km of stratigraphy in the Arrowie (Fig. 1) and Stansbury basins. The 10 stratigraphic sections and drill cores described and illustrated here were sampled synchronously for biostratigraphic, lithostratigraphic and chemostratigraphic data, and so become the basis for an integrated multi-proxy early Cambrian chronostratigraphy. The detailed biostratigraphy of sections AJX-M, MORO and WAR (Betts et al., 2016), and SCYW-791A, BHG, PIN and YALKALPO-2 (Betts et al., 2017b) are illustrated here, but further information is provided by Betts et al. (2016, appendices 1, 3 and 4; 2017b, appendices 1, 6, 10 and 11). New lithological data from these sections, as well as the  $\delta^{13}\text{C}$  chemostratigraphic curves are correlated to the recently established biostratigraphic zonation of Betts et al. (2016, 2017b). Stratigraphic sections WANG and WANG-S, measured through lower parts of the carbonate-dominated Normanville Group (Wangkonda and Sellick Hill formations) in the Stansbury Basin, capture important new biostratigraphic and chemostratigraphic data and are described in more detail below.

### 2.1. *Stansbury Basin*

Lower Cambrian facies in both the Stansbury and Arrowie basins include marginal marine to carbonate shelf, platform, ramp, outer shelf and slope deposits (Gravestock and Gatehouse, 1995; Jago et al., 2006), and shelly fossils allow for accurate correlation of strata between the basins (Betts et al., 2016, 2017b). Cambrian rocks crop out extensively on both the Yorke and Fleurieu peninsulas and on Kangaroo Island, and subsurface geology is relatively well known via extensive drill coring. Early Cambrian shelly fossils from the Stansbury Basin were central to the pioneering biostratigraphic work of Daily (1956), and were also applied to the development of regional molluscan and shelly fossil biozones developed by Gravestock et al. (2001). Shelly fossils from the Stansbury Basin supplemented abundant Arrowie Basin material to generate the biostratigraphic scheme developed by Betts et al. (2016, 2017b).

On the Fleurieu Peninsula in the eastern Stansbury Basin (Fig. 2), the Normanville Group consists of an approximately 1 km-thick succession of predominantly limestone, siltstone and shale, with minor arkosic and calcareous sandstone units towards the base, and significant deposits of black, pyritic and phosphatic shales towards the top (Daily and Milnes, 1973). The entire succession is upward-deepening and represents a transgressive marine event, beginning with a shallow, nearshore, subtidal environment at the base, followed by a shallow-marine shelf with biohermal reefs, through to a deep-water environment and eventually a carbonate-free basinal setting at the top (Alexander and Gravestock, 1990; Gravestock and Gatehouse, 1995). Regional tectonism has resulted in subtle, but key differences in the depositional regimes between the Stansbury and Arrowie basins, notably the development of carbonates at comparably low stratigraphic levels in the eastern Stansbury Basin, for example, the Wangkonda Formation on Fleurieu Peninsula (early in Sequence Set C1.1 of Gravestock and Gatehouse, 1995). At similar levels in the Arrowie Basin, shallow-marine and shoreline deposits such as the Uratanna and Parachilna formations accumulated,

and carbonates did not develop until later in Sequence Set €1.1 (Gravestock and Cowley, 1995).

Differences in depositional regimes across the Arrowie and Stansbury basins have affected the stratigraphic occurrence of shelly fossils. In the Stansbury Basin, the first shelly fossils include abundant, indeterminate hyoliths in the middle siltstone member of the Mount Terrible Formation (Sequence Set €1.0), below the Wangkonda Formation. Abundant shelly fossil assemblages, dominated by hyoliths, halkieriid sclerites and molluscs also occur in the upper-middle and topmost members of the Mount Terrible Formation (Jacquet et al., 2017b). Equivalent strata in the Arrowie Basin—namely the siliciclastic Uratanna and Parachilna formations—are notably devoid of shelly fossils. A single specimen of a helcionelloid mollusc, tentatively identified as *?Bemella* sp., has been reported from the Parachilna Formation (Daily, 1976b; Fig. 8G), although for the most part, the only fossils known from this unit are abundant U-shaped burrows of *Diplocraterion parallelum* (Daily, 1973; Mángano and Buatois, 2014; Jacquet et al., 2017b).

Thin carbonates in the upper Mount Terrible Formation of the Normanville Group on Fleurieu Peninsula record the first Australian occurrence of the globally distributed micromollusc, *Watsonella crosbyi* (Jacquet et al., 2017b). Early Cambrian correlation is commonly impeded by endemism, so the occurrence of *W. crosbyi* in the Normanville Group is significant, as it is one of the rare early Cambrian shelly taxa with a global distribution (Jacquet et al., 2017b). The shelly and trace fossil data, coupled with chemostratigraphic evidence presented herein, support a Terreneuvian, Stage 2 age assessment for *W. crosbyi* in South Australia, consistent with occurrences in other Cambrian terranes (Jacquet et al., 2017b).

In their detailed study of the lithology and stratigraphy of lower Cambrian rocks in the Normanville–Sellick Hill region, Abele and McGowran (1959) recognised four distinct and



predominantly calcareous units (in ascending order): the Wangkonda Formation; Sellick Hill Formation; Fork Tree Limestone; and Heatherdale Shale. Daily (1963) ascribed the name Mount Terrible Formation to the lower *Hyolithes* Sandstone of Abele and McGowran's Wangkonda Formation, recognising that it constituted a distinct stratigraphic unit, whilst retaining the name Wangkonda Formation for the overlying limestone member. The Normanville Group is overlain unconformably by the extensive greywackes and shales of the early to (?)middle Cambrian Kanmantoo Group (Jago et al., 1994, 2003). The chronostratigraphic data presented here are derived from new stratigraphic sections measured on Fleurieu Peninsula (Fig. 2), including the WANG, WANG-S (Fig. 3), SHL and FTL sections (Fig. 4), sampled for shelly fossils, as well as carbon and oxygen isotopes.

#### 2.1.1. *WANG and WANG-S sections (Wangkonda and Sellick Hill formations)*

The WANG (Wangkonda) section was measured through the Wangkonda (98 m-thick) and Sellick Hill (306 m-thick) formations along a new NW-oriented road, exposing the geology in a commercial quarry located approximately 2 km inland from Sellicks Beach (Fig. 2). The base of the WANG stratigraphic section is located at the boundary between the top of the Mount Terrible Formation and overlying Wangkonda Formation (Fig. 3). The top of the WANG section is located near the top of the Sellick Hill Formation, approximately 5–10 m below the lower boundary of the Fork Tree Limestone, which has been removed by large-scale quarrying activities. The WANG-S (Wangkonda South) section was measured through ~160 m of Wangkonda Formation and 23.7 m of overlying Sellick Hill Formation, along a road cut on Main South Road in the Sellicks Hill area, Fleurieu Peninsula (Fig. 2). The WANG-S section was measured as a supplementary section in an attempt to replicate biostratigraphic and chemostratigraphic signals in the Wangkonda and lower Sellick Hill Formations, as recovered from the WANG section (Fig. 3).

The Wangkonda Formation is primarily a blue-grey limestone comprising laminated microbialites, dolostones and micrites (Figs. 5A–C, E, 6A–E), with coarse clastic interbeds leached of carbonate, and a quartz-rich clay bed near the base (Abele and McGowran, 1959). The Wangkonda Formation is normally 100–110 m thick (e.g. WANG section), although regional mapping indicates that the unit thickens to the SW, and in the WANG-S section the formation is close to 160 m thick. Abrupt dip changes in this section may possibly indicate fault repetition in the upper 50 m of the section. The weathered nature of the rocks in the WANG-S section make it difficult to precisely correlate strata to the fresh exposures in the WANG section. The Wangkonda Formation comprises interbedded micritic fenestral limestones (Fig. 5F, G, L) and bioturbated (Fig. 5I, J), arkosic, cross-bedded sandstones that imply a peritidal sandflat to shallow nearshore setting. Interbedded oolitic grainstone (Fig 5K, 6A) likely formed as localized bars or shoals in a shallow subtidal environment. Fenestral fabrics are commonly found in association with microbialites (sometimes oncoids, Fig. 5D, K) and may indicate sub-aerial exposure, which is not conducive to high faunal diversity (Gravestock and Gatehouse, 1995; Gravestock et al., 2001). Stylolites and dissolution textures are common (Fig. 5H, M).

Few fossils have been recovered from the Wangkonda Formation. Chancelloriid sclerites were reported by Gravestock et al. (2001) and a few sclerite fragments of *Australohalkieria* sp. were illustrated by Bengtson et al. (1990, fig. 49). The low yields of microfossils from the Wangkonda Formation in both the WANG and WANG-S sections is thus not unexpected and confirms previous reports. In the WANG section, a single tube, cf. *Torella* sp., was recovered from 60 m above the base of the section (WANG/60.0). At WANG-S/190.0 (124.6 m above base) in the upper Wangkonda Formation, shelly fossils include hyolith conchs, halkieriid sclerites, helcionelloid mollusc steinkerns, and

chancelloriid spicules (Fig. 7A–L), and is similar in composition to the fauna from the Mt. Terrible Formation, but lacking *Watsonella crosbyi* (Jacquet et al., 2017a, fig. 4).

Daily (1976b) and Gravestock et al. (2001, p. 48) noted that the Wangkonda Formation was highly bioturbated at some levels, and Jacquet et al. (2017b) confirmed the presence of vertical burrows belonging to *Skolithos* sp. and *Diplocraterion* sp. in more sandy interbeds throughout the unit (Fig. 8A). The presence of well-developed vertical burrows in the Wangkonda Formation invites correlation with the quartz-rich sandstones of the Parachilna Formation in the Arrowie Basin that has similarly burrowed ‘piperock’ textures. *Bemella*-like helcionelloids also occur in both units (Daily, 1976b; Fig. 8G). The incoming of vertical burrowing is now taken as an important bilaterian evolutionary innovation that is characteristic of Cambrian Stage 2 (Mángano and Buatois, 2014, 2017).

The boundary between the Wangkonda Formation and the overlying Sellick Hill Formation is unconformable (Abele and McGowran, 1959; Daily, 1963). Much like the underlying Wangkonda Formation, the lower Sellick Hill Formation is sandy and relatively poorly fossiliferous, although Gravestock et al. (2001) reported a diverse shelly fauna including *Watsonella crosbyi*, *Mackinnonia rostrata*, *Figurina nana*, *Anuliconus truncatus*, *Obtusoconus brevis* and *Stenotheca drepanoidea* from Facies A in the Sellick Hill Formation (Myponga Beach section). Unfortunately, apart from the presence of indeterminate hyolithelminths, occurrences of these molluscs at low levels in the Sellick Hill Formation have not been reproduced in either the WANG or WANG-S sections.

Alexander and Gravestock (1990) divided the Sellick Hill Formation into five Facies Associations (A–E, all intersected by the WANG section; see Fig. 3), that can be separated into two depositional stages: a lower, predominantly clastic series of sediments (A, B); and an upper, carbonate-dominated sequence (C–E). The WANG-S section intersects only Facies A,

which consists of laminated and highly burrowed siliciclastics (Fig. 5N–P), and the SHL and FTL sections (discussed below) intersect Facies C–E (Fig. 4).

A poorly circulated, marginal basin setting appears to have prevailed through most of the deposition of the lower Sellick Hill Formation, with conditions improving in the upper parts with archaeocyaths, microbialites and stromatolites occurring within a lowstand systems tract (Gravestock and Gatehouse, 1995). Facies A and B correspond to an inner shelf depositional system (Mount and Kidder, 1993), characterised by an influx of detrital siliciclastic material, likely from the Gawler Craton that largely stifled carbonate development. Facies A consists of coarse, arkosic sandstones and siltstones with some bioturbation (Figs. 5N–P, 6F, H–I), and rare oolitic grainstones (Fig. 6G), whereas Facies B has finer, more calcareous sandstone interbedded with siltstone, shale and minor sandstone intervals (Fig. 6J) and exhibits extensive bioturbation (Fig. 6K). Trace fossils present in the cross-bedded sandstone beds of Facies B are dominated by horizontal traces, including *Treptichnus* sp. (WANG/146.5, Fig. 3). Gravestock et al. (2001) additionally reported (but did not figure) the trace fossils *Monocraterion*, *Plagiogmus* and *Taphrelminthopsis* from Facies B in their Section 5 at Myponga Beach.

Facies Associations C–E record a low-energy, carbonate ramp environment. Facies C includes ribbon limestones, calcareous shales, bioturbated interbedded carbonates and siliciclastics (Fig. 6L–O), and potential omission surfaces with quartz siltstone interbeds. Intraformational, flat-pebble conglomerates are a distinctive sedimentary feature in Facies C, suggestive of cyclic, submarine debris flows (Alexander and Gravestock, 1990). In the WANG section, Facies C contains a 13 m-thick (WANG/283.0–296.0) fault slip surface that may represent potential repetition of part of the section (Fig. 3). Faunal diversity is low in Facies C, with a single, partial, conical hyolithelminth tube recovered from WANG/190.0. Facies D is characterised by the cyclical establishment and intermittent partial destruction of

pioneer bioherms, consisting of mainly reworked archaeocyathan and other fossil debris, reflecting rapid deposition from high-energy events. Phosphatic hardgrounds are clearly developed at WANG/321 (Fig. 6P, Q) that have preserved abundant shelly fossils including tomotiids, brachiopods, halkieriids and various spicules (Fig. 3). Facies E is very similar to Facies C in depositional style, with well-developed thin-bedded carbonates (Fig. 6R, S) and comparatively minor development of hardground surfaces. Facies E also includes small (metre-scale) archaeocyathan buildups surrounded by thin-bedded and nodular limestones (not observed in the WANG section). Facies E has the highest faunal diversity, including the paterinid brachiopod *Askepasma* sp. cf. *A. saproconcha* (Fig. 9A–C), the tomotiids *Dailyatia ajax* (Fig. 9F–K, M, O), *D. bacata* (Fig. 9L, N, P) and *Sunnaginia imbricata* (Fig. 9D, E), cancelloriids (including *Archiasterella* sp.), the hyolith *Cupithecra* sp. (Fig. 9S), and palmate, cultrate and siculate halkieriid sclerites (Fig. 9T–W, including *Australohalkieria parva*, Fig. 9X), and hyolithelminth tubes (Fig. 9Q, R). Archaeocyaths from the Sellick Hill Formation were also described by Debrenne and Gravestock (1990). The lower boundary of the *Kulparina rostrata* Zone is defined at WANG/321.0, 83 m below the top of the section, based on the occurrence of *Askepasma* sp. cf. *A. saproconcha* and the accessory taxon, *D. ajax*. A single specimen recovered from WANG/251.0 may also belong to *Askepasma* sp. cf. *A. saproconcha*, but very poor preservation precludes confident identification. If further sampling were to confirm this lower occurrence of *Askepasma* sp. cf. *A. saproconcha*, then the base of the *K. rostrata* Zone could be placed lower within the Sellick Hill Formation (dotted line in Fig. 3). *Sunnaginia imbricata* is also recovered from Facies D and E from WANG/321.0 to WANG/350.0 (Figs. 3, 9C, D). These are key supplementary taxa in the *K. rostrata* Zone (Betts et al., 2016), and so provide good independent support for the definition of this zone in the upper part of the Sellick Hill Formation in the WANG section. The upper boundary of the *K. rostrata* Zone probably occurs high in the overlying Fork Tree Limestone,

but the lack of taxa representing the succeeding *Micrina etheridgei* Zone means the top of the *K. rostrata* Zone (and concordant base of the *M. etheridgei* Zone) occurs at a stratigraphic level considerably above the top of the WANG section.

### 2.1.2. SHL and FTL sections (*Sellick Hill Formation, Fork Tree Limestone and Heatherdale Shale*)

The SHL (Sellick Hill limestone) section is 62.5 m thick and incorporates Facies C–E of the Sellick Hill Formation, exposed in a gully at the coast, ~1.5 km south of Myponga Beach on Fleurieu Peninsula (Fig. 2). The lower 24 m of the SHL section (Facies C) is characterised by flat-pebble conglomerates in beds up to 20 cm thick (Figs. 4, 8E). Alexander and Gravestock (1990) documented these intraformational conglomerates at a locality to the northeast of Myponga Beach, noting the distinctive vertical or inclined stacking of the clasts. In the SHL section, the clasts are rounded and elongate, and are surrounded by a quartz sand matrix (Fig. 10A, I). The clasts commonly exhibit iron staining, a result of the alteration of pyrite crystals to limonite (Fig. 10D, H, I). Beds of laminated (Fig. 10B, C, E) and bioturbated limestones ~1–2 cm thick (Fig. 10F, G, J) are interbedded with the flat-pebble conglomerates, and the development of hardground surfaces is relatively common. Shelly fossils from Facies C in the Sellick Hill Formation are rare, although *Sunnaginia imbricata*, halkieriids and hyoliths were recovered from horizon SHL/22.

In the SHL section, Facies D is very thin (~3 m thick, Fig. 4), with well-developed anastomosing phosphatic hardgrounds, shelly fossil-rich bioclastic packstone intervals (Fig. 10L), and bioturbated intervals (Fig. 10K). These levels feature geopetal infills, dissolution of skeletal fragments, and well-sorted and sub-rounded quartz grains, suggesting a shallow depositional environment. Minor detrital glauconite occurs in SHL/50.7, which was also

noted in Facies D by Alexander and Gravestock (1990). Shelly fauna from horizon SHL/50.9 are particularly abundant, and include *Sunnaginia imbricata*, *Dailyatia ajax*, *Askepasma* sp. cf. *A. saproconcha*, hyoliths, *Australohalkieria parva*, *Hippopharangites dailyi* and *Sinosachites delicatus*. Shelly fossils are clearly observed in thin section (SHL/50.9, Fig. 10L) between phosphatic surfaces, suggesting intermittent cycles of low sedimentation or non-deposition. Skeletal and siliciclastic constituents of this microfacies show evidence of transportation, with well-sorted, sub-rounded quartz grains suggesting deposition of suspension load from more proximal sources. The top of the SHL section is situated near the base of the first archaeocyathan bioherm typical of Facies E (SHL/91.8, Fig. 4). The contact between the biohermal buildup and the surrounding thin-bedded limestones is undulating.

The FTL section overlaps with the top of the SHL section by approximately 10 m, in the biohermal deposit of Facies E, extending in a south-easterly direction through a dry creek bed of a coastal exposure near Myponga Beach (Figs. 2, 4). The base of the FTL section is underneath the first biohermal mound within the upper Sellick Hill Formation. The lower ~100 m of the FTL section intersects carbonate deposits typical of Facies E, including biohermal buildups and bioturbated ribbon limestones (sampled in the SHL section, Figs. 8F, 10M–O). The contact between the Sellick Hill Formation and the overlying Fork Tree Limestone is conformable. The FTL section intersects 266 m of Fork Tree Limestone and ends within the lower Heatherdale Shale (Fig. 4).

The Fork Tree Limestone in the FTL section has been variably recrystallised and dolomitised, which has affected preservation of bedding planes and archaeocyaths. The lower part of the Fork Tree Limestone, historically referred to as the "Archaeocyathinae" limestone (Howchin, 1897), is similar to the massive, biohermal complexes at the top of the underlying Sellick Hill Formation. The development of abundant archaeocyathan-calcimicrobial bioherms in these horizons indicate shallow-water conditions (Daily, 1976b).

The upper part consists of massive, occasionally brecciated limestones, transitioning to mottled, sandy limestones towards the top of the unit. Deposition of this upper portion is likely to represent a deeper-water environment in comparison to the lower part of the unit. The carbonates are commonly found in association with large aggregations of *Epiphyton* and *Renalcis*, or discontinuous laminae formed by microbial mats. Archaeocyaths, some with diameters of several centimetres, are common, as are shelly fossils. Overall, the depositional environment of the Fork Tree Limestone has been interpreted to be an outer carbonate ramp (Alexander and Gravestock, 1990), although this possibly extends to a basinal setting in the upper portion.

The Heatherdale Shale overlies the Fork Tree Limestone in the FTL section with apparent conformity, although outcrop is poor. The lower 30 m consists of an initially carbonate-rich siltstone facies that transitions upwards into dark, pyritic, carbonate-free siltstones and shales (Jacquet et al., 2017b). Deposition is considered to have taken place in a mid-shelf environment below wave base during rising sea levels, from a transgressive to highstand systems tract (Gravestock and Gatehouse, 1995). Nodules and stringers of phosphate can be found throughout, but occur most noticeably towards the top of the unit (Daily et al., 1976). The limited fossils that have been recovered from the Heatherdale Shale include molluscs (Jacquet et al., 2016), brachiopods and hyoliths, as well as rare organic-walled microfossils (Foster et al., 1985), conocoryphid trilobites (Jago et al., 1984; Jenkins and Hasenohr, 1989), and soft-bodied arthropods, such as *Isoxys* and *Tuzoia* (see Paterson et al., 2010, p. 377; JRP, DCGB and JBJ, unpublished data). The thickness of the Heatherdale Shale is highly variable (greatest thickness of ~350 m at Sellicks Hill; Jago et al., 1994), suggesting that the contact between the Heatherdale Shale and the overlying Carrickalinga Head Formation at the base of the Kanmantoo Group is erosional.



## 2.2. *Arrowie Basin*

In the Arrowie Basin (Fig. 1), the Hawker Group consists of a relatively continuous succession, up to 5 km thick, of predominantly lower Cambrian carbonates interbedded with subordinate siliciclastics that have exceptional exposure across the Stuart Shelf in the west, and entire Flinders Ranges in the central part of the basin. Despite having undergone folding and localized diapiric uplift during Delamerian orogenic events (514–490 Ma, Foden et al., 2006), Hawker Group sedimentary rocks remain mostly unaffected by heating or tectonic processes, and for the most part, have relatively low-grade thermal maturity, are generally lean in organic compounds, and are unprospective for petroleum recovery (Carr et al., 2012). Measured stratigraphic sections and sampled drill cores from the Arrowie Basin that were sampled for carbon and oxygen chemostratigraphic analyses include SCYW-791A, AJX-M, BHG, WAR, MORO, YALKALPO-2 and PIN (Fig. 1). For description of the lower Cambrian succession in the Arrowie Basin, see Betts et al. (2016), Brock et al. (2016a,b), Ceglar et al. (2004), Clarke (1986a,b,c; 1990a,b,c), Gravestock (1995), Gravestock and Hibbert (1991), Haslett (1975), Jago et al. (2012) and Zang et al. (2001, 2004).

### 2.2.1. *WAR section (Wirrapowie Limestone)*

The WAR (Waragee) section intersects ~600 m of Wirrapowie Limestone near Warragee Bore in the central Flinders Ranges (Fig. 1). The section is measured from the poorly exposed boundary between the Parachilna Formation and a thin (~25 m) development of Woodendinna Dolostone, which is conformably overlain (although the contact is covered) by the Wirrapowie Limestone (Fig. 11). The Woodendinna Dolostone is dominated by low

domical to columnar stromatolites (Fig. 8B). The Wirrapowie Limestone in the WAR section is developed as a variably laminated, muddy limestone with firm and phosphatic hardground surfaces, interbedded with sandy bioclastic to peloidal (Fig. 12A, B) limestones, and oolitic grainstones with sub-rounded intraclasts and rounded quartz grains (up to 1 mm) (Fig. 12D). Intraformational conglomerates (Fig. 12A, C, E), cross-beds and grainstones occur throughout the WAR section, indicating periodic higher-energy events. The Wirrapowie Limestone is interpreted as a relatively restricted upper intertidal to stagnant lagoonal environment (Haslett, 1975). However, the WAR section also has finely laminated bioturbated calc-mudstones (Fig. 12G), stromatolite growth (Fig. 12F), and microbial deposits with a distinctive shallowing interval from 396.0–432.0 m, where limestones become coarse and bioclastic. At these levels, *Askepasma saproconcha* is abundant (Betts et al., 2016, appendix 5). Change in depositional style can be attributed to a brief transition from a lagoonal environment to a less restricted, more open shallow shelf or shoaling facies, with development of microbial mounds and an abundant population of *A. saproconcha*. Upper parts of the section are less well bedded than the lower intervals and feature more clotted microbial fabrics. In outcrop, these limestones are massive, blocky and spalling, with occasional archaeocyath-rich framestones.

Archaeocyath debris is clear in thin sections, sourced from an interval ranging from WAR/396.0 to WAR/416.0, and in WAR/655.0 (Fig. 12H–J). Also, petrographic thin sections reveal widespread development of post-depositional pyritic and hematitic phases that have either been altered to limonite or have limonite alteration haloes.

### 2.2.2. MORO section (Hawker Group)

The MORO (Moro Gorge) section was measured from the top of the Parachilna Formation and intersects the Woodendinna Dolostone, Wilkawillina Limestone and interfingering Wirrapowie Limestone exposed on the eastern limb of the Arrowie Syncline (Betts et al., 2014) (Fig. 13). The Parachilna Formation consists of predominantly iron-rich, moderately to well-sorted, quartz-rich sandstones (Fig. 14A), deposited during the early stages of a transgression system tract during Cambrian Sequence €1.1A (Zang et al., 2004). The sandstones are thoroughly bioturbated, commonly dominated by “piperock”, vertical U-shaped burrows belonging to *Diplocraterion parallelum*. Alluvial cover obscures the contact between the Parachilna Formation and the unconformably overlying Woodendinna Dolostone (Fig. 13).

Pervasive dolomitisation occurs throughout the Woodendinna Dolostone in the type section (Haslett, 1975). Dolomitisation in the MORO section has also destroyed original rock fabrics in much of the Woodendinna Dolostone, which is interpreted to have been deposited in a supratidal environment with occasional subaerial exposure (Haslett, 1975). The fabric-retentive dolostones are dominated by laminated to columnar stromatolites (Fig. 14B; Haslett, 1975), and features now classified as microbially-induced sedimentary structures (MISS) (Davies et al., 2016). Shelly fossils are unknown from the Woodendinna Dolostone, likely due to the difficulties of surviving in such highly variable, hostile environments prone to episodic desiccation.

The Mt. Mantell, Hideaway Well and Winnitiny Creek members of the Wilkawillina Limestone are clearly developed in the southeastern Arrowie Syncline. The Mt. Mantell Member of the Wilkawillina Limestone is characterised by oolitic and peloidal (Fig. 14E) grainstones, as well as abundant microbialites amongst the stromatolites (Fig. 12C, D). Fragmented and transported archaeocyath debris occur in the Mt. Mantell Member in the MORO section, but dolomitisation in the uppermost parts has possibly destroyed evidence of

archaeocyaths and other shelly fossils (Fig. 14C, D). Clarke (1986c) reported abundant archaeocyaths representative of Faunal Assemblage 1 of Gravestock (1984) in the Mt. Mantell Member of the Wilkawillina Limestone type section in the Bunkers Graben, 66.5 km to the southwest.

The contact between the Mt. Mantell Member and the overlying Hideaway Well Member is gradational (Clarke, 1986a), but the members are easily distinguished. In contrast to the predominantly stromatolitic and microbial Mt. Mantell Member, the Hideaway Creek Member features abundant archaeocyaths (Fig. 14F–I, K) and the first shelly fauna (Fig. 13; see also Betts et al., 2014; James and Gravestock, 1990). The archaeocyathan-microbial buildups typical of the Hideaway Well Member are particularly well established in the MORO section. Individual bioherms exceed 100 m in diameter and have considerable relief, which is largely attributed to the binding properties of encrusting carbonate-secreting microbes such as *Epiphyton*, *Renalcis* and *Girvanella* (Fig. 14F–I; see also Betts, 2012; Brasier, 1976).

The topography of the biohermal facies is irregular, with deep channels filled with intraclastics, shelly debris and micrite shed from the flanks of the bioherm into deeper lagoonal or outer slope settings (Fig. 8C). Larger allochthonous blocks, up to 3 m in diameter, were shed from the biohermal deposits, coming to rest on the thin-bedded limestones occurring between build-ups (Fig. 8D).

The contact between the Hideaway Well Member and the overlying Winnitiny Creek Member is described as disconformable by Clarke (1986a) in the type section. Above the bioherm in the Hideaway Well Member, the lithology changes drastically to a succession of alternating micrites (Fig. 14L, M), wackestones (Fig. 14J) and laminated lime mudstones. The appearance of micritic limestones above the archaeocyathan-microbial bioherm suggests a rapid change in depositional environment, from a moderate to high-energy, shallow-water

reef platform to more restricted, lower-energy, intrashelfal, and probably slightly deeper shelf depressions.

At 711.7 m (Sample MORO/918.5) above the base of the section, the biohermal Wilkawillina Limestone transitions into lagoonal deposits of the Wirrapowie Limestone (Fig. 13). This facies is characterised by the development of phosphatic hardgrounds and firmgrounds (Fig. 14N) (Jacquet et al., 2017a), with thinly laminated phosphatic surfaces interpreted to have been deposited in a restricted shelf to lagoonal setting. The lack of cross-beds, dessication mudcracks or detrital material suggests that this environment remained submerged and stable (Haslett, 1975).

### 2.2.3. BHG section (*Hawker Group*)

The BHG (Bullock Head Gap) section is a 2.1 km-thick succession measured through the southern Arrowie Syncline in the central Flinders Ranges that intersects the Wirrapowie Limestone (including the Midwerta Shale Member), lower Mernmerna Formation (including the Nepabunna Siltstone Member), upper Mernmerna Formation and Oraparinna Shale (Fig. 15; see also Betts et al., 2017b, fig. 7). The lower 116.3 m of the Wirrapowie Limestone in BHG is a finely laminate, manganiferous limestone, with some firm- and hardground horizons interbedded with calcareous siltstones, and a shelly fauna representing the *Kulparina rostrata* Zone. The overlying 1015.7 m of Wirrapowie Limestone yields *Micrina etheridgei* Zone fossils (Fig. 15) and includes 202.6 m of the Midwerta Shale Member; a finely-bedded siliciclastic package consisting of fine-grained siltstones and sandy, spiculitic carbonates. Some horizons exhibit post-depositional pyrite growth with limonite alteration haloes (Fig. 16A–C) (see discussion in Betts et al., 2017b, p. 249). The Wirrapowie Limestone is interpreted as a shallow-lagoonal facies with occasional mudcracks, oolitic

intervals and interformational conglomerates (Haslett, 1975). However, lateral facies changes mean that these features are not always manifest (see Betts et al., 2017b for further discussion).

Typical shelly fossil assemblages from the conformably overlying Mernmerna Formation are of *Dailyatia odyssei* Zone age. Determination of the boundary between the Wirrapowie Limestone and the Mernmerna Formation in the BHG section is difficult because the Flinders Unconformity (FU) is not developed in this part of the basin, and the contact between the Wirrapowie Limestone and the Mernmerna Formation is therefore gradational. In all sections where it is manifest, the FU separates the *Micrina etheridgei* and *D. odyssei* zones (Betts et al., 2016, 2017b). Hence, the contact between the Wirrapowie Limestone and the Mernmerna Formation is likely to be approximately coincident with the boundary between the *M. etheridgei* and *D. odyssei* zones (Fig. 15).

The Nepabunna Siltstone is developed only in the northern parts of the Arrowie Basin, and represents an outer shelf/slope to basinal deposit that can interfinger with the Mernmerna Formation (Jago et al., 2013). The Nepabunna Siltstone is calcareous and manganiferous, having accumulated during the E1.2 highstand (Gravestock and Hibburt, 1991; Zang, 2002). In thin section, it is dark, often very finely laminated, with fine calcite veins typically oriented parallel to (but sometimes cross-cutting) bedding (Fig. 16D, E). Manganese oxide is disseminated throughout and commonly accumulates along bedding planes and calcite veins.

#### 2.2.4. AJX-M section (Ajax Limestone)

The AJX-M section (Fig. 17) was originally measured by Gravestock (1984, Section M) in the Mt. Scott Range, northern Flinders Ranges, where the Ajax Limestone crops out on

the southern limb of a northwest plunging syncline (Brock et al., 2006, 2016a) (Fig. 1). The AJX-M section has yielded abundant shelly fossils (Skovsted et al., 2009a,b, 2011, 2014b, 2015a; Topper et al., 2011a) and some of the oldest bradoriid arthropods known from East Gondwana (Topper et al., 2011b). Trilobites, including the eponyms for the two oldest trilobite zones in Australia, *Parabadiella huoi* and *Pararaia tatei*, occur in the AJX-M section, in addition to *Eoredlichia shensiensis*. The biostratigraphy of this section was compiled by Betts et al. (2016, fig. 2; see also Fig. 17 herein). Lithologies of the AJX-M section have been described in a number of papers (e.g. Brock et al., 2016a; Skovsted et al., 2009b, 2011; Topper et al., 2011a,b), and are summarized here with new lithological thin sections.

The lower parts of the section intersect dolomitised stromatolitic and microbial boundstones (Fig. 18A, B). The fossiliferous carbonates representing the *Micrina etheridgei* Zone interval include a hyolith-rich wackestone marker horizon near the defined lower boundary of the biozone (Fig. 18C), overlain by ~85 m of skeletal wackestone (Fig. 18D–E). The top of the zone is defined by a highly recrystallized, dolomitised sparitic limestone (Fig. 18F). The upper carbonates of the AJX-M section within the *Dailyatia odyssei* Zone interval host a variety of lithologies, including micritic and skeletal wackestones (Fig. 18G–I), intraclastic grainstones (Fig. 18J), as well as a redeposited, immature, intraclastic mix of calcareous and sandy conglomerates above a truncated disconformable horizon.

#### 2.2.5. *Yalkalpo-2 Drillcore (Mernmerna Formation)*

Yalkalpo-2 is a stratigraphic well drilled by the South Australian Department of Mines and Energy (1975–1976), east of the Benagerie Ridge (31°50'53.92" S/140°37'56.53" E), to a depth of 799.02 m, intersecting 541 m of lower Cambrian clastics and carbonates (Youngs,

1977; Youngs and Moorcroft, 1982) (Figs. 1, 19). Yalkalpo-2 has been investigated as part of many studies aimed at deciphering early Cambrian regional tectonics, depositional regimes, and biostratigraphy (using acritarchs, archaeocyaths, trilobites, and various other shelly fossils) (Gravestock et al., 2001; Zang et al., 2001, 2007).

Interpretations of lithological boundaries in Yalkalpo-2 differ slightly herein from assessments made by previous authors. Zang et al. (2001) and Gravestock et al. (2001) indicated that the lowermost parts of the drill core intersected the Parachilna Formation, which was interpreted to pass transitionally into the Woodendinna Dolostone at a depth of 788.7 m (Zang et al., 2001). The original drill core report documents *Chancelloria*, *Anabarella* and *Micromitra (Paterina) etheridgei* (= *Micrina etheridgei*) at a depth of 786.90 m (Youngs, 1977). New data (herein) reveal the occurrence of shelly fossils from the *Micrina etheridgei* Zone, including *M. etheridgei*, *Paterimitra pyramidalis*, *Dailyatia ajax*, *Dailyatia macroptera* and *Dailyatia bacata* at a lower interval (YALK/794.22–794.40 m; Fig. 19) that was previously interpreted to be Parachilna Formation (Zang et al., 2001). Whilst the upper parts of the Parachilna Formation are extensively burrowed (*Diplocraterion parallelum*), body fossils from this unit are extremely rare (Daily, 1976a). Similarly, the overlying Woodendinna Dolostone, an emergent intertidal–supratidal deposit, also lacks diverse fauna, aside from microbialites and stromatolites (Haslett, 1975).

In all other measured sections, the Parachilna Formation and the Woodendinna Dolostone are separated from the lowest shelly fossil-bearing horizons by hundreds of metres (e.g. MORO, BALC; see Betts et al., 2016, figs. 4, 7). Discovery of shelly fossils at this level in Yalkalpo-2 strongly suggest that the Woodendinna Dolostone has been misidentified in this drill core. There may be an undetected paraconformity or subsurface faulting between the Parachilna Formation and the overlying Wilkawillina Limestone (Winnitiny Creek Member) in the Yalkalpo-2 drill core (as in the BALC and MMT stratigraphic sections – see Betts et



al., 2016, figs. 7, 8). This may explain the rare occurrences of shelly fossils (including trilobites; see Gravestock et al. 2001, pl. I, figs. 1–3) in the Yalkalpo-2 drill core.

Nevertheless, the lowermost samples (798.85–799.00 m) consist of a mature, iron-rich quartz sandstone typical of the Parachilna Formation (Fig. 20A). The lithologies from 798.00 to 780.55 m consist of sandy, glauconitic and dolomitised intervals (Fig. 20B–E) – lithologies consistent with the interpretation of the lower parts of the Wilkawillina Limestone as shallow and subtidal (Gravestock, 1995). Additionally, the Yalkalpo Syncline, at the easterly limits of the Arrowie Basin (separated by the Benagerie Ridge) may have been part of a separate depositional system where shallow, supratidal–intertidal deposition persisted for a longer period.

Typical Wilkawillina Limestone facies occur from 779.78 m to 760.28 m, with common archaeocyath fragments and other phosphatic shelly debris indicative of the *Micrina etheridgei* Zone (Fig. 20F). Laminated and clotted limestones typical of the Mernmerna Formation occur from 760.28 m to 641.41 m. Throughout the Mernmerna Formation, much of the micrite is botryoidal or clotted and thrombolitic and is therefore likely to be microbially mediated (Fig. 20I, J). From 641.41 m to 625.45 m, carbonates increase in sand content, with abundant, rounded to sub-rounded quartz grains (Fig. 20M). Thin sections reveal that in some instances, shelly fossils have been secondarily replaced by sparry calcite, and that archaeocyaths commonly have calcitic spar infills (Fig. 20G). The shelly fauna is dominated by *Dailyatia odyssei* (Betts et al., 2017b). Framboidal hematite is present in places as an infilling or replacement texture of calcite spar in voids (Fig. 20H). Minor dolomitisation occurs in intervals throughout the lower and upper parts of the section (Fig. 20K, L), and dissolution features are generally rare.

### 2.2.6. PIN section (*Mernmerna* Formation)

The PIN (Pinyatta Creek) section (Fig. 21) was measured through the *Mernmerna* Formation cropping out in Pinyatta Creek, approx. 3.7 km SW of Chambers Gorge in the eastern Arrowie Basin (Fig. 1). Lithological textures are typical of the *Mernmerna* Formation (Clarke, 1986c, 1990a; Gravestock and Cowley, 1995), with bioclasts, archaeocyath and shelly debris (representing the *Dailyatia odyssei* Zone; Fig. 22A–C, F–I), as well as micritic or fine, granular carbonate mud clearly observable in thin section (Fig. 22D, E). Skeletal allochems are often silicified, with trilobite fragments common throughout the section. Localised microbial laminations are also clear in thin section in the upper horizons (Fig. 22H, I). The depositional environment is interpreted as mid-outer shelf, in calm waters that were occasionally disturbed by higher-energy events that introduced bioclastic debris.

### 2.2.7. SCYW-791A Drillcore (*Andamooka* Limestone)

The *Andamooka* Limestone is a relatively thin (max. ~300 m), weakly deformed and poorly age-constrained carbonate unit cropping out on the Stuart Shelf at the northern end of Lake Torrens, and as far west as Olympic Dam (Fig. 1). Because of minor tilting and the presence of erosional surfaces throughout the succession, the supratidal to marine shelf carbonates of the *Andamooka* Limestone were deposited on the Yarloo Shale (equivalent of the Bunyeroo Formation) in the north and on progressively older members of the Tent Hill Formation towards the south (Johns, 1968; Gravestock and Cowley, 1995).

The most complete section through the *Andamooka* Limestone occurs in drillhole SCYW-791A, located at 137°9'23.742" S, 30°7'29.726" E, drilled by Amoco Minerals (from 1979–1981) to a total depth of 1450.20 m, in search of copper and uranium (Fig. 23). The

recovered core of lower Cambrian sediments transects 24.87 m of Yarrowurta Shale (equivalent of the Billy Creek Formation) at the top of the succession, followed by a total of 196.7 m of peritidal and subtidal carbonates of the Andamooka Limestone (Fig. 23; see also Cowley, 1990). Below the Andamooka Limestone, the core penetrates the early Ediacaran Yarloo Shale (386.57 m of fine-grained red beds) and the Tent Hill Formation.

The upper 10 m of the Andamooka Limestone is dominated by clotted microbialite fabrics (*Renalcis*), with secondary dolomitisation filling vuggy cavities (Fig. 24A–C), and evaporitic deposits with low domical stromatolites near the very top of the unit, representing a supratidal to sabkha-type depositional setting. Lower in the core, Betts et al. (2017b, fig. 2; Fig. 23) documented a typical *Dailyatia odyssei* Zone fauna from a 32-m fossiliferous interval representing high-energy, shallow-shelf carbonates within fair-weather wave base that includes rich skeletal packstones, peloidal and occasional oolitic grainstone, with evidence of transport and redeposition (Fig. 24D, E). Clotted microbialites, including dendritic forms, along with archaeocyathan-rich grainstones (Fig. 24F–I) are also present in this interval.

### 3. Methods

#### 3.1. Sampling

Stratigraphic sections were sampled simultaneously for biostratigraphic (see Betts et al., 2016, 2017b), chemostratigraphic and lithologic data (herein). Carbon and oxygen isotope data are derived from bulk rock samples of a range of carbonate facies, including stromatolitic microbialites, archaeocyathan-microbial bioherms, and lagoonal-shoal, platform, ramp and slope deposits in the Arrowie and Stansbury basins. Carbonate-dominated

units sampled include the Woodendinna Dolostone, Wilkawillina, Wirrapowie and Ajax limestones, and the Mernmerna Formation in the Arrowie Basin, and the Andamooka Limestone on the Stuart Shelf. Sampled units in the Stansbury Basin include the Wangkonda Formation, Sellick Hill Formation and Fork Tree Limestone.

### 3.2. *Stable isotope methods*

Lithological samples were evaluated following the recommendations of Kaufman and Knoll (1995). Homogeneous regions of fine-grained (micritic) carbonate were selected on freshly cut faces of lithological samples using a stereo microscope, and powders (8–30 mg) were drilled with a low speed Dremel Digital 400-series drill. Carbon and oxygen isotope samples from all sections were processed and analysed at CSIRO North Ryde in Sydney, except for those from SCYW-791A and WANG, which were processed and analysed at the University of Adelaide in South Australia (Hall, 2012; Mathewson, 2016).

Samples from WANG-S, SHL, WAR, MORO, BHG, AJX-M, Yalkalpo-2 and PIN were reacted in evacuated Exutainer tubes with 104% phosphoric acid for about 24 hours at 25°C (analysed at Environmental Isotopes Pty. Ltd., Sydney). A subsample of the produced CO<sub>2</sub> was extracted using a gas syringe and the C and O isotope values were analyzed by injection into a He stream and separated from other gases by a GC attached to a Finnigan 252 mass spectrometer via a Conflo III. The internal laboratory carbonate standards CSIRO ( $\delta^{13}\text{C} = -13.46$  VPDB;  $\delta^{18}\text{O} = -5.26$  VPDB) and PRM-2 ( $\delta^{13}\text{C} = 1.15$  VPDB;  $\delta^{18}\text{O} = -17.63$  VPDB) were used to correct the data. The laboratory standards have been calibrated against international standards NBS19 and LSVEC (Coplen, 1995; Coplen et al., 2006). Replicate analysis of the standard calcites is generally better than  $\pm 0.1$  for C and O. Carbon and

oxygen isotope values are reported in permil (‰) relative to VPDB. Oxygen isotope values (see Supplementary Information) are also reported in permil (‰) relative to VSMOW.

SCYW-791A samples analysed at the University of Adelaide were reacted with 104% phosphoric acid within a Fisons Isocarb carbonate preparation system coupled to a Fisons Optima dual inlet isotope ratio mass spectrometer (IRMS). The internal laboratory carbonate standard (ANU-P3;  $\delta^{13}\text{C}_{\text{VPDB}}=2.24\text{‰}$ ;  $\delta^{18}\text{O}_{\text{VPDB}}=-0.30\text{‰}$ ) used to correct the data was calibrated to VPDB using the international standard NBS19 ( $\delta^{13}\text{C}=+1.95\text{ VPDB}$ ,  $\delta^{18}\text{O}=-2.20\text{ VPDB}$  (Coplen, 1995; Coplen et al., 2006). Total analytical errors ( $1\sigma$ ) for  $\delta^{13}\text{C}$  and  $\delta^{18}\text{O}$  are estimated at  $\pm 0.05\text{‰}$  and  $\pm 0.1\text{‰}$  based on repeat analyses of standards.

WANG samples analysed at the University of Adelaide were reacted in Exutainer tubes with 104% phosphoric acid for about 1 hour at  $70^{\circ}\text{C}$ . Vials were purged with He by the auto-sampler for 150 seconds each at 20 ml/min prior to acid addition. A subsample of the produced  $\text{CO}_2$  was then analysed via the gas bench preparation system on a Nu Horizon IRMS operating in continuous flow. The internal laboratory carbonate standards used to correct the data were ANU-P3 calcium carbonate ( $\delta^{13}\text{C}=+2.24$ ,  $\delta^{18}\text{O}=-0.32$ ), UAC-1 calcium carbonate ( $\delta^{13}\text{C}=-15.0$ ,  $\delta^{18}\text{O}=-18.4$ ), and IAEA CO-8 calcite ( $\delta^{13}\text{C}=-5.76$ ,  $\delta^{18}\text{O}=-22.7$ ). ANU-P3 calibrated and provided by ANU, UAC-1 calibrated to international standards IAEA CO-1, 8, and 9, and ANU-P3. Replicate analysis of the standard calcites is generally better than  $\pm 0.1$  for C and O. Carbon and oxygen isotope values are reported in permil (‰) relative to the international standard VPDB. Oxygen isotope values (see Supplementary Information) are also reported in permil (‰) relative to the international standards VSMOW.

### 3.3. CA-TIMS U-Pb geochronology methods

U-Pb dates were obtained by the chemical abrasion isotope dilution thermal ionization mass spectrometry (CA-TIMS) method from analyses using single zircon grains. Zircons were liberated from rocks first by crushing and grinding, followed by separation according to density in water and a heavy liquid and finally by magnetic susceptibility. The grains were mounted in epoxy and polished until the centres were exposed. Cathodoluminescence (CL) images were obtained with a JEOL JSM-1300 scanning electron microscope and Gatan MiniCL (Supplementary Information).

Zircons were removed from the epoxy mounts and subjected to a modified version of the chemical abrasion method of Mattinson (2005), reflecting analysis of single grains or fragments of grains. Grains were selected for dating based on CL images; grains with apparent inherited cores were avoided.

Zircons were placed in a muffle furnace at 900°C for 60 hours in quartz beakers. Single grains were transferred to 3 ml Teflon PFA beakers and loaded into 300 µl Teflon PFA microcapsules. Fifteen microcapsules were placed in a large-capacity Parr vessel, and the crystals partially dissolved in 120 µl of 29 M HF for 12 hours at 180°C or 190°C. The contents of each microcapsule were returned to 3 ml Teflon PFA beakers, the HF removed and the residual grains immersed in 3.5 M HNO<sub>3</sub>, ultrasonically cleaned for an hour, and fluxed on a hotplate at 80°C for an hour. The HNO<sub>3</sub> was removed and the grains were rinsed twice in ultrapure H<sub>2</sub>O before being reloaded into the same 300 µl Teflon PFA microcapsules (rinsed and fluxed in 6 M HCl during sonication and washing of the grains) and spiked with the EARTHTIME mixed <sup>233</sup>U–<sup>235</sup>U–<sup>205</sup>Pb tracer solution (Condon et al., 2015). The grains were dissolved in Parr vessels in 120 µl of 29 M HF with a trace of 3.5 M HNO<sub>3</sub> at 220°C for 48 hours, dried to fluorides, and re-dissolved in 6 M HCl at 180°C overnight. U and Pb were separated from the zircon matrix using an HCl-based anion-exchange chromatographic procedure (Krogh, 1973), eluted together and dried with 2 µl of 0.05 N H<sub>3</sub>PO<sub>4</sub>.

Pb and U were loaded on a single outgassed Re filament in 5  $\mu\text{l}$  of a silica-gel/phosphoric acid mixture (Gerstenberger and Haase, 1997), and U and Pb isotopic measurements made on a GV Isoprobe-T multicollector thermal ionization mass spectrometer equipped with an ion-counting Daly detector. Pb isotopes were measured by peak-jumping all isotopes on the Daly detector for 100 to 160 cycles, and corrected for  $0.16 \pm 0.03\%$ /a.m.u. (1 sigma error) mass fractionation. Transitory isobaric interferences due to high-molecular weight organics, particularly on  $^{204}\text{Pb}$  and  $^{207}\text{Pb}$ , disappeared within approximately 30 cycles, while ionization efficiency averaged  $10^4$  cps/pg of each Pb isotope. Linearity (to  $\geq 1.4 \times 10^6$  cps) and the associated deadtime correction of the Daly detector were monitored by repeated analyses of NBS982, and have been constant since installation. Uranium was analyzed as  $\text{UO}_2^+$  ions in static Faraday mode on  $10^{11}$  ohm or  $10^{12}$  ohm resistors for 200-300 cycles, and corrected for isobaric interference of  $^{233}\text{U}^{18}\text{O}^{16}\text{O}$  on  $^{235}\text{U}^{16}\text{O}^{16}\text{O}$  with an  $^{18}\text{O}/^{16}\text{O}$  of 0.00206. Ionization efficiency averaged 20 mV/ng of each U isotope. U mass fractionation was corrected using the known  $^{233}\text{U}/^{235}\text{U}$  ratio of the EARTHTIME tracer solution.

CA-TIMS U-Pb dates and uncertainties were calculated using the algorithms of Schmitz and Schoene (2007), EARTHTIME tracer solution (Condon et al., 2015) with calibration of  $^{235}\text{U}/^{205}\text{Pb} = 100.233$ ,  $^{233}\text{U}/^{235}\text{U} = 0.99506$ , and  $^{205}\text{Pb}/^{204}\text{Pb} = 11268$ , and U decay constants recommended by Jaffey et al. (1971).  $^{206}\text{Pb}/^{238}\text{U}$  ratios and dates were corrected for initial  $^{230}\text{Th}$  disequilibrium using  $D_{\text{Th/U}} = 0.20 \pm 0.05$  ( $1\sigma$ ) and the algorithms of Crowley et al. (2007), resulting in an increase in the  $^{206}\text{Pb}/^{238}\text{U}$  dates of  $\sim 0.09$  Ma. All common Pb in analyses was attributed to laboratory blank and subtracted based on the measured laboratory Pb isotopic composition and associated uncertainty. U blanks are estimated at  $0.013 \pm 0.009$  pg ( $1\sigma$ ).

Weighted mean  $^{206}\text{Pb}/^{238}\text{U}$  dates were calculated from equivalent dates using Isoplot 3.0 (Ludwig, 2003). Errors on the weighted mean dates are given as  $\pm x / y / z$ , where x is the

internal error based on analytical uncertainties only, including counting statistics, subtraction of tracer solution, and blank and initial common Pb subtraction, y includes the tracer calibration uncertainty propagated in quadrature, and z includes the  $^{238}\text{U}$  decay constant uncertainty propagated in quadrature. Internal errors should be considered when comparing our dates with  $^{206}\text{Pb}/^{238}\text{U}$  dates from other laboratories that used the same EARTHTIME tracer solution or a tracer solution that was cross-calibrated using EARTHTIME gravimetric standards. Errors including the uncertainty in the tracer calibration should be considered when comparing our dates with those derived from other geochronological methods using the U-Pb decay scheme (e.g., laser ablation ICPMS). Errors including uncertainties in the tracer calibration and  $^{238}\text{U}$  decay constant (Jaffey et al., 1971) should be considered when comparing our dates with those derived from other decay schemes (e.g.,  $^{40}\text{Ar}/^{39}\text{Ar}$ ,  $^{187}\text{Re}$ - $^{187}\text{Os}$ ). Errors for weighted mean dates and dates from individual grains are given at  $2\sigma$ .

## 4. Results

### 4.1. CA-TIMS Radiometric Dates

#### 4.1.1. Billy Creek Formation, Flinders Ranges, Arrowie Basin

Sample R1300537 is from a tuff in the Billy Creek Formation (upper part of the Warragee Member), Angorichina, Flinders Ranges ( $31^{\circ}11'14.3''\text{S}$ ;  $138^{\circ}52'58.2''\text{E}$ ). Eight grains yielded equivalent dates with a weighted mean of  $511.87 \pm 0.14 / 0.28 / 0.60$  Ma (MSWD = 0.9, probability of fit = 0.48) that is interpreted as being the eruption age (Fig. 25).

#### 4.1.2. Mernmerna Formation, Flinders Ranges, Arrowie Basin



The BG Tuff is located 25 m above the base of the Mernmerna Formation in Bunyeroo Gorge, Flinders Ranges, located at 31°24'45.15" S; 138°31'35.14" E (AMG coordinates: 264847 6522030). Seven grains yielded equivalent dates with a weighted mean of  $515.38 \pm 0.13 / 0.28 / 0.60$  Ma (MSWD = 2.0, probability of fit = 0.06) that is interpreted as being the eruption age (Fig. 25). One other date that is older and discordant is interpreted as being from a grain with an inherited component (Fig. 25).

Sample R1300538 is from a 10 cm thick green tuff layer in the Third Plain Creek Member of the Mernmerna Formation, Bunkers Range (MMF/58.1, 31°11'44"S; 138°52'32"E). Eight grains yielded equivalent dates with a weighted mean of  $514.56 \pm 0.13 / 0.28 / 0.60$  Ma (MSWD = 1.2, probability of fit = 0.29) that is interpreted as being the eruption age (Fig. 25). One other date that is slightly older at  $516.42 \pm 0.32$  Ma is interpreted as being from a grain that is detrital or inherited.

Sample 1830309 is a tuff from a volcanoclastic layer in the Mernmerna Formation in the Paralana 1B DW1 drill core (30°12'35.00"S/139°42'48.00"E). Six grains yielded equivalent dates with a weighted mean of  $514.46 \pm 0.13 / 0.28 / 0.60$  (MSWD = 1.6, probability of fit = 0.17) that is interpreted as being the eruption age (Fig. 25). One older date at  $514.84 \pm 0.32$  Ma is interpreted as being from a grain that is detrital or inherited. One younger date at  $513.62 \pm 0.31$  Ma is interpreted as being from a grain that underwent slight Pb loss that was not removed by chemical abrasion.

#### 4.1.3. Heatherdale Shale, Fleurieu Peninsula, Stansbury Basin

Zircons from a thin tuff in the upper Heatherdale Shale on Fleurieu Peninsula analyzed (35°20'17.18"S, 138°27'54.55"E). The four youngest dates are equivalent with a

weighted mean of  $514.98 \pm 0.22 / 0.33 / 0.63$  Ma (MSWD = 0.7, probability of fit = 0.57) that is interpreted as being the maximum depositional age (Fig. 25). Five other dates ( $515.78 \pm 0.38$  to  $516.24 \pm 0.34$  Ma) are interpreted as being from older detrital grains.

#### 4.2. *Stable carbon and oxygen isotopes*

Corresponding  $\delta^{13}\text{C}$  and  $\delta^{18}\text{O}$  profiles of the 10 sections are plotted against lithological and biostratigraphic information respectively in Figures 3 [WANG/WANG-S], 4 [SHL/FTL], 11 [WAR], 13 [MORO], 15 [BHG], 17 [AJX-M], 19 [YALKALPO-2], 21 [PIN], and 23 [SCYW-791A] (raw data in Supplementary Information). Wendler (2013) commented that diagenetic processes will have affected the isotopic signals of most sediments, but that generally this should not affect their application to chemostratigraphic work, as long as the overall trends are preserved. Select intervals that exhibit unusual  $\delta^{18}\text{O}$  values (e.g. more than  $\sim 3\%$  away from the moving average of adjacent 5 samples, or strongly covarying  $\delta^{13}\text{C}$  and  $\delta^{18}\text{O}$ ) were omitted from the isotope curves. This includes five sample horizons from the WANG isotope curves (Fig. 3). WANG/146.5 was not included in the curve as it was taken from a trace fossil sample off the main section line, and was heavily weathered and broken up by quarrying activities. The sharp negative  $\delta^{13}\text{C}$  values and sharp positive  $\delta^{18}\text{O}$  values of WANG/296.0 were excluded from the curve as they were taken from within a fault zone where there was significant dip change resulting from deformation. WANG/321.0 was also excluded from the curve as it (and Facies D of the Sellick Hill Formation in general) has been subjected to significant erosion and possible reworking (see also Gravestock et al., 2001), as well as frequent sub-aerial exposure (or sediment-starved omission surfaces) imparting strong diagenetic change in these samples. The omitted samples

in the WANG section group together in the cross-plot, separately from the rest of the data (Fig. 26).

In the WAR section, six samples from the lowermost horizons in the Woodendinna Dolostone were omitted (WAR/0.0 to WAR/56.6) (Figs. 11, 26). At these horizons, where dolomitisation is pervasive, the  $\delta^{18}\text{O}$  and  $\delta^{13}\text{C}$  values exhibit strong covariation. The simultaneous sharp positive  $\delta^{18}\text{O}$  spikes and negative  $\delta^{13}\text{C}$  spikes are likely produced by diagenetic alteration (Melim et al., 2001). An additional eight horizons in the Wirrapowie Limestone were also omitted due to strongly covarying values (Figs. 11, 26, Supplementary Information). The Wirrapowie Limestone is interpreted as a lagoonal facies with abundant sediment-starved hardground and incipient hardground development, which is likely to have affected isotope values.

In the MORO section, six horizons have been omitted from the curve (Figs. 13, 26). MORO/225.7 and MORO/241.3 are in the Woodendinna Dolostone and are likely to have undergone alteration associated with dolomitisation. Isotope values throughout the Hideaway Well Member of the Wilkawillina Limestone are highly variable, which may be associated with various diagenetic alteration processes affecting the biohermal facies (Fig. 13). MORO/589.3 exhibits a strong negative  $\delta^{13}\text{C}$  spike when compared to the horizons immediately adjacent, MORO/620.5 has strongly covarying  $\delta^{18}\text{O}$  and  $\delta^{13}\text{C}$ , MORO/699.5 also displays very negative  $\delta^{18}\text{O}$  values, and the strongly negative  $\delta^{18}\text{O}$  values at MORO/855.3 are suggestive of localized alteration.

Three horizons in the BHG section (BHG/0.0, BHG/1755.7 and BHG/2170) have been omitted (Figs. 15, 26). While the negative  $\delta^{13}\text{C}$  values at BHG/0.0 are consistent with  $\delta^{13}\text{C}$  values in the *Kulparina rostrata* Zone in other sections (WANG, WANG-S, WAR, MORO), the  $\delta^{13}\text{C}$  and  $\delta^{18}\text{O}$  signals covary, and plot separately from the other data (Fig. 26), suggesting diagenetic alteration at this horizon. BHG/1755.7 and BHG/2170 are at the lower and upper

boundaries of the Nepabunna Siltstone, and the aberrant isotope values are therefore likely to be related to facies changes.

In the AJX-M section, the five lowermost horizons were omitted from the curve (AJX-M/64 – AJX-M/159) (Figs. 17, 26). These samples are taken from the stromatolitic boundstone facies in the Ajax Limestone that was likely to have been very shallow, and also exhibits dolomitisation in thin section (Fig. 18A, B). AJX-M/345 exhibits a sharp spike in  $\delta^{13}\text{C}$  that is dissimilar to the values from horizons immediately adjacent. This horizon is also close to an extensively dolomitised and altered level at AJX-M/347.4 and may have been affected by similar diagenetic processes (Fig. 18F). Isotope values at AJX-M/357 and AJX-M/371 may also have been influenced by diagenetic alteration. AJX-M/427.7 is from the unconformity level, and isotope values are likely to have been affected by periods of non-deposition or erosion. In the cross-plot, AJX-M/357, AJX-M/371 and AJX-M/427.7 plot separately to the rest of the data (Fig. 26).

## 5. Discussion

### 5.1. *Isotopic excursions and global correlation*

Measured stratigraphic sections and drill cores from the Arrowie and Stansbury basins intersect packages of rocks that range in age from the Terreneuvian, Stage 2 to unnamed Series 2, Stage 4. They record important carbon isotope excursions, including (from oldest to youngest) the ZHUCE, SHICE, CARE and perhaps also the MICE. Combining the  $\delta^{13}\text{C}$  chemostratigraphic data with the shelly fossil biostratigraphic scheme developed by Betts et al. (2016, 2017b) facilitates more confident identification of these peaks, and enhances correlation of the lower Cambrian successions in South Australia with other parts of the

world. Radiometric dates from tuff horizons in the Arrowie and Stansbury basins also enable the scheme to be independently time-calibrated, facilitating more accurate age assessments.

#### 5.1.1. *The Zhujiqing Carbon-Isotope Excursion (ZHUCE)*

The ZHUCE event (also referred to as I' in Siberian sections, 6p in Maloof et al., 2010a, L4 in Landing et al., 2013; Li et al., 2009) is named for the positive  $\delta^{13}\text{C}$  excursion identified on the Yangtze Platform in South China (Zhu et al., 2006), and follows a major radiation of the first biomineralised organisms within the Cambrian. Positive  $\delta^{13}\text{C}$  values associated with the ZHUCE occur just after the transition between the undefined Fortunian–Stage 2 boundary (Fan et al., 2011).

The chemostratigraphic curves for the WANG and WANG-S sections are presented in Fig. 3. Sample WANG/1.0 has an initial positive  $\delta^{13}\text{C}$  value of +2.3‰. After dropping to –1.2‰ at WANG/90.0, a major positive anomaly occurs at horizon WANG/120.0, where the  $\delta^{13}\text{C}$  curve reaches values of +5.7‰. The WANG-S section overlaps with the lower ~100 m of the WANG section through the Wangkonda Formation.  $\delta^{13}\text{C}$  data through this interval are similar in both sections, although in WANG-S they are generally shifted toward more positive values. The positive carbon isotope peak in Facies A of the Sellick Hill Formation also lies within the purported range of *Watsonella crosbyi* (see Jacquet et al., 2017b), and is of a similar  $\delta^{13}\text{C}$  value to ZHUCE maxima recorded elsewhere (discussed below).

The ZHUCE is characterised by the highest positive  $\delta^{13}\text{C}$  values throughout the entire Cambrian Period, and has been recorded at multiple localities across the globe, including China (up to +7‰, Zhou et al., 1997; Li et al., 2009), India (up to +6‰, Aharon et al., 1987; Knoll et al., 1995), Mongolia (“6p”, up to +7‰, Smith et al., 2016; although this

identification of the ZHUCE event has been questioned, see below), Morocco (“6p”, +6–7‰, Maloof et al., 2005), and Siberia (“I”+6‰, Kouchinsky et al., 2001). Discovery of the ZHUCE  $\delta^{13}\text{C}$  positive event in the lower Normanville Group represents the first report of this carbon isotopic excursion from Australia.

Landing and Kouchinsky (2016) have suggested that the lower boundary of Cambrian Stage 2 should be placed at a stratigraphic level marked by the first appearance of the micro-molluscs *Watsonella crosbyi* and *Aldanella attleborensis*, which occur below the ZHUCE  $\delta^{13}\text{C}$  positive event. The first appearances of *W. crosbyi* and the genus *Aldanella* (represented by *Aldanella* sp. cf. *A. golubevi*) in Australia occur within the upper member of the Mount Terrible Formation, which underlies the Wangkonda Formation (Jacquet et al., 2017b). This fossiliferous level occurs ~140 m below the ZHUCE  $\delta^{13}\text{C}$  positive peak within Facies A of the Sellick Hill Formation, which means that the FAD of *W. crosbyi* and *Aldanella* sp. cf. *A. golubevi* in the Mount Terrible Formation may represent the lower boundary of Cambrian Stage 2 (*sensu* Landing and Kouchinsky, 2016) in South Australia (Jacquet et al., 2017b).

As pointed out by Jacquet et al. (2017b), the only terrane where the range of *Watsonella crosbyi* does not conform to the global norm is Avalonia, where it has a 650-m composite range from the Chapel Island Formation to the Fosters Point Formation (Landing and Benus, 1988; Landing et al., 2013; Landing and Kouchinsky, 2016). Also, in Avalonia, the  $\delta^{13}\text{C}$  values associated with the *W. crosbyi* Zone are generally negative, climbing toward positive values (~+1‰) (Landing et al., 2013, fig. 5), but never reaching the distinctive positive values commonly associated with this event elsewhere.

The  $\delta^{13}\text{C}$  values reported by Ishikawa et al. (2008, 2014) through the Yanjiahe Formation in the Three Gorges area of South China are not as positive as typical ZHUCE values elsewhere (+4.24‰). However, shelly fossils from the lower Yanjiahe Formation

represent a typical Nemakit-Daldynian fauna, including *Protohertzina anabarica* and *Anabarites trisulcatus* (Guo et al., 2008). Diversity of shelly fauna increases toward the middle of the Yanjiahe Formation, and taxa such as *Aldanella* and *Maidipingoconus* occur 3 m below the disconformable upper boundary with the overlying Shuijingtuo Formation (equivalent to the Niutitang Formation in Guizhou Province, Chen and Jin, 1996) (Chen, 1984; Guo et al., 2008). A trend towards positive  $\delta^{13}\text{C}$  values, in combination with taxa such as *Aldanella*, are suggestive of the ZHUCE, and therefore a Terreneuvian, Stage 2 age for this part of the succession in the Three Gorges area. Ishikawa et al. (2008) correlate this excursion (P2) with the positive  $\delta^{13}\text{C}$  values through the Zhujiqing Formation in the Meishucun section (Brasier et al., 1990). Fauna associated with this excursion include taxa of the *Anabarites-Protohertzina* Zone (“Zone I”) and *Paragloborilus-Siphogonuchites* Zone (“Zone II”) (Brasier et al., 1990, fig. 4).

In the Xiaotan section in Yongshan County, Yunnan, positive  $\delta^{13}\text{C}$  values (+7.3‰) through the Dahai Member are likely to be the ZHUCE (Zhang et al., 1997; Zhou et al., 1997). Shelly fossils from the Dahai Member have been assigned to the *Watsonella crosbyi* Assemblage Zone (Steiner et al., 2007; Li et al., 2011). In addition to *W. crosbyi*, common shelly fossils found throughout this interval include molluscs such as *Bemella*, hyolithelminths and cancelloriids, which are also found in association with the ZHUCE in the WANG and WANG-S sections (Fig. 3).

Data from Siberia demonstrate that the ZHUCE is commonly composed of a number of positive  $\delta^{13}\text{C}$  peaks of a similar magnitude, referred to as I’ (Kouchinsky et al., 2001). The ZHUCE occurs in sub-Tommotian strata, such as the lower Pestrotsvet Formation on the southeastern Siberian Platform (Selinde section) (Kouchinsky et al., 2005, fig. 2). Similar  $\delta^{13}\text{C}$  values also occur in the Emyaksin Formation (*Anabarella plana*–*Allatheca anabarica* zones) (Kouchinsky et al., 2001, fig. 3). The ZHUCE has also been recorded in the

Medvezhya Formation in the Kotuikan River section, Anabar Uplift, northern Siberia (Knoll et al., 1995; Kaufman et al., 1996; Kouchinsky et al., 2017). Shelly fossils from the Medvezhya Formation include *Anabarites* spp., *Purella cristata*, *Aldanella* spp., halkieriids and orthothecid hyoliths (see Kouchinsky et al., 2017, figs. 4, 5).

The  $\delta^{13}\text{C}$  values attributed to the ZHUCE also occur in upper Krol carbonates in the Lesser Himalayas (I', up to +6‰, Aharon et al., 1987; Knoll et al., 1995). However, the stratigraphic level of the peak interpreted to be I' (ZHUCE) by Knoll et al. (1995) occurs below strata that contain Ediacaran fossils, in what is logged as 'terminal Proterozoic strata' (Aharon et al., 1987; Jiang et al., 2002). Fortunian-type shelly fauna such as *Anabarites*, *Circotheca*, *Olivoooides*, *Spirellus*, *Tiksitheca* and *Turcutheca* occur in the overlying Deo Ka Tibba Formation (Jiang et al., 2002), suggesting that the true ZHUCE event may occur in younger strata in this region.

Maloof et al. (2005, 2010a,b) produced a  $\delta^{13}\text{C}_{\text{CaCO}_3}$  age model through extensive integrated chemostratigraphic work and radiometric dating in units spanning the latest Ediacaran to lower Botoman (=Agdzian) in the western Anti-Atlas of Morocco. The  $\delta^{13}\text{C}$  curve through the stratigraphic section at Oued Sdas captures the ZHUCE ("6p", +6–7‰) in the Tifnout Member of the Adoudounian Formation (Taroudant Group). An ash layer dated at  $525.343 \pm 0.088$  Ma occurs at a stratigraphic level slightly above the peak of the event (Maloof et al., 2005, fig. 2), calibrating this event within Stage 2 of the Terreneuvian.

Recent work has documented the sequence stratigraphy and stable isotope stratigraphy of the Zavkhan Terrane in western Mongolia (Bold et al., 2016; Smith et al., 2016). Despite extensive mapping and measurement of numerous stratigraphic sections across the terrane, global correlation of the Precambrian–lower Cambrian units in the region remains contentious. Central to this problem is the identification by Smith et al. (2016) of the ZHUCE excursion ("6p" in Smith et al., 2016) through the Salaany Gol Formation, which



contrasts markedly with previous biostratigraphic age assessments that correlate it with the Atdabanian–Botoman in Siberia (Kruse et al., 1996; Landing and Kruse, 2017). Smith et al. (2016, 2017) argue, based on highly enriched  $\delta^{13}\text{C}$  values (up to +7‰), that this excursion through the Salaany Gol Formation could only be the ZHUCE, as peaks of similar magnitude are seen nowhere else in the global Cambrian  $\delta^{13}\text{C}$  curve. However, these highly positive  $\delta^{13}\text{C}$  values are restricted to an interval in their Orolgo Gorge section (Smith et al., 2016, fig. 9). In other sections measured by Smith et al. (2016) through the Salaany Gol Formation,  $\delta^{13}\text{C}$  values are lower (maximum +5.8‰ in the SE Taishir section, +5.9‰ in the Kunkher Gorge section and +4.3‰ in the Salaany Gorge section). Landing and Kruse (2017) suggest that this is, in fact, an anomalously enriched expression of the CARE event, placing the Salaany Gol Formation within the upper Tommotian–Atdabanian, despite previous claims by Kruse et al. (1996) that, according to archaeocyathan biostratigraphy, the Salaany Gol Formation is late Atdabanian–early Botoman in age. However, a complication with the interpretation of this excursion as the CARE is that  $\delta^{13}\text{C}$  values following the 6p excursion of Smith et al. (2016) in the upper Salaany Gol Formation are negative: –2.2‰ in the SE Taishir section; –1.6‰ in composite section E1328, E1329 and E1331; and –4.0‰ in section E1340 in the SE Khukh–Davaa area (Smith et al., 2016). These values are inconsistent with global post-CARE  $\delta^{13}\text{C}$  values that are generally closer to 0‰ (Maloof et al., 2010a,b). Previous  $\delta^{13}\text{C}$  chemostratigraphic work through the Bayan Gol and Salaany Gol formations by Brasier et al. (1996, fig. 11) show results that are more consistent with the global curve.

Shelly fossils have been reported from numerous horizons throughout the Bayan Gol and Salaany Gol formations. Khomentovsky and Gibsher (1996) recorded *Anabarites tripartitus*, *Protohertzina unguiformis*, and other shelly fauna indicative of the *Purella antiqua* Zone in the lower Bayan Gol Formation. Tommotian-type faunas, including *Lapworthella tortuosa* and *Heraultipegma varensalensis* (= *Watsonella crosbyi*, Landing and

Kouchinsky 2016), are found higher in the Bayan Gol Formation (Dorjnamjaa et al., 1993; Khomentovsky and Gibsher, 1996; Voronin et al., 1982). Other fauna that suggest a Terreneuvian, Stage 2 age for the Bayan Gol Formation include the micromolluscs *Nomgoliella*, *Barskovia*, *Latouchella* and *Salanyella* in BG3-4 in the Taishir area (MJB, personal observation). Presentation of high-resolution, coeval chemostratigraphic and biostratigraphic data through the lower Cambrian sequences in the Zavkhan Terrane is forthcoming. Until these data are fully integrated, all age assessments and correlations of the units will remain speculative.

#### 5.1.2. *Shiyantou Carbon Isotope Excursion (SHICE)*

The SHICE is named for the negative  $\delta^{13}\text{C}$  excursion in the Shiyantou Member of the Chiungchussu Formation in eastern Yunnan, South China (Zhang et al., 1997; Zhu et al., 2006). It succeeds the ZHUCE, and is associated with the extinction of many shelly taxa around the middle of Stage 2 (Zhu et al., 2006). It has been identified in China ( $-6\%$ , Zhang et al., 1997; Zhou et al., 1997), Morocco ( $\sim-5\%$ , Maloof et al., 2010a,b) and Siberia (“6n”,  $\sim-1.9\%$ , Kouchinsky et al., 2007). Previous chemostratigraphic work in South Australia (Tucker, 1989, fig. 7) has also captured  $\delta^{13}\text{C}$  values suggestive of the SHICE. The  $\delta^{13}\text{C}$  data from the Woodendinna Dolostone in the Flinders Ranges exhibit values of up to  $\sim-6\%$ , curving back to positive values in the overlying lower Wilkawillina Limestone (Tucker, 1989). This is similar to results obtained through the Woodendinna Dolostone and lower Wilkawillina Limestone in the WAR section (Fig. 11).

The SHICE  $\delta^{13}\text{C}$  negative excursion within the Normanville Group lies within Facies C of the Sellick Hill Formation ( $-4.9\%$  at WANG/283, Fig. 3). In both the Arrowie and Stansbury basins, it is clear that the peak of the SHICE occurs below the lower boundary of

the *Kulparina rostrata* Zone. In the WANG section, the peak is approximately 126 m below the lower boundary of the *K. rostrata* Zone (Fig. 3). In the WANG and SHL sections, the peak of the SHICE also occurs below the range of *Sunnaginia imbricata*, which first occurs below the lower boundary of the *K. rostrata* Zone in the SHL/FTL sections (Figs. 3, 4).

SHICE  $\delta^{13}\text{C}$  negative values also occur in the SHL and WAR sections. However, the results from neither of these sections fully captures the event, as they omit the lower parts (Figs. 4, 11). In the WAR section,  $\delta^{13}\text{C}$  values have an overall trend from negative ( $-6.2\text{‰}$  at WAR/87.3) to positive ( $1.0\text{‰}$  at WAR/779, Fig. 11), consistent with the upper part of the SHICE. The first occurrence of the paterinid brachiopod *Askepasma saproconcha* and the tommotiid *Dailyatia macroptera* is in WAR/396. Upper parts of the WAR section (WAR/396 to WAR/799) also contain *Dailyatia ajax* and *Kulparina rostrata*, thus indicating a *K. rostrata* Zone age (Betts et al., 2016). In other sections where the *K. rostrata* Zone has been identified,  $\delta^{13}\text{C}$  isotopes show similar negative values, or a general trend toward negative values, for example, in the BHG (Fig. 6) and MORO sections (Fig. 11).

In the SHL section in the Stansbury Basin, the lowest  $\delta^{13}\text{C}$  values are  $-4.4\text{‰}$  in SHL/0.0, closer to typical SHICE values seen worldwide (Figs. 4, 26). Here, the peak of the excursion is not captured, and the section only preserves relatively stable  $\delta^{13}\text{C}$  values (around  $-2.0\text{‰}$ ) that are likely to represent the middle–upper parts of the event. These results are consistent with an observation by Brasier et al. (1994), who noted a profound increase in faunal diversity, including paterinid brachiopods, tommotiids, molluscs and archaeocyaths, associated with the negative  $\delta^{13}\text{C}$  anomaly preceding the positive II and III events.

Occurrences of *Sunnaginia imbricata* in South Australia, Siberia, and Avalonia (Newfoundland and eastern USA), potentially make it an important taxon for correlation. *Sunnaginia* cf. *imbricata* from the Comley Limestones Formation in the UK (*S. angulata* in

Brasier, 1986, 1989) is superficially similar to *S. imbricata*. However, sclerites of *S. cf. imbricata* have different internal structures and may be a separate taxon (Murdock et al., 2012). Composite  $\delta^{13}\text{C}$  chemostratigraphy of lower Cambrian strata in western Avalonia shows a negative isotope excursion (up to  $-2\%$ ) through most of the Cuslett Formation, which becomes a positive trend in the Fosters Point Formation (Brasier et al., 1992, fig. 14). In the WANG section, the first occurrence of *S. imbricata* is 201 m above the ZHUCE peak in the lower Sellick Hill Formation, and its range is associated with negative  $\delta^{13}\text{C}$  values ( $\sim -2\%$ ) (Fig. 3). However, the Avalonian composite  $\delta^{13}\text{C}$  curve (Brasier et al., 1992, fig. 14; Landing et al., 2013, fig. 5) shows positive values (up to  $\sim +4\%$ ) through the *S. imbricata* Zone in the lower Bonavista Group, making correlation difficult.

Brasier et al. (1992) correlated the Avalonian and Siberian curves and suggested that the Tommotian–Atdabanian boundary is located within the Fosters Point Formation of the uppermost Bonavista Group (although no trilobites have been recovered from this unit). The magnitude of the negative  $\delta^{13}\text{C}$  event through the Cuslett Formation is comparable to the global SHICE, and the occurrence of *Sunnaginia imbricata* through the Cuslett Formation seems to support an older age interpretation of this unit. However, in western Avalonia, *S. imbricata* commonly co-occurs with apparently long-ranging taxa such as *Eccentrotheca kanesia*, making accurate age assessment difficult. Additionally, reports of *Rhombocorniculum cancellatum* in the Fosters Point Formation (and Weymouth Formation) further complicates correlations, as it suggests a younger (Series 2, Stage 3–4) age for these strata.

In the eastern Stansbury Basin, *Sunnaginia imbricata* is restricted to a narrow interval in the upper Sellick Hill Formation, overlapping with the lower *Kulparina rostrata* Zone (Fig. 20), which equates to a pre-trilobitic Terreneuvian (Stage 2) age (Jacquet et al., 2017b). However, in Newfoundland, *S. imbricata* co-occurs with *Lapworthella ludvigseni* and

*Eccentrotheca kanesia* throughout the Bonavista Group in the Petley Formation, West Centre Cove Formation (Landing, 1992), Cuslett Formation (also with *Watsonella crosbyi*) (Landing, 1989) and the Fosters Point Formation (Landing, 1995). In the Fosters Point Formation, *S. imbricata* co-occurs with *Camenella baltica* (Landing, 1995, fig. 6.15, 6.17). *Sunnaginia imbricata* also co-occurs with *C. baltica* and *E. kanesia*, other shelly fossils, and the trilobite *Callavia broeggeri* in the basal Brigus Formation (Bengtson and Fletcher, 1983). Additionally, the Weymouth Formation in eastern Massachusetts, which has been correlated with the Bonavista Group and overlying Brigus Formation, also contains *S. imbricata*, *E. kanesia* and *Rhombocorniculum cancellatum*, linguloid brachiopods and the trilobite *Strenuella strenua* (Landing, 1988, fig. 1, HNR/68.9, ER/9.6). Co-occurrence of *R. cancellatum* (~*Eoredlichia-Wutingaspis* Zone in South China) and *Callavia broeggeri* (*Callavia* Zone) imply a much younger age than that of *S. imbricata* in South Australia, and disparate stratigraphic occurrences suggest a much longer range for *S. imbricata* in Avalonia than in any other terrane.

It would seem that shelly taxa that have restricted stratigraphic ranges in most terranes commonly have much longer ranges in Avalonia (Landing, 1988). Landing (1992) ascribes these long ranges to the re-appearance of Lazarus taxa that repopulate the inner shelf after an absence caused by environmental changes. However, material from Avalonia is often poorly preserved and taxonomically ambiguous (for e.g., see crack-out specimens of *Watsonella crosbyi* from Avalonia illustrated by Landing, 1988, figs. 5.16, 5.17, 5.20), and thus needs careful re-assessment, especially of micro-ornament and micro-structure.

In the Xiaotan section, Yunnan, South China, post-ZHUCE  $\delta^{13}\text{C}$  values through the Shiyantou Member of the Chiungchussu Formation become negative (~-6‰) (Zhang et al., 1997, fig. 2; Zhu et al., 2006). In the overlying Yu'anshan Member,  $\delta^{13}\text{C}$  values are even more depleted (up to ~-10 to -9.5‰, Zhang et al., 1997, fig. 2), which may be suggestive of

diagenetic overprinting (see Ishikawa et al., 2008, fig. 5), as post-SHICE  $\delta^{13}\text{C}$  values generally do not reach significant nadirs until much later in the Cambrian (e.g. ROECE and SNICE). The Meishucun section at Jinning, Yunnan, intersects a similar period of time, although  $\delta^{13}\text{C}$  values demonstrate that this package is affected by numerous time breaks (Zhang et al., 1997). Zhang et al. (1997) suggest that the Shiyantou Member is associated with shelly fossil Zone III, the *Sinosachites-Lapworthella* assemblage. However, recognition of biozones in the East Yunnan sections has been complicated by key taxa that often range between zones (Steiner et al., 2007). Additionally, the lower parts of the Shiyantou Member are mostly siliciclastic, and shelly fossils are generally rare (Steiner et al., 2007). Updated stratigraphic correlation includes a “poorly fossiliferous interzone” (or barren interval) through the lower part of the Shiyantou Member (and equivalent units) where the SHICE peaks, with taxa of the *Sinosachites flabelliformis*–*Tannuolina zhangwentangi* Assemblage Zone occurring in the upper parts (Steiner et al., 2007, figs. 9 and 10). Betts et al. (2016, 2017b) broadly correlated the *S. flabelliformis*–*T. zhangwentangi* Assemblage Zone with the *Micrina etheridgei* Zone in South Australia, which succeeds the *Kulparina rostrata* Zone above the peak of the SHICE (Fig. 27).

Ishikawa et al. (2014, fig. 7) correlated the positive  $\delta^{13}\text{C}$  excursion at the top of the Meishucunian-aged Yanjiahe Formation (“P2” excursion of Ishikawa et al., 2008) with the ZHUCE. In the Three Gorges area in South China, there is a disconformity between the Yanjiahe Formation and the overlying Shuijingtuo Formation.  $\delta^{13}\text{C}$  isotope values at this boundary exhibit a negative trend (Ishikawa et al., 2008, fig. 7), which may correspond with SHICE (Zhu et al., 2006). However, due to the disconformity between the Yanjiahe and Shuijingtuo formations, this excursion is not fully developed in the Three Gorges area. *Tsunyiidiscus* is among the oldest trilobites recovered from the Shuijingtuo Formation in the Three Gorges section (Ishikawa et al., 2014), and in the Xiaoyangba and Zengjiapo sections

(Yang et al., 2015), indicating an absence of the older *Parabadiella huoi* Zone. Hence, strata of Terreneuvian, Stage 2 to Series 2, Stage 3 age (equivalent to the *Kulparina rostrata* and *Micrina etheridgei* zones; Betts et al., 2016, 2017b) are missing at Three Gorges, due to the hiatus at the top of the Yanjiahe Formation, and positive excursions II and III, in addition to the CARE (IV) event, are unlikely to have been preserved. Ishikawa et al. (2014) interpreted the positive  $\delta^{13}\text{C}$  excursion in the upper Shuijingtuo Formation as the MICE, and the subsequent negative excursion in the Shipai Formation as the AECE. As such, the Shuijingtuo Formation in the Three Gorges area is most reasonably correlated with the *Dailyatia odyssei* Zone in South Australia.

Similarly, in the Yanjiahe area (“Anjiahe” in Ishikawa et al., 2008) of Hubei Province, there is a negative  $\delta^{13}\text{C}$  spike down to  $-9.3\text{‰}$  post-ZHUCE, 1.4 m below the Yanjiahe–Shuijingtuo boundary (Ishikawa et al., 2008). These anomalously low values occur in a thin limestone bed that shows no evidence for diagenesis or alteration, and are interpreted as the original  $\delta^{13}\text{C}$  signature (Ishikawa et al., 2008), possibly representing the SHICE. The  $\delta^{13}\text{C}$  values in the overlying Shuijingtuo Formation decrease gradually from  $-5\text{‰}$  to  $0\text{‰}$ , and then increase gradually to  $+3.0\text{‰}$  in the upper Shuijingtuo Formation and lower Shipai Formation. Yang et al. (2015) note that the *Cambroclavus fangxianensis*–*Rhombocorniculum cancellatum* Zone ranges from the base of the Xihaoping Member of the Shuijingtuo Formation in the southeastern Shaanxi and northwestern Hubei provinces, and they record *Tsuniyidiscus niutitangensis* in the lower Shuijingtuo Formation. The *C. fangxianensis*–*R. cancellatum* Zone is correlated with the *Eoredlichia*-*Wutingaspis* Zone (including the *Tsuniyidiscus* and *Yunnanocephalus* subzones) in South China, and the majority of the *Dailyatia odyssei* Zone in South Australia, based on similar trilobites and other shelly fossils (see Paterson and Brock, 2007). Faunal correlation supports the conclusions of Ishikawa et al. (2014), who identified the positive  $\delta^{13}\text{C}$  MICE in the Three Gorges section (Nangaoan) after

the hiatus. This suggests that the  $\delta^{13}\text{C}$  curve through the Shuijingtuo Formation in the Hubei Province is most likely to be post-CARE, hence most of the SHICE and excursions II and III are also missing in this region. This is reinforced by shelly fossil correlations by Betts et al. (2017b), who suggested that the Shuijingtuo Formation (including the Xihaoping Member) correlates with the *D. odyssei* Zone in South Australia, based on the occurrence of *Beshtashella tortilis*, *Cambroclavus absonus*, *Eohadrotreta* sp. cf. *E. zhenbaensis*, *Haoia* sp. cf. *H. shaanxiensis* and *Kelanella* sp. in both regions.

In Siberia, the SHICE is commonly referred to as “6n”, and occurs in the uppermost Sukharikha Formation and the Pestrotsvet Formation (Selinde and Lena-Aldan sections) (Brasier et al., 1993, 1994; Kouchinsky et al., 2005, 2007; Magaritz et al., 1986). However, isotopic anomalies through this interval can be difficult to resolve, due to the unconformity at the base of the Tommotian, particularly in the eastern and northeastern Siberian Platform (Knoll et al., 1995; Kaufman et al., 1996). For example, in the Lena-Aldan area, biostratigraphic and chemostratigraphic data demonstrate that the appearance of shelly fauna is affected by a hiatus between the Ust'-Yudoma and Pestrotsvet formations, which also manifests as an abbreviated isotopic record. In the Selinde section, the base of the Pestrotsvet Formation (Manykajan Stage) exhibits additional  $\delta^{13}\text{C}$  excursions not recognized in the Lena-Aldan area, due to the hiatus (Kouchinsky et al., 2005, see also Kouchinsky et al., 2007, fig. 3).

In the Sukharikha section, the SHICE (6n) occurs in the uppermost Sukharikha Formation (Kouchinsky et al., 2007). Archaeocyaths suggest a *Nochoroicyathus sunnaginicus* Zone age, and shelly fossils present in the upper Sukharikha Formation include *Tannuolina* sp., halkieriid sclerites, *Torelella*, and the micromolluscs *Aldanella* and *Bemella* (Rowland et al., 1998; see also Kouchinsky et al., 2010). Similar shelly fauna occur through the Sellick Hill Formation on the Fleurieu Peninsula, South Australia (WANG/WANG-S and SHL/FTL



sections) where the SHICE is also developed (Figs. 3, 4). The Sukharikha section also exhibits a positive peak (“7p”) at the boundary between the Sukharikha and Krasnoporog formations that is not developed elsewhere. Kouchinsky et al. (2007) suggest that this is also likely related to the pre-Tommotian hiatus.

Maloof et al. (2005, 2010a,b) developed a U/PB- $\delta^{13}\text{C}_{\text{CaCO}_3}$  age model by coalescing global  $\delta^{13}\text{C}$  data and ID-TIMS zircon dates to form a temporally-constrained global composite curve. Maloof et al. (2010b, fig. 1) dated the boundary between the Nemakit-Daldynian and the Tommotian to  $524.837 \pm 0.092$  Ma ( $^{206}\text{U}$ - $^{238}\text{Pb}$  ID-TIMS), located between the positive ZHUCE and negative SHICE events. In the Moroccan Anti-Atlas, the SHICE is apparent in the Oued Sdas (Maloof et al., 2005) and Sidi Msal (Maloof et al., 2010b) sections. It begins to develop in the upper Adoudounian Formation (Tifnout Member), peaking in the Lie de Vin Formation, with values of  $\sim -4$  to  $-3\%$  (Maloof et al., 2010b). The oldest Cambrian shelly fossils in Morocco are from the overlying Igoudine Formation (*Eofallotaspis* Zone) (Geyer and Landing, 1995; Maloof et al., 2005). The Lie de Vin Formation consists of interbedded siliciclastics and carbonates, but shelly fossils are not known from this unit; fossils are limited to stromatolites and ichnofossils, including *Diplocraterion* (Devaere et al., 2014a). Volcanic ash beds from the upper Tifnout Member of the Adoudounian Formation yielded ages of  $524.837 \pm 0.092$  Ma and  $525.343 \pm 0.088$  Ma (Maloof et al., 2010b). In the Lie de Vin Formation, tuff horizons provided  $^{206}\text{U}$ - $^{238}\text{Pb}$  ID-TIMS dates of  $520.93 \pm 0.14$  Ma and  $523.17 \pm 0.16$  Ma. These dates bracket the SHICE, placing it securely within upper Stage 2 of the Terreneuvian.

### 5.1.3. Excursions II and III

Two relatively minor  $\delta^{13}\text{C}$  peaks occur within Stage 2 of the Terreneuvian, between the major SHICE negative anomaly and the positive CARE event. In Siberian sections, these are referred to as excursions II and III (Magaritz et al., 1986; Kirschvink et al., 1991;). Excursion II reaches values of up to  $\sim+1$  to  $+2\text{‰}$ , while excursion III is a weaker peak with values hovering around  $0.0\text{‰}$  (Fig. 27). Excursions II and III are most clearly seen in  $\delta^{13}\text{C}$  curves through lower Cambrian strata measured in Morocco (Maloof et al., 2010b) and Siberia. In South Australia, excursions II and III are also obvious in the BHG and MORO sections (Figs. 6, 11). The peak  $\delta^{13}\text{C}$  values for excursions II and III in the BHG section are  $+2.9\text{‰}$  and  $-0.3\text{‰}$ , respectively. In the MORO section, excursion II has a peak value of  $+2.3\text{‰}$  and III has a peak value of  $+0.2\text{‰}$ . Timing of these events in South Australia is constrained by excursion II, which straddles the boundary between the *Kulparina rostrata* and *Micrina etheridgei* zones in both sections, but peaks in the lower *M. etheridgei* Zone (Figs. 13, 15).

A similar series of peaks occurs in the Lie de Vin Formation (Oued Sdas section) in the Anti-Atlas of Morocco (Maloof et al., 2005), although these show more depleted values than observed elsewhere (see Maloof et al., 2010a, fig. 5). In Morocco, positive excursions II and III are bracketed by zircon  $^{206}\text{U}$ - $^{238}\text{Pb}$  ID-TIMS dates of  $523.17 \pm 0.16$  Ma and  $520.93 \pm 0.14$  Ma (see Fig. 27).

In Siberia, excursions II and III occur in the *Dokidocyathus regularis* Zone in the Pestrotsvet Formation (Dvortsy section, Magaritz et al., 1986; Brasier et al., 1993; and the Selinde section, Kouchinsky et al., 2005), Krasnoporog Formation (Kouchinsky et al., 2007) and Emyaksin Formation (Kouchinsky et al., 2001, 2015). Shelly fossils associated with excursions II and III in the Emyaksin Formation include *Camenella garbowskae*, *Lapworthella tortuosa* and abundant hyolithelminths, including *Torelella* (Kouchinsky et al., 2015). Kirschvink et al. (1991) also identified excursion II in the Isis section on the Lena

River, and Magaritz et al. (1986) showed “cycles” II and III in the Dvortsy section on the Aldan River. In the Siberian sections, Brasier et al. (1994) noted the appearance of bivalves, true hyoliths, calcitic brachiopods and the earliest coralomorphs associated with excursion II, which is consistent with the occurrence of these groups through the *Micrina etheridgei* Zone (and excursion II) in South Australia (MORO and BHG sections, Figs. 13, 15).

#### 5.1.4. Cambrian Arthropod Radiation Event (CARE)

The CARE (or excursion IV) is a positive  $\delta^{13}\text{C}$  peak near the base of Series 2, Stage 3 that has been identified in lower Cambrian strata in Siberia (Brasier et al., 1993, 1994; Derry et al., 1994; Kouchinsky et al., 2005, 2007), Morocco (Maloof et al., 2010a), Canada (Dilliard et al., 2007) and Australia (herein). Maximum  $\delta^{13}\text{C}$  values for the CARE range from  $+1.4\text{‰}$  in Siberia to  $+3.4\text{‰}$  in Morocco. The CARE is associated with the appearance of diverse arthropod (especially trilobite) taxa, and peaks after the first appearance of trilobites worldwide (Zhu et al., 2006, Fig. 27). In South Australian sections, the CARE has been identified in the Mernmerna Formation (BHG section,  $+3.5\text{‰}$ , Fig. 15; Yalkalpo-2 drillcore,  $+1.9\text{‰}$ , Fig. 19), and the Ajax Limestone (AJX-M section,  $+1.9\text{‰}$ , Fig. 17). In all South Australian sections where the CARE is apparent, it straddles the boundary between the *Micrina etheridgei* and *Dailyatia odyssei* zones, with positive values increasing through the upper *M. etheridgei* Zone, and peaking in the lower *D. odyssei* Zone. This is consistent with biostratigraphic trends, which show arthropod diversity increasing through the *M. etheridgei* Zone (including first appearances of a wide variety of bradoriid taxa in the lower-mid *M. etheridgei* Zone), and the first occurrence of the oldest South Australian trilobite, *Parabadiella huoi* in the upper *M. etheridgei* Zone (Betts et al., 2014, 2016, 2017b).

Previous studies have suggested that the first appearance of trilobites is diachronous around the world (see Zhang et al., 2017) and, despite little evidence, that they appear considerably later in Australia and South China (Peng et al., 2012; Landing et al., 2013). However, in the Arrowie Basin, *Parabadiella huoi* first occurs in the *Micrina etheridgei* Zone of the AJX-M section (Betts et al., 2016), below the positive  $\delta^{13}\text{C}$  peak interpreted as the CARE (IV) in the lowermost *Dailyatia odyseii* Zone. This suggests that the first appearance of trilobites in Australia is either at, or very close to the base of Stage 3, in keeping with the first occurrences of trilobites elsewhere in the world (Figs. 17, 27).

The Tommotian–Atdabanian boundary in Siberia (= Terreneuvian, Stage 2–Series 2, Stage 3 boundary, Peng et al., 2012) is associated with a gradual increase in  $\delta^{13}\text{C}$  values toward the CARE (Brasier et al., 1994, fig. 4). The CARE in Siberia is associated with the incoming of fallotaspoid trilobites, and the upper parts of the excursion are associated with the eodiscoid genus *Delgadella* (= *Pagetiellus* in Brasier et al., 1994; Derry et al., 1994). Brasier et al. (1994) noted a radiation of bradoriids at levels F–H (in composite Siberian sections) where the CARE is developed, which corresponds closely with the increase in bradoriid diversity throughout the *Micrina etheridgei* and lower *Dailyatia odyseii* zones in South Australia (Topper et al., 2011; Betts et al., 2014, 2016, 2017b).

The CARE is apparent in the Zhurinsky Mys section (Pestrotsvet Formation), measured on the Lena River (Kirschvink et al., 1991), although supporting biostratigraphic data are lacking (Brasier et al., 1993). The CARE is also recorded in the Pestrotsvet Formation in the Selinde section, southeastern Siberian Platform (Kouchinsky et al., 2005) and in the Krasnoporog Formation (Sukharikha section, northwestern Siberian Platform, Kouchinsky et al., 2007). In the southeastern Siberian Platform, biostratigraphy is based mostly on archaeocyaths and trilobites (Rozanov et al., 1992; Rozanov and Zhuravlev, 1992). Archaeocyaths indicative of the *Nochoroicyathus sunnaginicus*, *Dokidocyathus regularis* and

*Dokidocyathus lenaicus* zones occur in the Pestrotsvet Formation, leading up to the CARE event (summarised by Kouchinsky et al., 2005). However, Kouchinsky et al. (2005) also note that  $\delta^{13}\text{C}$  chemostratigraphic data from lower Cambrian successions in Siberia indicate that archaeocyathan biostratigraphy may suffer from local diachronism, as occurrences of key archaeocyathan taxa in the Pestrotsvet Formation contradict correlations with the stratotype sections in the Lena-Aldan region. Trilobites occur in Bed 36 (in thin section), and body fossils of *Profallotaspis* occur in Bed 37, at the base of the CARE (Kouchinsky et al., 2005).

The CARE is also clearly developed in the Kuonamka River sections through the Emyaksin Formation in northern Siberia (Kouchinsky et al., 2015). Fossil occurrences through this interval are sparse, but taxa from immediate post-CARE levels in the Kuonamka sections, where the  $\delta^{13}\text{C}$  curve declines to  $\sim 0\text{‰}$ , include *Lapworthella dentata*, *Microdictyon* spp., palaeoscolecids, and a high diversity mollusc assemblage featuring *Yochelcionella* and *Bemella* (Kouchinsky et al., 2015). In South Australia, *Lapworthella fasciculata* is common in the upper *Micrina etheridgei* Zone, but ranges through (in greater abundance) to the *Dailyatia odyssei* Zone. Diverse mollusc faunas (Betts et al., 2017b; Jacquet and Brock 2016), including *Yochelcionella* spp., occur in the *D. odyssei* Zone. However, co-occurrence with the trilobite *Pararaia bunyeroensis* in the MMF section (Betts et al., 2017b) indicates they are likely to be slightly younger than those from the Kuonamka Formation.

In South Australia, the PIN section (Fig. 21) and SCYW-791A drillcore (Fig. 23) both have fauna and  $\delta^{13}\text{C}$  values consistent with a post-CARE, mid-*Dailyatia odyssei* Zone age. The SCYW-791A drillcore through the Andamooka Limestone displays  $\delta^{13}\text{C}$  values that remain at  $\sim 0\text{‰}$  through the lower-mid levels (where the *D. odyssei* Zone has been identified; Betts et al., 2017b). However, the increasing trend for positive values through the upper parts of the core may represent the MICE, but as no shelly fauna have been recovered from this interval, this remains to be confirmed.

The CARE is also clearly developed in sections measured through the upper Lie de Vin and Igoudine formations in the Anti-Atlas of Morocco (Maloof et al., 2005, 2010a,b). The event is captured in the Oued Salas section (maximum of +2.2‰) (Maloof et al., 2005), the Talat n' Yissi section (maximum of +3.4‰) (Maloof et al., 2005), and the Sidi Msal section (maximum of +3.7‰) (Maloof et al., 2010b). The trend for positive values increases through the Lie de Vin Formation, with the peak occurring in the upper Lie de Vin Formation, and curving back toward neutral and negative  $\delta^{13}\text{C}$  values in the Igoudine Formation (Maloof et al., 2010b, fig. 1). Animal body fossils are not known from the Lie de Vin Formation (Geyer and Landing, 1995). The oldest animal fossils known from Morocco occur in the Tiout Member of the overlying Igoudine Formation, including the trilobites *Eofallotaspis*, *Hupetina antiqua* and 'bigotinid' redlichiods (Geyer and Landing, 1995; Zhang et al., 2017), but other shelly fauna are not known from this unit (Skovsted et al., 2014a). Shelly fossils from the overlying Amouslek Formation include tomotiids such as *Tannuolina maroccana*. However, as it occurs above the CARE  $\delta^{13}\text{C}$  anomaly, it cannot be used to correlate the Amouslek Formation with the *Sinosachites flabelliformis*-*Tannuolina zhangwentangi* Zone in South China.

Dilliard et al. (2007) conducted high-resolution sequence-stratigraphic and stable isotope chemostratigraphic work through the lower Cambrian Sekwi Formation in the Northwest Territories of Canada. Curves from Canada show some differences with regard to the magnitude and absolute timing of events, which are likely related to tectonism, sea-level transgressions and regressions, and/or diagenesis, but can be correlated with the global curve (Dilliard et al., 2007). Dilliard et al. (2007) note that the maximum value of their "cycle A" (+1.2‰) coincides generally with the *Fallotaspis*-*Nevadella* Zone boundary, and correlate this excursion with the CARE/IV excursion in Siberia. Trilobites provide broad biostratigraphic control in the Sekwi Formation, which spans the upper *Fallotaspis*,

*Nevadella* and *Bonnia-Olenellus* zones. The chancelloriids *Archiasterella fletchergryllus* and *Chancelloria* cf. *eros* have also been reported from the Sekwi Formation (Randell et al., 2005). Chancelloriids have a wide geographic distribution (Yun et al., 2017), but their problematic taxonomy and long stratigraphic ranges make them poor biostratigraphic tools. Hyoliths have also been noted in the field (Dilliard et al., 2007), however, other than trilobites, useful shelly fossil biostratigraphic data from the Sekwi Formation are lacking. The underlying Vampire Formation is composed of fine siliciclastics, and so  $\delta^{13}\text{C}$  data cannot be generated, and ichnofauna have been the only fossils recovered from this unit (Macnaughton and Narbonne, 1999). However, its stratigraphic relationship with the Sekwi Formation would suggest it is likely to have a Terreneuvian, Stage 2–early Series 2, Stage 3 age (Fig. 27).

Brasier et al. (1990) and Zhou et al., (1997) analysed  $\delta^{13}\text{C}$  trends through coeval lower Cambrian sections in Yunnan. Both the Xiaotan and Meishucun sections display negative  $\delta^{13}\text{C}$  values in the lower Shiyantou Member of the Chiungchussu Formation, which either conformably or disconformably overlies the Dahai Member of the Zhujiaping Formation (Brasier et al., 1990; Zhang et al., 1997; Zhou et al., 1997) that contains *Watsonella crosbyi* (Li et al., 2001) and has  $\delta^{13}\text{C}$  values indicative of the ZHUCE event. The  $\delta^{13}\text{C}$  results from both sections reveal a similar trajectory through the overlying Shiyantou and Yu'anshan members, with the curves tracking from negative values in the Shiyantou Member toward neutral values in the Yu'anshan Member (Ishikawa et al., 2008, fig. 5). As in the Three Gorges sections (Ishikawa et al., 2008, 2014), time breaks in the Yunnan sections have resulted in an abbreviated  $\delta^{13}\text{C}$  curve, and excursions II and III, in addition to the CARE, are not developed. However, the occurrence of *Parabadiella huoi* in the basal Yu'anshan Member (Steiner et al., 2001) suggests that the  $\delta^{13}\text{C}$  values through the Shiyantou

Member likely lead into the CARE, which is not fully captured in the basal Yu'an-shan Member (Brasier et al., 1990; Zhou et al., 1997).

## 5.2 Radiometric dating

The boundary between Cambrian Stages 3 and 4 in the global geological timescale remains unrati-fied but has been suggested to be at approximately 514 Ma (Peng et al., 2012). Three tuff horizons from within the upper *Dailyatia odyssei* Zone (= *Pararaia bunyeroensis* Zone) in the lower Mernmerna Formation (Third Plain Creek Member) yielded new  $^{206}\text{U}$ – $^{238}\text{Pb}$  CA-TIMS eruption ages of  $515.38 \pm 0.13$  Ma (Bunyeroo Gorge),  $514.56 \pm 0.13$  Ma (MMF section) and  $514.46 \pm 0.13$  Ma (Paralana -1B core) (see Figs. 25 and 27). A tuff from the upper Heatherdale Shale on Fleurieu Peninsula produced a CA-TIMS maximum depositional age of  $514.98 \pm 0.22$  Ma (Fig. 25). Similar-aged volcanic ash beds occur in the Comley Limestones Formation (*Callavia* Zone) in the UK (horizon Ac1;  $514.45 \pm 0.36$  Ma, ID-TIMS method; Harvey et al., 2011), and in the upper Tata Group in the High Atlas of Morocco (= lower Issafene Formation in the Lemdad syncline;  $517 \pm 1.5$  Ma, ID-TIMS method; Maloof et al., 2010b). This latter date, and a date from the underlying Taroudant Group (Lie De Vin Formation, ID-TIMS method,  $520.93 \pm 0.14$  Ma) bracket the CARE positive peak (Maloof et al., 2010b). Correlation of the CARE in the South Australian successions with the global curve, calibrated by the age model of Maloof et al. (2010b), suggests the boundary between the *Micrina etheridgei* and *D. odyssei* zones is close to the base of Cambrian Series 2, Stage 3 (Fig. 27). An additional tuff horizon in the Warragee Member of the Billy Creek Formation in the Bunkers Range has produced a CA-TIMS date of  $511.87 \pm 0.14$  Ma (Fig. 25), indicating that the Stage 4–5 (traditional Early–Middle Cambrian) boundary, currently estimated at 509 Ma (Peng et al., 2012), could be within the



Lake Frome Group of the Arrowie Basin; this is also partly supported by limited trilobite data from the Wirrealpa Limestone and Moodlatana Formation (Jell in Bengtson et al., 1990; Paterson and Brock, 2007). Moreover, the Billy Creek Formation CA-TIMS date provides an absolute age approximation for the Cambrian Stage 4 Emu Bay Shale and underlying Marsden Sandstone on Kangaroo Island in the Stansbury Basin (Paterson et al., 2016), as all three units contain the emuellid trilobite *Balcoracania dailyi* (Pocock, 1970; Paterson and Edgecombe, 2006; Paterson et al., 2007; Gehling et al., 2011). Unfortunately, an apparent paucity of active arc volcanism during Fortunian to Cambrian Stage 3 times in both the Arrowie and Stansbury basins means that it may not be possible to obtain radiometric dates from ash beds from lower parts of the Hawker Group and equivalent successions.

## 6. Conclusions

Accurate correlations of lower Cambrian strata in South Australia with other parts of the world have been difficult, due to a lack of abundant and integrated biostratigraphic, chemostratigraphic, lithostratigraphic and radiometric data. Intensive sampling over more than 15 years of field campaigns demonstrates that South Australia has one of the best preserved, best exposed, most complete and easily accessible lower Cambrian successions anywhere in the world. Biostratigraphic data from 21 measured stratigraphic sections and drill cores from the Stansbury and Arrowie basins have led to the development of a new shelly fossil biostratigraphic scheme for the early Cambrian of Australia (Betts et al., 2016, 2017b). This has now been complemented with  $\delta^{13}\text{C}$  curves through 10 of the sections sampled for palaeontological data, providing the first, tightly integrated multi-proxy dataset for the early Cambrian of South Australia (Terreneuvian, Stage 2–Series 2, Stage 4). New  $^{206}\text{U}$ – $^{238}\text{Pb}$  CA-TIMS dates from critical levels in the Mernmerna Formation (Arrowie Basin)

and Heatherdale Shale (Stansbury Basin) provide geochronologic calibration for the chronostratigraphic scheme, embedding it within the global timescale.

While increasingly applied as the premier correlation technique for lower Cambrian rocks worldwide, it is clear that chemostratigraphy on its own must be used with great caution. The most reliable results are generated when  $\delta^{13}\text{C}$  data are integrated with high-resolution biostratigraphic and lithostratigraphic data and accurate radiometric dates. In South Australia, the  $\delta^{13}\text{C}$  data have a clear and repeatable relationship with the biostratigraphic zones developed by Betts et al. (2016, 2017b). The  $\delta^{13}\text{C}$  curves from the South Australian sections echo very closely the global curve, allowing robust global correlation of the lower Cambrian succession and linking the (commonly endemic) shelly fossils from South Australia with contemporaneous faunas from around the world.

The ZHUCE positive  $\delta^{13}\text{C}$  event through the WANG and WANG/S sections on the Fleurieu Peninsula occurs beneath the *Kulparina rostrata* Zone, in strata containing a shelly fauna supporting a Terreneuvian, Stage 2 age. Negative  $\delta^{13}\text{C}$  values prior to and throughout the *K. rostrata* Zone in the WANG, SHL and WAR sections correspond with the SHICE  $\delta^{13}\text{C}$  anomaly during the late Terreneuvian, Stage 2. Excursions II and III are evident in the AJX-M, BHG and MORO sections in the Arrowie Basin, with excursion II straddling the boundary between the *K. rostrata* and *M. etheridgei* zones. The positive CARE (IV) excursion occurs in the AJX-M and BHG sections and the Yalkalpo-2 drillcore. Corresponding with the established relationship between CARE (IV) and increasing arthropod diversity, this  $\delta^{13}\text{C}$  event in South Australia also coincides with an increase in bradoriid diversity and abundance, as well as the first appearance of trilobites in East Gondwana. The relatively close association between the *Parabadiella huoi* Zone and the CARE excursion in the AJX-M section suggests that the first occurrence of trilobites in Australia is closer to the base of Stage 3 than previously understood. A younger positive event occurring in drillcore SCYW-791A reaches

+3.29‰ and may represent the MICE event, but lack of shelly fossils at these levels makes this difficult to determine.

The new CA-TIMS dates from the upper *Daliyatia odyssei* Zone (=Pararaia *bunyerensis* Zone) in the Mernmerna Formation (Arrowie Basin) and the Heatherdale Shale (Stansbury Basin) securely embed the upper part of new chronostratigraphic scheme in a global geochronological context. This has been the first detailed investigation that integrates shelly fossil biostratigraphy,  $\delta^{13}\text{C}$  chemostratigraphy, and  $^{206}\text{U}$ – $^{238}\text{Pb}$  CA-TIMS radiometric dates in an effort to regionally and globally correlate lower Cambrian strata from South Australia. The clear relationship of the South Australian  $\delta^{13}\text{C}$  curves with the stratigraphic position and magnitude of global  $\delta^{13}\text{C}$  excursions, in combination with biostratigraphic data, clearly links South Australian successions with regions such as North and South China, Siberia, Mongolia, Laurentia, east and west Avalonia, and West Gondwana. The comprehensive data documented here demonstrate the power of utilizing these contemporaneous, yet independent proxies to constrain the timing of events during the early Cambrian, and provides a new, robust temporal framework for correlating lower Cambrian strata in South Australia.

## Acknowledgements

This is a contribution to the Flinders Ranges World Heritage nomination. Funding for this project was provided by an Australian Research Council (ARC) Discovery Project #120104251 (to GAB and JRP), Linnean Society of NSW and Macquarie University HDR funds (to MJB), an ARC Future Fellowship (FT120100770 to JRP), and the Spanish Ministry of Science Project CGL2009-07073 (to DCGB and JRP). JBJ was supported by the University of South Australia. We would like to thank field and lab team members, including Hayley Bell, Sarah Collison, Bo Jonak, David Keith, Malcolm Lambert, Briony Mamo, David Mathieson, Brett Pyemont, Mitch Smith, Bonnie Teece and James Valentine. Thanks also to: Nick Langsford for providing the BG tuff for dating; Linda and Luke Nothdurft (QUT) and David Adams (MQ) for discussion about isotope sample analyses; Simon George for the image of the Wirrealpa thrombolites; Erin Fletcher (nee Casey) for access to her unpublished Honours thesis on the Andamooka Limestone; Dean Oliver for initial drafting of maps; and Liang Yue and Yun Hao at Northwest University for sourcing critical Chinese literature. We are grateful to property owners Julie and Bill Reschke (Mulga View Station), Ian and Di Fargher (Angorichina), Graham and Laura Ragless (Beltana), and Jim and Linda Stacey (Myponga Beach) for accommodation and field access. Thanks to Michael Close and Trevor Smith at the Sellick Hill quarry for their assistance. We are also grateful to the Adnyamathanha People of Nepabunna for allowing the field teams to conduct fieldwork on their land. We would like to thank Peng Shanchi and an anonymous reviewer for their constructive comments on the manuscript.

**References**

- Abele, C., McGowran, B., 1959. The geology of the Cambrian south of Adelaide (Sellick Hill to Yankalilla). *Transactions of the Royal Society of South Australia* 82, 301–320.
- Aharon, P., Schidlowski, M., Singh, I.B., 1987. Chronostratigraphic markers in the end-Precambrian carbon isotope record of the Lesser Himalaya. *Nature* 327, 699–702.
- Alexander, E.M., Gravestock, D.I., 1990. Sedimentary facies in the Sellick Hill Formation, Fleurieu Peninsula, South Australia. *Geological Society of Australia, Special Publication* 16, 269–289.
- Babcock, L.E., Peng, S-C., 2007. Cambrian chronostratigraphy: current state and future plans. *Palaeogeography, Palaeoclimatology, Palaeoecology* 254, 62–66.
- Babcock, L.E., Peng, S-C., Brett, C.E., Zhu, M-Y., Ahlberg, P., Bevis, M., Robison, R.A., 2015. Global climate, sea level cycles, and biotic events in the Cambrian period. *Palaeoworld* 24, 5–15.
- Babcock, L.E., Peng, S-C., Geyer, G., Shergold, J.H., 2005. Changing perspectives on Cambrian chronostratigraphy and progress toward subdivision of the Cambrian System. *Geosciences Journal* 9, 101–106.
- Babcock, L.E., Robison, R.A., Rees, M.N., Peng, S-C., Saltzman, M.R., 2007. The global boundary stratotype section and point (GSSP) of the Drumian Stage (Cambrian) in the Drum Mountains, Utah, USA. *Episodes* 30, 84–94.
- Bengtson, S., Fletcher, T.P., 1983. The oldest sequence of skeletal fossils in the Lower Cambrian of southeastern Newfoundland. *Canadian Journal of Earth Sciences* 20, 525–536.
- Bengtson, S., Conway Morris, S., Cooper, B.J., Jell, P.A., Runnegar, B.N., 1990. Early Cambrian fossils from South Australia. *Memoirs of the Association of Australasian Palaeontologists* 9, 1–364.

- Betts, M.J. 2012. Small shelly fossils and archaeocyath bioherms from lower Cambrian Hawker Group carbonates at Moro Gorge, central Flinders Ranges. Honours thesis, Macquarie University, Sydney.
- Betts, M.J., Paterson, J.R., Jago, J.B., Jacquet, S.M., Skovsted, C.B., Topper, T.P., Brock, G.A., 2016. A new lower Cambrian shelly fossil biostratigraphy for South Australia. *Gondwana Research* 36, 176–208.
- Betts, M.J., Paterson, J.R., Jago, J.B., Jacquet, S.M., Skovsted, C.B., Topper, T.P., Brock, G.A., 2017a. A new lower Cambrian shelly fossil biostratigraphy for South Australia: Reply. *Gondwana Research* 44, 262–264.
- Betts, M.J., Paterson, J.R., Jago, J.B., Jacquet, S.M., Skovsted, C.B., Topper, T.P., Brock, G.A. 2017b. Global correlation of the early Cambrian of South Australia: Shelly fauna of the *Dailyatia odyssei* Zone. *Gondwana Research* 46, 240–279.
- Betts, M.J., Topper, T.P., Valentine, J.L., Skovsted, C.B., Paterson, J.R., Brock, G.A. 2014. A new early Cambrian bradoriid (Arthropoda) assemblage from the northern Flinders Ranges, South Australia. *Gondwana Research* 25, 420–437.
- Bicknell, R.D.C., Paterson, J.R., 2018. Reappraising the early evidence of durophagy and drilling predation in the fossil record: implications for escalation and the Cambrian Explosion. *Biological Reviews* 93, 754–784.
- Bold, U., Crowley, J.L., Smith, E.F., Sambuu, O., Macdonald, F.A., 2016. Neoproterozoic to early Paleozoic tectonic evolution of the Zavkhan terrane of Mongolia: Implications for continental growth in the Central Asian orogenic belt. *Lithosphere* 8, 729–750.
- Bradbury, H.J., Vandeginste, V., John, C.M., 2015. Diagenesis of phosphatic hardgrounds in the Monterey Formation: A perspective from bulk and clumped isotope geochemistry. *Geological Society of America Bulletin* 127, 1453–1463.

- Brand, U., Veizer, J., 1981. Chemical diagenesis of a multicomponent carbonate system – 2: Stable Isotopes. *Journal of Sedimentary Petrology* 51, 987–997.
- Brasier, M.D., 1976. Early Cambrian intergrowths of archaeocyathids, *Renalcis*, and pseudostromatolites from South Australia. *Palaeontology* 19, 35–37.
- Brasier, M.D. 1986. The succession of small shelly fossils (especially conoidal microfossils) from English Precambrian–Cambrian boundary beds. *Geological Magazine* 123, 237–256.
- Brasier, M.D., 1989. Chapter 5, Sections in England and their correlation. In: Cowie, J.W., Brasier, M.D. (Eds.), *The Precambrian–Cambrian Boundary*. Clarendon Press, Oxford, UK, pp. 82–98.
- Brasier, M.D., 1993. Towards a carbon isotope stratigraphy of the Cambrian System: potential of the Great Basin succession. In: Hailwood, E.A., Kidd, R.B. (Eds.), *High Resolution Stratigraphy*. Geological Society Special Publication 70, pp. 341–350.
- Brasier, M.D., Anderson, M.M., Corfield, R.M., 1992. Oxygen and carbon isotope stratigraphy of early Cambrian carbonates in southeastern Newfoundland and England. *Geological Magazine* 129, 265–279.
- Brasier, M.D., Corfield, R., Derry, L., Rozanov, A.Y., Zhuravlev, A.Y. 1994. Multiple  $\delta^{13}\text{C}$  excursions spanning the Cambrian explosion to the Botomian crisis in Siberia. *Geology* 22, 455–458.
- Brasier, M.D., Khomentovsky, V.V., Corfield, R.M. 1993. Stable isotopic calibration of the earliest skeletal fossil assemblages in eastern Siberia (Precambrian-Cambrian boundary). *Terra Nova* 5, 225–232.
- Brasier, M.D., Magaritz, M., Corfield, R., Luo, H-L., Wu, X-C., Ouyang, L., Jiang, Z-W., Hamdi, B., He, T-G. and Fraser, A.G., 1990. The carbon-and oxygen-isotope record

- of the Precambrian–Cambrian boundary interval in China and Iran and their correlation. *Geological Magazine* 127, 319–332.
- Brasier, M.D., Shields, G., Kuleshov, V.N., Zhegalov, E.A. 1996. Integrated chemo- and biostratigraphic calibration of early animal evolution: Neoproterozoic–early Cambrian of southwest Mongolia. *Geological Magazine* 133, 445–485.
- Brock, G.A., Paterson, J.R., 2004. A new species of *Tannuella* (Helcionellida, Mollusca) from the Early Cambrian of South Australia. *Memoirs of the Association of Australasian Palaeontologists* 30, 133–143.
- Brock, G.A., Alexander, E.M., Paterson, J.R., Jago, J.B., Gatehouse, C.G., 2006. Mt. Scott Range and Ajax Mine. In: Jago, J.B., Zang, W-L. (Eds.), *South Australia 2006, XI International Conference of the Cambrian Stage Subdivision Working Group Field Guide*. South Australia. Geological Society of Australia, South Australian Division, Adelaide, pp. 26–31.
- Brock, G.A., Betts, M. J., Paterson, J.R., Jago, J.B., Kruse, P.D., 2016a. Day 6 – Thursday 7 July. Ajax Mine archaeocyaths and AJX-M section, Mount Scott Range. In: Kruse, P.D., Jago, J.B. (Eds.), *Palaeo Down Under 2. Geological field excursion guide: Cryogenian-Ediacaran-Cambrian of the Adelaide Fold Belt*. Report Book 2016/00011. Department of State Development, South Australia, Adelaide, pp. 27–29.
- Brock, G.A., Engelbretsen, M.J., Jago, J.B., Kruse, P.D., Laurie, J.R., Shergold, J.H., Shi, G-R., Sorauf, J.E., 2000. Palaeobiogeographic affinities of Australian Cambrian faunas. *Memoirs of the Association of Australasian Palaeontologists* 23, 1–61.
- Brock, G.A., Jago, J.B., Kruse, P.D., Betts, M.J., Jacquet, S.M., Paterson, J.R., García-Bellido, D.C., 2016b. Chapter 4. Cambrian of the Stansbury and Arrowie Basins. In: Kruse, P.D., Jago, J.B. (Eds.), *Palaeo Down Under 2. Geological field excursion*



- guide: Cryogenian-Ediacaran-Cambrian of the Adelaide Fold Belt. Report Book 2016/00011. Department of State Development, South Australia, Adelaide, pp. 10–24.
- Carr, L.K., Korsch, R.J., Stuckmeyer, H., Jones, L.E.A., Holzschuh, J., Costelloe, R.D., Meixner, A.J., 2012. The architecture and petroleum potential of Australia's onshore sedimentary basins from deep seismic reflection data and petroleum systems maturation modelling: The Arrowie, Georgina and Darling basins. *Geoscience Australia, Record* 2012/36, 1–84.
- Ceglar, N., Reilly, M.R.W., Payenberg, T.H.D., Lang, S.C., 2004. Deep water outcrop analogue study: basal Bunkers Sandstone, Donkey Bore Syncline, Northern Flinders Ranges, Australia. In: Boulton, P.J., Johns, D.R., Lang, S.C. (Eds.), *Eastern Australian Basins Symposium II, Petroleum Exploration Society of Australia Special Publication* 2, pp. 499–509.
- Chang, C., Hu, W.-X., Wang, X.-L., Yu, H., Yang, A.-H., Cao, J., Yao, S.-P., 2017. Carbon isotope stratigraphy of the lower to middle Cambrian on the eastern Yangtze Platform, South China. *Palaeogeography, Palaeoclimatology, Palaeoecology* 479, 90–101.
- Chen, P., 1984. Discovery of Lower Cambrian small shelly fossils from Jijiapo, Yichang, west Hubei and its significance. *Professional Papers of Stratigraphy and Palaeontology* 2, 49–65.
- Chen, G.-X., Jin, J.-W. (Eds.), 1996. Multiple classification and correlation of the stratigraphy of China 42: Stratigraphy (Lithostratic) of Hubei Province. Bureau of Geology and Mineral Resources of Hubei Province. China University of Geosciences Press. Wuhan, Hubei Province. 284 pp.

- Clarke, J.D.A., 1986a. Subdivision of the lower part of the Wilkawillina Limestone, eastern Flinders Ranges. *Quarterly Geological Notes - Geological Survey of South Australia* 97, 12–17.
- Clarke, J.D.A., 1986b. Subdivision of the Early Cambrian Parara Limestone at Wilkawillina Gorge, Flinders Ranges. *Quarterly Geological Notes - Geological Survey of South Australia* 99, 1–7.
- Clarke, J.D.A., 1986c. Stratigraphy and sedimentology of the upper part of the Wilkawillina Limestone, Wilkawillina Gorge, Flinders Ranges. *Quarterly Geological Notes - Geological Survey of South Australia* 100, 2–7.
- Clarke, J.D.A., 1990a. Slope facies deposition and diagenesis of the Early Cambrian Parara Limestone, Wilkawillina Gorge, South Australia. *Geological Society of Australia Special Publication* 16, 230–246.
- Clarke, J.D.A., 1990b. Platform carbonate deposition and diagenesis. Woodendinna Dolomite and Lower Wilkawillina Limestone (Early Cambrian), Wilkawillina Gorge, South Australia. *Geological Society of Australia Special Publication* 16, 247–268.
- Clarke, J.D.A., 1990c. An early Cambrian carbonate platform near Wilkawillina Gorge, South Australia. *Australian Journal of Earth Sciences* 37, 471–483.
- Clarke, L.J., Jenkyns, H.C., 1999. New oxygen isotope evidence for long-term Cretaceous climatic change in the Southern Hemisphere. *Geology* 27, 699–702.
- Claybourn, T.M., 2016. Investigating the molluscan fauna of the Shackleton Limestone (Transantarctic Mountains, Antarctica) with outline morphometrics. PalAss Meeting, Lyon, France. DOI: 10.13140/RG.2.2.25492.30083.
- Compston, W., Zhang, Z-C, Cooper, J.A., Ma, G-G, Jenkins, R.J.F., 2008. Further SHRIMP geochronology on the early Cambrian of South China. *American Journal of Science* 308, 399–420.

- Condon, D.J., Schoene B., McLean N.M., Bowring S.A., Parrish R., 2015. Metrology and traceability of U-Pb isotope dilution geochronology (EARTHTIME Tracer Calibration Part I). *Geochimica et Cosmochimica Acta* 164, 464–480.
- Coplen, T., 1995. Reporting of stable hydrogen, carbon, and oxygen isotopic abundances. *Geothermics* 24, 707–712.
- Coplen, T.B., Brand, W.A., Gehre, M., Gröning, M., Meijer, H.A., Toman, B., Verkouteren, R.M., 2006. New guidelines for  $\delta^{13}\text{C}$  measurements. *Analytical Chemistry* 78, 2439–2441.
- Cowley, W.M., 1990. Early Cambrian Andamooka Limestone and Yarrowurta Shale of the Stuart Shelf. Mines and Energy South Australia. Report Book 90/00017.
- Cremonese, L., Shields-Zhou, G.A., Struck, U., Ling, H.-F., Och, L.M., 2014. Nitrogen and organic carbon isotope stratigraphy of the Yangtze Platform during the Ediacaran-Cambrian transition in south China. *Palaeogeography, Palaeoclimatology, Palaeoecology* 398, 165–186.
- Crowley, J.L., Schoene, B., Bowring, S.A., 2007. U-Pb dating of zircon in the Bishop Tuff at the millennial scale. *Geology* 35, 1123–1126.
- Daily, B., 1956. The Cambrian in South Australia. In: Rodgers, J. (Ed.), *El Sistema Cambrico, su paleogeografía y el problema de su base*, Report 20th International Geological Congress, Mexico 2, pp. 91–147.
- Daily, B., 1963. The fossiliferous Cambrian succession on the Fleurieu Peninsula, South Australia. *Records of the South Australian Museum* 14, 579–602.
- Daily, B., 1969. Fossiliferous Cambrian sediments and low-grade metamorphics, Fleurieu Peninsula, South Australia. In: Daily, B. (Ed.), *Geological Excursions Handbook*, ANZAAS, 41<sup>st</sup> Congress, Section 3, pp. 49–54.

- Daily, B., 1973. Discovery and significance of basal Cambrian Uratanna Formation, Mt Scott Range, Flinders Ranges, South Australia. *Search* 4, 202–205.
- Daily, B., 1976a. The Cambrian of the Flinders Ranges. In Thompson, B.P., Daily, B., Coats, R.P. and Forbes, B.G. (compilers), *Late Precambrian and Cambrian geology of the 'Adelaide Geosyncline' and Stuart Shelf, South Australia*. 25th International Geological Congress Excursion Guide, 33A, 15–19.
- Daily, B. 1976b. New data on the base of the Cambrian in South Australia. *Izvestiya Akademii Nauk. SSSR, Seriya Geologicheskaya*. 3, 45–52.
- Daily, B., Milnes, A.R., 1973. Stratigraphy, structure and metamorphism of the Kanmantoo Group (Cambrian) in its type section east of Tunkalilla Beach, South Australia. *Transactions of the Royal Society of South Australia* 97, 231–242.
- Daily, B., Firman, J.B., Forbes, B.G., Lindsay, J.M., 1976. Geology. In: Twidale, C.R., Tyler, M.J., Webb, B.P. (Eds.), *Natural History of the Adelaide Region*. Royal Society of South Australia, Adelaide, pp. 5–42.
- Davies, N.S., Liu, A.G., Gibling, M.R., Miller, R.F., 2016. Resolving MISS conceptions and misconceptions: A geological approach to sedimentary surface textures generated by microbial and abiotic processes. *Earth-Science Reviews* 154, 210–246.
- Debrenne, F., Gravestock, D.I., 1990. Archaeocyatha from the Sellick Hill Formation and Fork Tree Limestone on Fleurieu Peninsula, South Australia. *Geological Society of Australia Special Publication* 16, 290–309.
- Derry, L.A., 2010. A burial diagenesis origin for the Ediacaran Shuram–Wonoka carbon isotope anomaly. *Earth and Planetary Science Letters* 294, 152–162.
- Derry, L.A., Brasier, M.D., Corfield, R.E.A., Rozanov, A.Y., Zhuravlev, A.Y., 1994. Sr and C isotopes in Lower Cambrian carbonates from the Siberian craton: A

- paleoenvironmental record during the ‘Cambrian explosion’. *Earth and Planetary Science Letters* 128, 671–681.
- Devaere, L., Clausen, S., Álvaro, J.J., 2014a. Stratigraphic overview of the Ediacaran and Cambrian from the Anti-Atlas, Morocco. University Lille1, France. ISBN: 978-2-9601543-0-6.
- Devaere, L., Clausen, S., Steiner, M., Álvaro, J.J., Vachard, D., 2013. Chronostratigraphic and palaeogeographic significance of an early Cambrian microfauna from the Héraultia Limestone, northern Montagne Noire, France. *Palaeontologia Electronica* 16, 1–91.
- Devaere, L., Clausen, S., Monceret, E., Vizcaïno, D., Vachard, D., Genge, M.C., 2014b. The tommotiid *Kelanella* and associated fauna from the early Cambrian of southern Montagne Noire (France): implications for camenellan phylogeny. *Palaeontology* 57, 979–1002.
- Dilliard, K.A., Pope, M.C., Coniglio, M., Hasiotis, S.T., Lieberman, B.S., 2007. Stable isotope geochemistry of the lower Cambrian Sekwi Formation, Northwest Territories, Canada: Implications for ocean chemistry and secular curve generation. *Palaeogeography, Palaeoclimatology, Palaeoecology* 256, 174–194.
- Dorjnamjaa, D., Bat-Ireedui, Y.A., Dashdavaa, Z., Soelmaa, D., 1993. Precambrian-Cambrian Geology of the Dzavkhan Zone. IGCP Project 303 “Precambrian-Cambrian Event Stratigraphy”, Guidebook for Excursion Precambrian-Cambrian Geology Khasagt-Khavrhan Ridge, Goby-Altay Province, Mongolia. Earth Sciences Department, Oxford, pp. 1–36.
- Erwin, D.H., Laflamme, M., Tweedt, S.M., Sperling, E.A., Pisani, D., Peterson, K.J., 2011. The Cambrian conundrum: early divergence and later ecological success in the early history of animals. *Science* 334, 1091–1097.

- Erwin, D.H., Valentine, J.W., 2013. The Cambrian explosion: The Construction of Animal Biodiversity. Roberts, Greenwood Village, 416 pp.
- Fan, R., Deng, S-H., Zhang, X-L., 2011. Significant carbon isotope excursions in the Cambrian and their implications for global correlations. *Science China Earth Sciences* 54, 1686–1695.
- Fanton, K., Holmden, C., 2007. Sea-level forcing of carbon isotope excursions in epeiric seas: implications for chemostratigraphy. *Canadian Journal of Earth Sciences* 44, 807–818.
- Foden, J., Elburg, M.A., Dougherty-Page, J., Burt, A., 2006. The timing and duration of the Delamerian Orogeny: Correlation with the Ross Orogen and implications for Gondwana assembly. *Journal of Geology* 114, 189–210.
- Foster, C.B., Cernovskis, A., O'Brien, G.W., 1985. Organic-walled microfossils from the Early Cambrian of South Australia. *Alcheringa* 9, 259–268.
- Fricke, H.C., Clyde, W.C., O'Neil, J.R., Gingerich, P.D., 1998. Evidence for rapid climate change in North America during the latest Paleocene thermal maximum: oxygen isotope compositions of biogenic phosphate from the Bighorn Basin (Wyoming). *Earth and Planetary Science Letters* 160, 193–208.
- Gehling, J.G., Jago, J.B., Paterson, J.R., García-Bellido, D.C., Edgecombe, G.D., 2011. The geological context of the Lower Cambrian (Series 2) Emu Bay Shale Lagerstätte and adjacent stratigraphic units, Kangaroo Island, South Australia. *Australian Journal of Earth Sciences* 58, 243–257.
- Gerstenberger, H., Haase, G., 1997. A highly effective emitter substance for mass spectrometric Pb isotope ratio determinations. *Chemical Geology* 136, 309–312.
- Geyer, G., Landing, E. 1995. Morocco '95—The Lower–Middle Cambrian standard of western Gondwana. *Beringeria*, Special Issue 2, 269 pp.

- Gravestock, D.I., 1984. Archaeocyatha from lower parts of the Lower Cambrian carbonate sequence in South Australia. *Memoirs of the Association of Australasian Palaeontologists* 2, 1–139.
- Gravestock, D.I., 1995. Chapter 7, Early and Middle Palaeozoic. In: Drexel, J.F., Preiss, W.V. (Eds.), *The Geology of South Australia, Volume 2, The Phanerozoic*. Geological Survey of South Australia, Bulletin 54, pp. 3–61.
- Gravestock, D.I., Alexander, E.M., Demidenko, Y.E., Esakova, N.B., Holmer, L.E., Jago, J.B., Lin, T.-R., Melnikova, N., Parkhaev, P.Y., Rozanov, A.Y., Ushatinskaya, G.T., Sang, W.-L., Zhegallo, E. A. and Zhuravlev, A.Y. 2001. The Cambrian biostratigraphy of the Stansbury Basin, South Australia. *Transactions of the Palaeontological Institute of the Russian Academy of Sciences* 282, 1–341.
- Gravestock, D.I., Cowley, W.M. 1995. Chapter 7, Arrowie Basin. In: Drexel, J.F., Preiss, W.V. (Eds.), *The Geology of South Australia, Volume 2, The Phanerozoic*. Geological Survey of South Australia, Bulletin 54, pp. 20–31.
- Gravestock, D.I., Gatehouse, C.G. 1995. Chapter 7, Stansbury Basin. In: Drexel, J.F., Preiss, W.V. (Eds.), *The Geology of South Australia, Volume 2, The Phanerozoic*. Geological Survey of South Australia, Bulletin 54, pp. 5–19.
- Gravestock, D.I., Hibbert, J.E., 1991. Sequence stratigraphy of the eastern Officer and Arrowie Basins: a framework for Cambrian oil search. *APEA Journal*, 31, 177–190.
- Guo, J-F., Li, Y., Han, J., Zhang, X-L., Zhang, Z-F., Ou, Q., Liu, J., Degan, S., Maruyama, S., Komiya, T., 2008. Fossil association from the lower Cambrian Yanjiahe formation in the Yangtze Gorges area, Hubei, South China. *Acta Geologica Sinica (English Edition)* 82, 1124–1132.

- Hall, P.A., 2012. Elemental, isotopic and molecular signatures of early Cambrian marine sediments and a phantom petroleum system in South Australia. University of Adelaide, South Australia. PhD thesis.
- Halverson, G.P., Hurtgen, M.T., Porter, S.M., Collins, A.S., 2009. Neoproterozoic-Cambrian Biogeochemical Evolution. *Developments in Precambrian Geology* 16, 51–365.
- Harvey, T.H., Williams, M., Condon, D.J., Wilby, P.R., Siveter, D.J., Rushton, A.W., Leng, M.J., Gabbott, S.E., 2011. A refined chronology for the Cambrian succession of southern Britain. *Journal of the Geological Society* 168, 705–716.
- Haslett, P. 1975. The Woodendinna Dolomite and Wirrapowie Limestone; two new lower Cambrian formations, Flinders Ranges, South Australia. *Transactions of the Royal Society of South Australia* 99, 211–219.
- Higgins, J.A., Blättler, C.L., Lundstrom, E.A., Santiago-Ramos, D.P., Akhtar, A.A., Ahm, A.C., Bialik, O., Holmden, C., Bradbury, H., Murray, S.T. and Swart, P.K., 2018. Mineralogy, early marine diagenesis, and the chemistry of shallow-water carbonate sediments. *Geochimica et Cosmochimica Acta* 220, 512–534.
- Holmden, C., Creaser, R.A., Muehlenbachs, K., Leslie, S.A., Bergström, S.M., 1998. Isotopic evidence for geochemical decoupling between ancient epeiric seas and bordering oceans: implications for secular curves. *Geology* 26, 567–570.
- Howchin, W., 1897. On the occurrence of lower Cambrian fossils in the Mount Lofty Ranges. *Transactions of the Royal Society of South Australia* 21, 74–86.
- Ishikawa, T., Ueno, Y., Komiya, T., Sawaki, Y., Han, J., Shu, D., Li, Y., Maruyama, S., Yoshida, N., 2008. Carbon isotope chemostratigraphy of a Precambrian/Cambrian boundary section in the Three Gorge area, South China: prominent global-scale isotope excursions just before the Cambrian Explosion. *Gondwana Research* 14, 193–208.



- Ishikawa, T., Ueno, Y., Shu, D-G., Li, Y., Han, J., Guo, J-F., Yoshida, N., Maruyama, S., Komiya, T., 2014. The  $\delta^{13}\text{C}$  excursions spanning the Cambrian explosion to the Canglangpuian mass extinction in the Three Gorges area, South China. *Gondwana Research* 25, 1045–1056.
- Jacquet, S.M., Brock, G.A., 2016. Lower Cambrian helcionelloid macromolluscs from South Australia. *Gondwana Research* 36, 333–358.
- Jacquet, S.M., Betts, M.J., Brock, G.A., 2017a. Facies controls on Cambrian molluscan faunas. Geological Society of America Annual Meeting, Seattle, Washington, USA. Abstracts with Programs 49, p. 233
- Jacquet, S.M., Brougham, T., Skovsted, C.B., Jago, J.B., Laurie, J.R., Betts, M.J., Topper, T.P., Brock, G.A., 2017b. *Watsonella crosbyi* from the lower Cambrian (Terreneuvian, Stage 2) Normanville Group in South Australia. *Geological Magazine* 154, 1088–1104.
- Jacquet, S.M., Jago, J.B., Brock, G.A., 2016. An enigmatic univalve macromollusc from the lower Cambrian (Series 2, Stage 3) Heatherdale Shale, South Australia. *Australasian Palaeontological Memoirs* 49, 21–30.
- Jaffey, A.H., Flynn, K.F., Glendenin, L.E., Bentley, W.C., Essling, A.M., 1971. Precision measurements of half-lives and specific activities of  $^{235}\text{U}$  and  $^{238}\text{U}$ . *Physical Review C* 4, 1889–1906.
- Jago, J.B., Daily, B., Von Der Borch, C.C., Cernovskis, A., Saunders, N., 1984. First reported trilobites from the Lower Cambrian Normanville Group, Fleurieu Peninsula, South Australia. *Transactions of the Royal Society of South Australia* 108, 207–211.
- Jago, J.B., Dyson, I.A., Gatehouse, C.G., 1994. The nature of the sequence boundary between the Normanville and Kanmantoo Groups on Fleurieu Peninsula, South Australia. *Australian Journal of Earth Sciences* 41, 445–453.

- Jago, J.B., Gatehouse, C.G., Powell, C.M., Casey, T., 2013. Implications of cross-bedding data from the upper part of the Cambrian succession, Arrowie Basin, South Australia. *Australian Journal of Earth Sciences* 60, 231–240.
- Jago, J.B., Gehling, J.G., Paterson, J.R., Brock, G.A., Zang, W.-L., 2012. Cambrian stratigraphy and biostratigraphy of the Flinders Ranges and the north coast of Kangaroo Island, South Australia. *Episodes* 35, 247–255.
- Jago, J.B., Gum, J.C., Burt, A.C., Haines, P.W., 2003. Stratigraphy of the Kanmantoo Group: a critical element of the Adelaide Fold Belt and the Palaeo-Pacific plate margin, Eastern Gondwana. *Australian Journal of Earth Sciences* 50, 343–363.
- Jago, J.B., Lin, T.-R., Dunster, J.N., 2002. A new species of the trilobite *Abadiella* from the Lower Cambrian of the eastern Officer Basin, South Australia. *Acta Palaeontologica Sinica* 41, 428–433.
- Jago, J.B., Zang, W.-L., Sun, X., Brock, G.A., Paterson, J.R., Skovsted, C.B., 2006. A review of the Cambrian biostratigraphy of South Australia. *Palaeoworld* 15, 406–423.
- James, N.P., Gravestock, D.I., 1990. Lower Cambrian shelf and shelf margin buildups, Flinders Ranges, South Australia. *Sedimentology* 37, 455–480.
- Jell, P.A., Jago, J.B., Gehling, J.G., 1992. A new conocoryphid trilobite from the Lower Cambrian of the Flinders Ranges, South Australia. *Alcheringa* 16, 189–200.
- Jenkins, R.J.F., Cooper, J.A., Compston, W., 2002. Age and biostratigraphy of Early Cambrian tuffs from SE Australia and southern China. *Journal of the Geological Society* 159, 645–658.
- Jenkins, R.J., Hasenohr, P., 1989. Trilobites and their trails in a black shale: Early Cambrian of the Fleurieu Peninsula, South Australia. *Transactions of the Royal Society of South Australia* 113, 195–203.

- Jiang, G-Q., Christie-Blick, N., Kaufman, A.J., Banerjee, D.M., Rai, V., 2002. Sequence stratigraphy of the Neoproterozoic Infra Krol Formation and Krol Group, lesser Himalaya, India. *Journal of Sedimentary Research* 72, 524–542.
- Johns, R.K., 1968. Geology and Mineral Resources of the Andamooka-Torrens Area. Geological Survey of South Australia Bulletin 41, 1–103.
- Johnsen, S.J., Dahl-Jensen, D., Gundestrup, N., Steffensen, J.P., Clausen, H.B., Miller, H., Masson-Delmotte, V., Sveinbjörnsdóttir, A.E., White, J., 2001. Oxygen isotope and palaeotemperature records from six Greenland ice-core stations: Camp Century, Dye-3, GRIP, GISP2, Renland and NorthGRIP. *Journal of Quaternary Science* 16, 299–307.
- Kaufman, A.J., Knoll, A.H., 1995. Neoproterozoic variations in the C-isotopic composition of seawater: stratigraphic and biogeochemical implications. *Precambrian Research* 73, 27–49.
- Kaufman, A.J., Knoll, A.H., Semikhatov, M.A., Grotzinger, J.P., Jacobsen, S.B., Adams, W., 1996. Integrated chronostratigraphy of Proterozoic–Cambrian boundary beds in the western Anabar region, northern Siberia. *Geological Magazine* 133, 509–533.
- Khomentovsky, V.V., Gibsher, A.S., 1996. The Neoproterozoic–lower Cambrian in northern Gobi-Altay, western Mongolia: Regional setting, lithostratigraphy and biostratigraphy. *Geological Magazine* 133, 371–390.
- Kirschvink, J.L., Magaritz, M., Ripperdan, R.L., Zhuravlev, A.Y., Rozanov, A.Y., 1991. The Precambrian-Cambrian boundary: Magnetostratigraphy and carbon isotopes resolve correlation problems between Siberia, Morocco, and South China. *GSA Today* 1, 69–91.
- Knauth, L.P., Kennedy, M.J., 2009. The late Precambrian greening of the Earth. *Nature* 460, 728–732.

- Knoll, A.H., Kaufman, A.J., Semikhatov, M.A., Grotzinger, J.P., Adams, W., 1995. Sizing up the sub-Tommotian unconformity in Siberia. *Geology* 23, 1139–1143.
- Kouchinsky, A., Bengtson, S., Clausen, S., Vendrasco, M.J., 2015. An early Cambrian fauna of skeletal fossils from the Emyaksin formation, northern Siberia. *Acta Palaeontologica Polonica* 60, 421–512.
- Kouchinsky, A., Bengtson, S., Landing, E., Steiner, M., Vendrasco, M., Ziegler, K., 2017. Terreneuvian stratigraphy and faunas from the Anabar Uplift, Siberia. *Acta Palaeontologica Polonica* 62, 311–440.
- Kouchinsky, A., Bengtson, S., Missarzhevsky, V.V., Pelechaty, S., Torssander, P., Val'kov, A.K., 2001. Carbon isotope stratigraphy and the problem of a pre-Tommotian Stage in Siberia. *Geological Magazine* 138, 387–396.
- Kouchinsky, A., Bengtson, S., Murdock, D.J., 2010. A new tannuolinid problematic from the lower Cambrian of the Sukharikha River in northern Siberia. *Acta Palaeontologica Polonica* 55, 321–331.
- Kouchinsky, A., Bengtson, S., Pavlov, V., Runnegar, B.N., Torssander, P., Young, E., Ziegler, K., 2007. Carbon isotope stratigraphy of the Precambrian–Cambrian Sukharikha River section, northwestern Siberian platform. *Geological Magazine* 144, 609–618.
- Kouchinsky, A., Bengtson, S., Pavlov, V., Runnegar, B.N., Val'kov, A.K., Young, E., 2005. Pre-Tommotian age of the lower Pestrotsvet Formation in the Selinde section on the Siberian platform: Carbon isotopic evidence. *Geological Magazine* 142, 319–325.
- Kouchinsky, A., Bengtson, S., Runnegar, B.N., Skovsted, C.B., Steiner, M., Vendrasco, M.J., 2012. Chronology of early Cambrian biomineralization. *Geological Magazine* 149, 221–251.

- Krogh, T.E., 1973. A low contamination method for hydrothermal decomposition of zircon and extraction of U and Pb for isotopic age determination. *Geochimica et Cosmochimica Acta* 37, 485–494.
- Kruse, P.D., 1991. Cyanobacterial-archaeocyathan-radiocyathan bioherms in the Wirrealpa Limestone of South Australia. *Canadian Journal of Earth Sciences* 28, 601–615.
- Kruse, P.D., Gandin, A., Debrenne, F., Wood, R., 1996. Early Cambrian bioconstructions in the Zavkhan Basin of western Mongolia. *Geological Magazine* 133, 429–444.
- Kruse, P.D., Jago, J.B., Laurie, J.R., 2009. Recent developments in Australian Cambrian biostratigraphy. *Journal of Stratigraphy* 33, 35–47.
- Kruse, P.D., West, P.W., 1980. Archaeocyatha of the Amadeus and Georgina basins. *Journal of Australian Geology and Geophysics* 5, 165–181.
- Kruse, P.D., Zhuravlev, A.Y., Parkhaev, P.Y., Zhu, M-Y., 2017. Comment: A new lower Cambrian shelly fossil biostratigraphy for South Australia by Marissa J. Betts, John R. Paterson, James, B. Jago, Sarah M. Jacquet, Christian B. Skovsted, Timothy P. Topper, Glenn A. Brock. *Gondwana Research* 44, 258–261.
- Landing, E., 1988. Lower Cambrian of eastern Massachusetts: Stratigraphy and small shelly fossils. *Journal of Paleontology* 62, 661–695.
- Landing, E., 1989. Paleoecology and distribution of the Early Cambrian rostroconch *Watsonella crosbyi* Grabau. *Journal of Paleontology* 63, 566–573.
- Landing, E. 1992. Lower Cambrian of southeastern Newfoundland: Epirogeny and Lazarus faunas, lithofacies-biofacies linkages, and the myth of a global biostratigraphy. In: Lipps, J., Signor, P.W. (Eds). *Origin and Early Evolution of the Metazoa*. Plenum Press, New York, pp. 283–309.

- Landing, E., 1995. Upper Placentian—Branchian series of mainland Nova Scotia (middle-upper Lower Cambrian): Faunas, paleoenvironments, and stratigraphic revision. *Journal of Paleontology* 69, 475–495.
- Landing, E., Bartowski, K.E., 1996. Oldest shelly fossils from the Taconic allochthon and late Early Cambrian sea-levels in eastern Laurentia. *Journal of Paleontology* 70, 741–761.
- Landing, E., Benus, A.P. 1988. Cambrian depositional history and stratigraphy, Avalon-Bonavista region, southeastern Newfoundland. Geological Association of Canada, Field Trip Guidebook, pp. 1–50.
- Landing, E., Geyer, G. 2012. Misplaced faith—limitations of the first appearance datum (FAD) in chronostratigraphy and proposal of more robust Lower Cambrian correlation standards. *Journal of Guizhou University (Natural Science)* 29, 170–171.
- Landing, E., Westrop, S.R., 1998. Cambrian faunal sequence and depositional history of Avalonian Newfoundland and New Brunswick: Field workshop. *New York State Museum Bulletin*, 492, pp. 5–75.
- Landing, E., Geyer, G., Brasier, M.D., Bowring, S.A., 2013. Cambrian Evolutionary Radiation: Context, correlation, and chronostratigraphy—overcoming deficiencies of the first appearance datum (FAD) concept. *Earth-Science Reviews* 123, 133–172.
- Landing, E., Kouchinsky, A., 2016. Correlation of the Cambrian Evolutionary Radiation: Geochronology, evolutionary stasis of earliest Cambrian (Terreneuvian) small shelly fossil (SSF) taxa, and chronostratigraphic significance. *Geological Magazine* 153, 750–756.
- Landing, E., Kruse, P.D., 2017. Integrated stratigraphic, geochemical, and paleontological late Ediacaran to early Cambrian records from southwestern Mongolia: Comment. *Geological Society of America Bulletin* 129, 1012–1015.

- Larsson, C.M., Skovsted, C.B., Brock, G.A., Balthasar, U., Topper, T.P., Holmer, L.E., 2014. *Paterimitra pyramidalis* from South Australia: scleritome, shell structure and evolution of a lower Cambrian stem group brachiopod. *Palaeontology* 57, 417–446.
- Li, D., Ling, H.F., Jiang, S.Y., Pan, J.Y., Chen, Y.Q., Cai, Y.F., Feng, H.Z., 2009. New carbon isotope stratigraphy of the Ediacaran–Cambrian boundary interval from SW China: Implications for global correlation. *Geological Magazine* 146, 465–484.
- Li, G-X., Xiao, S-H., 2004. *Tannuolina* and *Micrina* (Tannuolinidae) from the Lower Cambrian of eastern Yunnan, south China, and their scleritome reconstruction. *Journal of Paleontology* 78, 900–913.
- Li, G-X., Zhao, X., Gubanov, A., Zhu, M-Y., Na, L., 2011. Early Cambrian mollusc *Watsonella crosbyi*: a potential GSSP index fossil for the base of the Cambrian Stage 2. *Acta Geologica Sinica* 85, 309–319.
- Ludwig, K.R., 2003. User's Manual for Isoplot 3.00. Berkeley Geochronology Center. Berkeley, CA. 1–70.
- MacNaughton, R.B., Narbonne, G.M., 1999. Evolution and ecology of Neoproterozoic–Lower Cambrian trace fossils, NW Canada. *Palaios* 14, 97–115.
- Magaritz, M., Holser, W.T., Kirschvink, J.L., 1986. Carbon-isotope events across the Precambrian/Cambrian boundary on the Siberian Platform. *Nature* 320, 258–259.
- Malooof, A.C., Porter, S.M., Moore, J.L., Dudás, F.Ö., Bowring, S.A., Higgins, J.A., Fike, D.A., Eddy, M.P. 2010a. The earliest Cambrian record of animals and ocean geochemical change. *Geological Society of America Bulletin* 122, 1731–1774.
- Malooof, A.C., Ramezani, J., Bowring, S.A., Fike, D.A., Porter, S.M., Mazouad, M., 2010b. Constraints on Early Cambrian carbon cycling from the duration of the Nemakit-Daldynian-Tommotian boundary  $\delta^{13}\text{C}$  shift, Morocco. *Geology* 38, 623–626.

- Maloof, A.C., Schrag, D.P., Crowley, J.L., Bowring, S.A., 2005. An expanded record of Early Cambrian carbon cycling from the Anti-Atlas Margin, Morocco. *Canadian Journal of Earth Sciences* 42, 2195–2216.
- Mángano, M.G., Buatois, L.A., 2014. Decoupling of body-plan diversification and ecological structuring during the Ediacaran–Cambrian transition: Evolutionary and geobiological feedbacks. *Proceedings of the Royal Society, B* 281, No. 1780, 20140038.
- Mángano, M.G., Buatois, L.A., 2017. The Cambrian revolutions: Trace-fossil record, timing, links and geobiological impact. *Earth-Science Reviews* 173, 96–108.
- Marshall, C.R., 2006. Explaining the Cambrian “Explosion” of Animals. *Annual Review of Earth and Planetary Science* 34, 355–384.
- Marshall, J.D., 1992. Climatic and oceanographic isotopic signals from the carbonate rock record and their preservation. *Geological Magazine* 129, 143–160.
- Mathewson, C.P., 2016. Biostratigraphy and chemostratigraphy of the lower Cambrian Normanville Group, South Australia. Macquarie University, Sydney. Masters thesis, unpublished.
- Matthews, S.T., Missarzhevsky, V.V., 1975. Small shelly fossils of late Precambrian and early Cambrian age: a review of recent work. *Journal of the Geological Society* 131, 289–303.
- Mattinson, J.M., 2005. Zircon U-Pb chemical abrasion (“CA-TIMS”) method: combined annealing and multi-step partial dissolution analysis for improved precision and accuracy of zircon ages. *Chemical Geology* 220, 47–66.
- Melim, L.A., Swart, P.K., Maliva, R.G., 2001. Meteoric and marine-burial diagenesis in the subsurface of Great Bahama Bank. In: Ginsberg, R.N. (Ed.), *Subsurface Geology of a Prograding Carbonate Platform Margin, Great Bahama Bank: Results of the Bahamas Drilling Project*. SEPM Special Publication 70, pp. 137–162.



- Missarzhevsky, V.V., Mambetov, A. 1981. Stratigrafiya i fauna pogranichnykh sloev kembriya i dokembriya Malogo Karatau. Trudy Ordena Trudovogo Krasnogo Znameni Geologicheskii Institut, Akademiya Nauk SSSR 326, 92 [In Russian].
- Mount, J.F., Kidder, D., 1993. Combined flow origin of edgewise intraclast conglomerates: Sellick Hill Formation (Lower Cambrian), South Australia. *Sedimentology* 40, 315–329.
- Pan, B., Brock, G.A., Skovsted, C.B., Betts, M.J., Topper, T.P., Li, G-X., In press. *Paterimitra pyramidalis* Laurie, 1986, the first tommotiid discovered from the early Cambrian of North China. *Gondwana Research*.
- Pan, B., Topper, T.P., Skovsted, C.B., Miao, L-M., Li, G-X., 2017. Occurrence of *Microdictyon* from the lower Cambrian Xinji Formation along the southern margin of the North China Platform. *Journal of Paleontology* 92, 59–70.
- Parkhaev, P.Y., 2014. On the stratigraphy of *Aldanella attleborensis*—potential index species for defining the base of Cambrian Stage 2. In IGCP Project 591 Field Workshop, pp. 102–105.
- Parkhaev, P.Y., Karlova, G.A., 2011. Taxonomic revision and evolution of Cambrian mollusks of the genus *Aldanella* Vostokova, 1962 (Gastropoda: Archaeobranchia). *Paleontological Journal* 45, 1145–1205.
- Paterson, J.R., Brock, G.A., 2007. Early Cambrian trilobites from Angorichina, Flinders Ranges, South Australia, with a new assemblage from the *Pararaia bunyeroensis* Zone. *Journal of Paleontology* 81, 116–142.
- Paterson, J.R., Edgecombe, G.D., 2006. The Early Cambrian trilobite family Emuellidae Pocock, 1970: systematic position and revision of Australian species. *Journal of Paleontology* 80, 496–513.

Paterson, J.R., Edgecombe, G.D., García-Bellido, D.C., Jago, J.B., Gehling, J.G., 2010.

Nektaspid arthropods from the lower Cambrian Emu Bay Shale Lagerstätte, South Australia, with a reassessment of lamellipedian relationships. *Palaeontology* 53, 377–402.

Paterson, J.R., García-Bellido, D.C., Jago, J.B., Gehling, J.G., Lee, M.S.Y., Edgecombe, G.D., 2016. The Emu Bay Shale Konservat-Lagerstätte: a view of Cambrian life from East Gondwana. *Journal of the Geological Society* 173, 1–11.

Paterson, J.R., Jago, J.B., Brock, G.A., Gehling, J.G., 2007. Taphonomy and palaeoecology of the emuellid trilobite *Balcoracania dailyi* (early Cambrian, South Australia). *Palaeogeography, Palaeoclimatology, Palaeoecology* 249, 302–321.

Peng, S-C., Babcock, L.E., 2011. Continuing progress on chronostratigraphic subdivision of the Cambrian System. *Bulletin of Geosciences* 86, 391–396.

Peng, S-C., Babcock, L., Cooper, R. 2012. The Cambrian Period. In: Gradstein, F.M., Ogg, J.G., Schmitz, M., Ogg, G. (Eds.), *The geologic time scale, Volume 2*. Elsevier, Amsterdam, pp. 437–488.

Peng, S-C., Babcock, L.E., Robison, R.A., Lin, H-L., Rees, M.N., Saltzman, M.R., 2004. Global Standard Stratotype-section and Point (GSSP) of the Furongian Series and Paibian Stage (Cambrian). *Lethaia* 37, 365–379.

Peng, S-C., Robison, R.A., 2000. Agnostoid biostratigraphy across the Middle-Upper Cambrian boundary in Hunan, China. *Paleontological Society Memoir* 53, 1–104.

Pocock, K.J., 1970. The Emuellidae, a new family of trilobites from the Lower Cambrian of South Australia. *Palaeontology* 13, 522–562.

Randell, R.D., Lieberman, B.S., Hasiotis, S.T., Pope, M.C., 2005. New cancelloriids from the Early Cambrian Sekwi Formation with a comment on cancelloriid affinities. *Journal of Paleontology* 79, 987–996.

- Remane, J., Basset, M.G., Cowie, J.W., Gohrbandt, K.H., Lane, H.R., Michelsen, O., Naiwen, W. 1996. Revised guidelines for the establishment of global chronostratigraphic standards by the International Commission on Stratigraphy (ICS). *Episodes* 19, 77–81.
- Ren, Y., Zhong, D-K., Gao, C-L., Liang, T., Sun, H-T., Wu, D., Zheng, X-W., 2017. High-resolution carbon isotope records and correlations of the lower Cambrian Longwangmiao formation (stage 4, Toyonian) in Chongqing, South China. *Palaeogeography, Palaeoclimatology, Palaeoecology* 485, 572–592.
- Ripperdan, R.L., 1994. Global variations in carbon isotope composition during the latest Neoproterozoic and earliest Cambrian. *Annual Reviews of Earth and Planetary Science* 22, 385–417.
- Rowland, S.M., Luchinina, V.A., Korovnikov, I.V., Sipin, D.P., Tarletskov, A.I., Fedoseev, A.V., 1998. Biostratigraphy of the Vendian-Cambrian Sukharikha River section, northwestern Siberian Platform. *Canadian Journal of Earth Sciences* 35, 339–352.
- Rožanov, A.Y., Missarzhevsky, V.V., Volkova, N., Voronova, L., Krylov, I., Keller, B., Korolyuk, I., Lenzion, K., Michniak, R., Pyrkhova, N., 1969. The Tommotian Stage and the Cambrian lower boundary problem. *Transactions of the Academy of Sciences of the USSR Nauka* 206, 1–380.
- Rožanov, A.Y., Repina, L.N., Apollonov, M.K., Shabanov, Y.Y., Zhuravlev, A.Y., Pegel', T.V., Fedorov, A.B., Astashkin, V.A., Zhuravleva, I.T., Egorova, L.I., Chugaeva, M.N., Dubinina, S.V., Ermak, V.V., Esakova, N.V., Sundukov, V.V., Sukhov, S.S., Zhemchuzhnikov, V.G. 1992. *Kembrij Sibiri [The Cambrian of Siberia]*. Novosibirsk, Nauka, 135 pp. [In Russian].

- Rozanov, A.Y., Zhuravlev, A.Y., 1992. The lower Cambrian fossil record of the Soviet Union. In: Lipps, J. and Signor, P.W. (Eds.), Origin and Early Evolution of the Metazoa. Plenum Press, New York, pp. 205–282.
- Schmid, S., 2017. Chemostratigraphy and palaeo-environmental characterisation of the Cambrian stratigraphy in the Amadeus Basin, Australia. *Chemical Geology* 451, 169–182.
- Schmitz, M.D., Schoene, B., 2007. Derivation of isotope ratios, errors and error correlations for U-Pb geochronology using  $^{205}\text{Pb}$ - $^{235}\text{U}$ -( $^{233}\text{U}$ )-spiked isotope dilution thermal ionization mass spectrometric data. *Geochemistry, Geophysics, Geosystems* 8, Q08006, doi:10.1029/2006GC001492.
- Skovsted, C.B., 2004. Mollusc fauna of the Early Cambrian Bastion Formation of north-east Greenland. *Bulletin of the Geological Society of Denmark* 51, 11–37.
- Skovsted, C.B., Balthasar, U., Brock, G.A., Paterson, J.R., 2009a. The tommotiid *Camarella reticulosa* from the early Cambrian of South Australia: Morphology, scleritome reconstruction, and phylogeny. *Acta Palaeontologica Polonica* 54, 525–540.
- Skovsted, C.B., Betts, M.J., Topper, T.P., Brock, G.A., 2015a. The early Cambrian tommotiid genus *Dailyatia* from South Australia. *Memoirs of the Association of Australasian Palaeontologists* 48, 1–117.
- Skovsted, C.B., Brock, G., Holmer, L., Paterson, J.R., 2009b. First report of the early Cambrian stem group brachiopod *Mickwitzia* from East Gondwana. *Gondwana Research* 16, 145–150.
- Skovsted, C.B., Brock, G.A., Holmer, L.E., Topper, T.P., Larsson, C.M., 2015b. The early Cambrian tommotiid *Kulparina rostrata* from South Australia. *Journal of Paleontology* 89, 920–932.
- Skovsted, C.B., Brock, G.A., Paterson, J.R., 2006. Bivalved arthropods from the Lower Cambrian Mernmerna Formation, Arrowie Basin, South Australia and their

- implications for identification of Cambrian 'small shelly fossils'. *Memoirs of the Association of Australasian Palaeontologists* 32, 7–41.
- Skovsted, C.B., Brock, G.A., Paterson, J.R., Holmer, L.E., Budd, G.E., 2008. The scleritome of *Eccentrotheca* from the Lower Cambrian of South Australia: Lophophorate affinities and implications for tommotiid phylogeny. *Geology* 36, 171–174.
- Skovsted, C.B., Pan, B., Topper, T.P., Betts, M.J., Li, G-X., Brock, G.A., 2016. The operculum and mode of life of the lower Cambrian hyolith *Cupithea* from South Australia and North China. *Palaeogeography, Palaeoclimatology, Palaeoecology* 443, 123–130.
- Skovsted, C.B., Brock, G.A., Topper, T.P., Paterson, J.R., Holmer, L.E., 2011. Scleritome construction, biofacies, biostratigraphy and systematics of the tommotiid *Eccentrotheca helenia* sp. nov. from the Early Cambrian of South Australia. *Palaeontology* 54, 253–286.
- Skovsted, C.B., Clausen, S., Álvaro, J.J., Ponlevé, D., 2014a. Tommotiids from the early Cambrian (Series 2, Stage 3) of Morocco and the evolution of the tannuolinid scleritome and setigerous shell structures in stem group brachiopods. *Palaeontology* 57, 71–192.
- Skovsted, C.B., Peel, J.S., 2007. Small shelly fossils from the argillaceous facies of the Lower Cambrian Forteau Formation of western Newfoundland. *Acta Palaeontologica Polonica* 52, 729–748.
- Skovsted, C.B., Topper, T.P., Betts, M.J., Brock, G.A., 2014b. Associated conchs and opercula of *Triplicatella disdoma* (Hyolitha) from the early Cambrian of South Australia. *Alcheringa* 38, 148–153.

- Smith, A.G., Barry, T., Bown, P., Cope, J., Gale, A., Gibbard, P., Gregory, J., Hounslow, M., Kemp, D., Knox, R. 2015. GSSPs, global stratigraphy and correlation. Geological Society, London, Special Publication 404, 37–67.
- Smith, D.G., Bailey, R.J., Burgess, P.M., Fraser, A.J., 2015. Strata and time: probing the gaps in our understanding. Geological Society, London, Special Publication 404, 1–10.
- Smith, E.F., Macdonald, F.A., Petach, T.A., Bold, U., 2017. Integrated stratigraphic, geochemical, and paleontological late Ediacaran to early Cambrian records from southwestern Mongolia: Reply. Geological Society of America Bulletin 129, 1016–1018.
- Smith, E.F., Macdonald, F.A., Petach, T.A., Bold, U. and Schrag, D.P. 2016. Integrated stratigraphic, geochemical, and paleontological late Ediacaran to early Cambrian records from southwestern Mongolia. Geological Society of America Bulletin 128, 442–468.
- Steiner, M., Li, G-X., Qian, Y., Zhu, M., 2004. Lower Cambrian small shelly fossils of northern Sichuan and southern Shaanxi (China), and their biostratigraphic importance. *Geobios* 37, 259–275.
- Steiner, M., Li, G-X., Qian, Y., Zhu, M-Y., Erdtmann, B.-D., 2007, Neoproterozoic to Early Cambrian small shelly fossil assemblages and a revised biostratigraphic correlation of the Yangtze Platform (China). *Palaeogeography, Palaeoclimatology, Palaeoecology* 254, 67–99.
- Steiner, M., Weber, B., Geyer, G., 2001. The lower Cambrian of eastern Yunnan: Trilobite-based biostratigraphy and related faunas. *Acta Palaeontologica Sinica* 40, 63–79.
- Steiner, M., Yang, B., 2017. The chronostratigraphic subdivision of the traditional “Lower Cambrian” – How reliable are chemostratigraphy and biostratigraphy? McIlroy, D.

- (Ed.), International Symposium on the Ediacaran-Cambrian Transition, St. John's, Newfoundland, Canada. Abstract Volume, p. 113.
- Swart, P.K., 2008. Global synchronous changes in the carbon isotopic composition of carbonate sediments unrelated to changes in the global carbon cycle. *Proceedings of the National Academy of Sciences* 105, 13741–13745.
- Swart, P.K., 2015. The geochemistry of carbonate diagenesis: The past, present and future. *Sedimentology* 62, 1233–1304.
- Swart, P.K., Eberli, G., 2005. The nature of the  $\delta^{13}\text{C}$  of periplatform sediments: implications for stratigraphy and the global carbon cycle. *Sedimentary Geology* 175, 115–129.
- Swart, P.K., Kennedy, M., 2012. Does the global stratigraphic reproducibility of  $\delta^{13}\text{C}$  in Neoproterozoic carbonates require a marine origin? A Pliocene–Pleistocene comparison. *Geology* 40, 87–90.
- Topper, T.P., Brock, G.A., Skovsted, C.B., Paterson, J.R., 2009. Shelly fossils from the Lower Cambrian *Pararaia bunyerooensis* Zone, Flinders Ranges, South Australia. *Memoirs of the Association of Australasian Palaeontologists* 37, 199–246.
- Topper, T.P., Brock, G.A., Skovsted, C.B., Paterson, J.R., 2010. Palaeoscolecid scleritome fragments with *Hadimopanella* plates from the early Cambrian of South Australia. *Geological Magazine* 147, 86–97.
- Topper, T.P., Brock, G.A., Skovsted, C.B., Paterson, J.R., 2011. *Microdictyon* plates from the lower Cambrian Ajax Limestone of South Australia: Implications for species taxonomy and diversity. *Alcheringa* 35, 427–443.
- Topper, T.P., Holmer, L.E., Skovsted, C.B., Brock, G.A., Balthasar, U., Larsson, C.M., Petterson-Stolk, S., Harper, D.A.T., 2013. The oldest brachiopods from the lower Cambrian of South Australia. *Acta Palaeontologica Polonica* 58, 93–109.

- Topper, T.P., Skovsted, C.B., Brock, G.A., Paterson, J.R., 2007. New bradoriids from the lower Cambrian Mernmerna Formation, South Australia: Systematics, biostratigraphy and biogeography. *Memoirs of the Association of Australasian Palaeontologists* 33, 67–100.
- Topper, T.P., Skovsted, C.B., Brock, G.A., Paterson, J.R., 2011. The oldest bivalved arthropods from the early Cambrian of East Gondwana: Systematics, biostratigraphy and biogeography. *Gondwana Research* 19, 310–326.
- Tucker, M.E., 1989. Carbon isotopes and Precambrian—Cambrian boundary geology, South Australia: Ocean basin formation, seawater chemistry and organic evolution. *Terra Nova* 1, 573–582.
- Voronin, Y.I., Voronova, L.G., Grigorieva, N.V., Drosdova, N.A., Zhegallo, E.A., Zhuravlev, A.Y., Ragozina, A.L., Rozanov, A.Y., Sayutina, T.A., Sysoiev, V.A., Fonin, V.D., 1982. Granitsa dokembriya i kembriya v geosinklinal'nykh rayonakh (opornyy razrez Salany-Gol, Mongol'skaya narodnaya respublika) [The Precambrian and Cambrian boundary in the Geosynclinal Areas (Reference Section of Salany-Gol, Mongolian People's Republic)]. *The Joint Soviet-Mongolian Paleontological Expedition, Transactions* 18, 1–150.
- Weiner, S., Dove, P.M., 2003. An overview of biomineralization processes and the problem of the vital effect. *Reviews in Mineralogy and Geochemistry* 54, 1–29.
- Weissert, H., Erba, E., 2004. Volcanism, CO<sub>2</sub> and palaeoclimate: a Late Jurassic–Early Cretaceous carbon and oxygen isotope record. *Journal of the Geological Society* 161, 695–702.
- Weissert, H., Joachinski, M., Sarnthein, M. 2008. Chemostratigraphy. *Newsletters on Stratigraphy* 42, 145–179.



- Wendler, I., 2013. A critical evaluation of carbon isotope stratigraphy and biostratigraphic implications for Late Cretaceous global correlation. *Earth-Science Reviews* 126, 116–146.
- Wood, R., Zhuravlev, A.Y., 2012. Escalation and ecological selectivity of mineralogy in the Cambrian Radiation of skeletons. *Earth-Science Reviews* 115, 249–261.
- Yang, C., Li, X-H., Zhu, M-Y., Condon, D.J., Chen, J-Y. 2018. Geochronological constraint on the Cambrian Chengjiang biota, South China. *Journal of the Geological Society*. doi.org/10.11445/jgs2017-103.
- Yang, B., Steiner, M., Keupp, H., 2015. Early Cambrian palaeobiogeography of the Zhenba–Fangxian Block (South China): Independent terrane or part of the Yangtze Platform? *Gondwana Research* 28, 1543–1565.
- Youngs, B.C., 1977. The sedimentology of the Cambrian Wirrealpa and Aroona Creek limestones. *Geological Survey of South Australia Bulletin* 47, 1–73.
- Youngs, B.C., Moorcroft, E., 1982. The petroleum potential of the eastern Arrowie Basin and Frome Embayment. *The APPEA Journal* 22, 82–101.
- Yun, H., Zhang, X-L., Li, L-Y., 2017. Chancelloriid *Allonnia erjiensis* sp. nov. from the Chengjiang Lagerstätte of South China. *Journal of Systematic Palaeontology* 16, 435–444.
- Yun, H., Zhang, X-L., Li, L-Y., Zhang, M-Q., Liu, W., 2016. Skeletal fossils and microfacies analysis of the lowermost Cambrian in the southwestern margin of the North China Platform. *Journal of Asian Earth Sciences* 129, 54–66.
- Zang, W-L., 2002. Sequence analysis and petroleum potential in the Arrowie Basin, South Australia. Department of Primary Industries and Resources, South Australia, Report Book 24, 1–170.

- Zang, W-L., Jago, J.B., Alexander, E.M., Paraschivoiu, E., 2004. A review of basin evolution, sequence analysis and petroleum potential of the frontier Arrowie Basin, South Australia. In: Boulton, P. J., Johns, D.R., Lang, S.C. (Eds.), Eastern Australian Basins Symposium II. Petroleum Exploration Society of Australia, Special Publication, pp. 243–256.
- Zang, W-L., Jago, J.B., Lin, T.R. 2001. Early Cambrian acritarchs, trilobites and archaeocyathids from Yalkalpo 2, eastern Arrowie Basin, South Australia. Department of Primary Industries and Resources, South Australia, Report Book 2001/00002, 1–41.
- Zang, W-L., Moczydlowska, M., Jago, J.B., 2007. Early Cambrian acritarch assemblage zones in South Australia and global correlation. *Memoirs of the Association of Australasian Palaeontologists* 33, 141–170.
- Zhang, X-L., Ahlberg, P., Babcock, L.E., Choi, D.K., Geyer, G., Gozalo, R., Hollingsworth, J.S., Li, G-X., Naimark, E.B., Pegel, T., Steiner, M., Wotte, T. Zhang, Z-F., 2017. Challenges in defining the base of Cambrian Series 2 and Stage 3. *Earth-Science Reviews* 172, 124–139.
- Zhang, J-M., Li, G-X., Zhou, C-M., Zhu, M-Y., Yu, Z-Y., 1997. Carbon isotope profiles and their correlation across the Neoproterozoic–Cambrian boundary interval on the Yangtze Platform, China. *Bulletin of the National Museum of Natural Science* 10, 107–116.
- Zhou, C-M., Zhang, J-M., Li, G-X., Yu, Z-Y., 1997. Carbon and oxygen isotopic record of the Early Cambrian from the Xiaotan Section, Yunnan, South China. *Scientia Geologica Sinica*. 32, 201–211.

- Zhu, M-Y., Babcock, L., Peng, S-C., 2006. Advances in Cambrian stratigraphy and paleontology: Integrating correlation techniques, paleobiology, taphonomy and paleoenvironmental reconstruction. *Palaeoworld* 15, 216–222.
- Zhu, M-Y., Zhang, J-M., Li, G-X., Yang, A-H., 2004. Evolution of C isotopes in the Cambrian of China: implications for Cambrian subdivision and trilobite mass extinctions. *Geobios* 37, 287–301.
- Zhuravlev, A.Y., 1995. Preliminary suggestions on the global Early Cambrian zonation. In: Geyer, G., Landing, E. (Eds.), *Morocco 95. The Lower-Middle Cambrian standard of western Gondwana. Beringeria Special Issue 2*, pp. 147–160.
- Zhuravlev, A.Y., Gravestock, D.I., 1994. Archaeocyaths from Yorke Peninsula, South Australia and archaeocyathan Early Cambrian zonation. *Alcheringa* 18, 1–54.

## Figure captions

Fig. 1. Extent of the Arrowie Basin, South Australia showing Cambrian outcrop and locations of measured sections and drill cores used to generate the shelly fossil biostratigraphy of Betts et al. (2016, 2017b). Sections and drill cores also targeted for stable isotope analyses (present study) are highlighted in orange.

Fig. 2. Regional geological map of the Normanville Group between Sellicks Hill and Normanville along the Fleurieu Peninsula, South Australia. Locations of the SHL, FTL, WANG-S and WANG sections are indicated.

Fig. 3. WANG-S and WANG stratigraphic sections through the Wangkonda and Sellick Hill formations on the Fleurieu Peninsula. Positions of the ZHUCE and SHICE (7p)  $\delta^{13}\text{C}$  excursions are indicated. In the WANG section, the *Kulparina rostrata* Zone occurs in Facies D and E of the Sellick Hill Formation. Ich = ichnofossils, Tomm + SSF = tommotiids and small shelly fossils, Brach = brachiopods.

Fig. 4. SHL and FTL stratigraphic sections through the Sellick Hill Formation and Fork Tree Limestone on the Fleurieu Peninsula. The *Kulparina rostrata* Zone occurs in the upper Sellick Hill Formation and through the Fork Tree Limestone. Upper part of the SHICE is captured through the SHL section.

Fig. 5. Thin section photomicrographs of fabrics and textures in carbonates from the Wangkonda and Sellick Hill formations in the WANG-S section, Fleurieu Peninsula. A, WANG-S/10, micritic lime mudstone with microcrystalline dolomite. B, WANG-S/50, medium crystalline, anhedral nonplanar fabric-obliterative dolomite. C, Magnification of B;

tightly packed anhedral nonplanar dolomite spar. D, WANG-S/80, dolomitised oncoidal grainstones with microsparite (light) and fine crystalline iron-rich dolomites (dark) replacing the intergranular matrix and interiors of some oncoids. E, magnification of D; fine crystalline, porphyrotopic iron-rich dolomites interdispersed through clotted microsparite. F, WANG-S/90, fenestral limestone. G, Magnification of F; vugs filled with coarse-crystalline euhedral planar dolomite and calcite cements. H, WANG-S/130, fenestral limestone, vugs filled mostly with calcite, partial dissolution associated with stylolites. I, WANG-S/151, bioturbated quartz-rich lime mudstone with mottled silty layers. J, WANG-S/181, micritic lime mudstone contact with microcrystalline dolomite. K, WANG-S/191, recrystallised oolitic grainstone with ooids replaced by microcrystalline dolomite within a microsparite matrix. L, WANG-S/219, fenestral limestone. M, WANG-S/230 (top of Wangkonda Formation), peloidal grainstone with fenestral fabric in top-most part of the thin section, strong dissolution in association with stylolites. N-P (base of Sellick Hill Formation, Facies Association A), WANG-S/230, WANG-S/237, WANG-S/250, laminated to bioturbated fine sandstones and mudstones, with some soft sediment deformation.

Fig. 6. Thin section photomicrographs of fabrics and textures in carbonates from the Wangkonda and Sellick Hill formations in the WANG section, Fleurieu Peninsula. A–E, Wangkonda Formation. A, WANG/1.0, replaced oolitic grainstone with euhedral well-zoned dolomites occupying void space left by individual ooids within microsparite matrix. B, WANG/40, medium-coarse crystalline planar-s to nonplanar-a, fabric-obliterative dolomite. C–D, WANG/60, WANG/70, fine to coarse crystalline, planar-s to nonplanar-a, fabric-obliterative dolomite. E, WANG/90, fine-grained quartz sandstone with framboidal pyritic clusters. F–I, Sellick Hill Formation, Facies Association A. F, WANG/100, very fine-grained quartz sandstone, silty stringers indicate bioturbation. G, WANG/110A, slightly deformed

oolitic grainstone. H, WANG/130, peloidal grainstone with stylolites, dissolution seams and very fine quartz grains. I, WANG/132, peloidal grainstone shows deformation by tectonic processes. J, Facies Association B, WANG/146.5, poorly sorted, sub-rounded quartz sandstone. K-O, Facies Association C. WANG/167, WANG/184, WANG/210, WANG/225 WANG/256, bioturbated, laminated fine-grained calcareous sandstones and siltstones. P-Q, WANG/321, Facies Association D, phosphatic hardground characterized by bioclastic wackestones and darkened omission surfaces. R-S, Facies Association E. R, WANG/331, fine-grained calcareous sandstones with silty interbeds. S, WANG/342, nodular lime mudstone with silty interstitial matrix.

Fig. 7. Phosphatised steinkerns of shelly fauna from WANG-S/190. A-E, *Hyolithellus* sp. steinkerns, SAM P55487, SAM P55488, SAM P55489, SAM P55490, SAM P55491. F, *Australohalkieria* sp. siculate sclerite, SAM P55492. G, tube-shaped problematica, SAM P55493. H-J, hyolith steinkerns, SAM P55494, SAM P55495, SAM P55496. K, *?Bemella* sp., SAM P55497. L. *?Anabarella* sp., SAM P55498. Specimens are lodged in the South Australian Museum (palaeontological collections).

Fig. 8. A. *Diplocraterion* sp. in sandy intervals in the Wangkonda Formation, Fleurieu Peninsula, scale bar = 5 cm. B. Thrombolites in the Wirrealpa Limestone, southern Flinders Ranges, scale bar = 0.5 m. C, Archaeocyath talus in the biohermal Hideaway Creek Member of the Wilkawillina Limestone (MORO section), northern Flinders Ranges, hammer = 34 cm long. D, boulder of archaeocyath-rich biohermal Wilkawillina Limestone resting on laminated, ribbon limestones, hammer = 34 cm long. E, flat-pebble conglomerate in Facies C of the Sellick Hill Formation, Fleurieu Peninsula. F, ribbon limestones in Facies E of the Sellick Hill Formation, Fleurieu Peninsula, hammer = 30 cm long. G, cast of *?Bemella* sp.

from the Parachilna Formation, Mt. Scott Range (Brian Daily Collections, SAM P40145), scale in millimeters.

Fig. 9. Phosphatic and secondarily phosphatised shelly fauna from the WANG section. A–C, *Askepasma* cf. *A. saproconcha*. A, WANG/380.0, SAM P55499, B, WANG/388, SAM P55500, C, WANG/251, SAM P55501. D, E, *Sunnaginia imbricata*, WANG/321, SAM P55502, SAM P55503. F–K, M, O, *Dailyatia ajax*. F, WANG/388, SAM P55504, G, WANG/321, SAM P55505. H, WANG/321, SAM P55506. I, WANG/404, SAM P55507. J, WANG/380, SAM P55508. K, WANG/321, SAM P55509. M, WANG/388, SAM P55510. O, WANG/358, SAM P55511. L, N, P, *Dailyatia bacata*. L, WANG/358, SAM P55512. N, WANG/358, SAM P55513. P, WANG/358, SAM P55514. Q–R, indeterminate hyolithelminths. P, WANG/321, SAM P55515. Q, WANG/321, SAM P55516. S, *Cupithec* sp., WANG/404, SAM P55517. S–V, indeterminate halkieriid sclerites. T, siculate sclerite, WANG/321, SAM P55518. U, cultrate sclerite, WANG/321, SAM P55519. V, palmate sclerite, WANG/321, SAM P55520. W, cultrate sclerite, WANG/321, SAM P55521. X, *Australohalkieria parva*, palmate sclerites, WANG/404, SAM P55522. Specimens are lodged in the South Australian Museum (palaeontological collections).

Fig. 10. Thin section photomicrographs of fabrics and textures in carbonates and siliciclastics from the SHL section, Sellick Hill Formation. A–J, Facies Association C. A–B (SHL/0.0, SHL/2.1), I, H (SHL/23.7), rounded clasts of lime mudstone with varying proportions of very fine-grained quartz sand within a quartz-rich matrix. C–E, SHL/3.1, fine quartz sandstone, with fine, calc-mud laminations. D–E. Magnifications of C; D, pyritic framboidal clusters within very fine-grained quartz sand, E, Shows sharp contact between calcareous mudstone layer and overlying very fine-grained sands. F–G, SHL/6.3, laminated, bioturbated calcareous

siltstone. G, Magnification of F; cross-section of burrow infilled with very fine-grained quartz sand. H, magnification of I; pyrite framboids, and limonite alteration haloes. J, K, SHL/37.0, SHL/50.8, well-laminated, slightly bioturbated lime mudstone with very-fine quartz grains between interstitial layers of silt. L, SHL/50.9, Facies Association D, bioclastic wackestone to packstone with closely spaced, phosphate-rich omission surfaces. Small shelly fossils including hyoliths and chancelloriids are easily distinguishable. Very fine quartz grains are present throughout, occasionally lining the top of omission surfaces. M–O, Facies Association E. M, SHL/82.5, bioturbated interbedded lime mudstone, fine quartz sandstone and siltstone. N–O, SHL/91.8, bioclastic wackestone with complete and fragmented archaeocyaths within a lime mud matrix. O, magnification of N; cross-section of regular archaeocyath.

Fig. 11. WAR stratigraphic section through the Woodendinna Dolostone and the Wirrapowie Limestone at Warragee Bore, central Flinders Ranges, with ranges of key taxa through the *Kulparina rostrata* Zone. The upper SHICE is captured in the Wirrapowie Limestone in the WAR section. Br = Brachiopods.

Fig. 12. Thin section photomicrographs of fabrics and textures in carbonates from the Wirrapowie Limestone in the WAR section. A–C, WAR/20.6, WAR, 56.6, intraclastic packstones; clasts composed of laminated to homogenous micritic mudstones with peloidal grainstone as the interstitial matrix (B). D, WAR/175, well-sorted intraclastic grainstone composed mostly of rounded calcareous mudstone and some radial calcitic ooids. E, WAR/296.3, poorly sorted intraclastic packstone with predominantly elongate homogenous lime mudstone clasts in a micritic matrix; umbrella voids under clasts filled with calcite. F, WAR/208, finely-laminated columnar stromatolite bindstone. G, WAR/362, bioturbated lime



mudstone with very fine quartz sand. H, WAR/396, archaeocyath packstone with clotted textures in micrites and calcite filled vugs, most archaeocyaths fragmented. I–J, WAR/405.7, WAR/655, bioclastic packstones containing abundant fragmented archaeocyaths and other shelly fauna. K. WAR/779, stylotised lime mudstone.

Fig. 13. MORO stratigraphic section through the Parachilna Formation, Woodendinna Dolostone, and Wilkawillina and Wirrapowie limestones in the Arrowie Syncline, northern Flinders Ranges, with key shelly fossil taxa through the *Kulparina rostrata* and *Micrina etheridgei* zones.  $\delta^{13}\text{C}$  values suggestive of the SHICE occur in the lower parts of the section, and positive  $\delta^{13}\text{C}$  events II and III occur in the Hideaway Well and Winnytinn Creek members of the Wilkawillina Limestone, with the III excursion straddling the boundary between the *K. rostrata* and *M. etheridgei* zones. Brach = brachiopods.

Fig. 14. Thin section photomicrographs of fabrics and textures in carbonates from the Parachilna Formation, Woodendinna Dolostone and Wilkawillina and Wirrapowie limestones in the MORO section. A, MORO/0.0, iron-rich, moderately to well-sorted, quartz-rich sandstone. B–C, MORO/239.4, MORO/401.1, finely-laminated to columnar stromatolitic bindstone. D, magnification of C; recrystallization and dolomitization of micrites in association with dissolution via stylolites. E, MORO/448.8, peloidal grainstone. F–I (MORO/604, MORO/612, MORO/625), K (MORO665), archaeocyath framestones and packstones, with clotted *Renalcis* calcimicrobes. J (MORO/829.7), N (MORO933.2), bioclastic wackestone. L–M, MORO775, homogenous lime mudstone. M, magnification of L.

Fig. 15. BHG stratigraphic section through the Wirrapowie Limestone, Midwerta Shale, lower Mernmerna Formation, Nepabunna Siltstone, upper Mernmerna Formation and the Oraparinna Shale in the south-west Arrowie Syncline, northern Flinders Ranges. Ranges of key taxa through the *Kulparina rostrata*, *Micrina etheridgei* and *Dailyatia odyssei* zones are shown. The  $\delta^{13}\text{C}$  events II and III are developed in the Wirrapowie Limestone, where event II is straddling the boundary between the *K. rostrata* and *M. etheridgei* zones. The CARE occurs in the lower Mernmerna Formation, straddling the boundary between the *M. etheridgei* and *D. odyssei* zones, peaking in the lower *D. odyssei* Zone. Moll = molluscs.

Fig. 16. Thin section photomicrographs of fabrics and textures in carbonates from the Nepabunna Siltstone and Midwerta Shale in the BHG section. A, BHG/620, mottled lime mudstone with fine silt. B, BHG/765, laminar, spiculitic lime mudstone. C, BHG/765, magnification of B; showing pyrite and limonite alteration haloes. D, BHG/1851, lime mudstone with recrystallised sparite. E, BHG/2170, finely-laminated lime mudstone with silty bands and secondary calcite spar infills between laminations.

Fig. 17. AJX-M stratigraphic section through the Ajax Limestone at Mt. Scott Range, north-western Flinders Ranges, with ranges of key shelly fossil taxa through the *Micrina etheridgei* and *Dailyatia odyssei* zones. The CARE straddles the boundary between the *M. etheridgei* and *D. odyssei* zones, and the upper part of the *Parabadiella huoi* Zone and the lower *Pararaia tatei* Zone.

Fig. 18. Thin section photomicrographs of fabrics and textures in carbonates from the Ajax Limestone in the AJX-M section. A, AJX-M/52.2, equigranular sparite (dark) and fabric-obliterative dolomite (light). B, AJX-M/131.7, stylolitic equigranular sparite with limonite

staining. C, AJX-M/198, hyolith-rich bioclastic wackestone. D–E, AJX-M/261.1, bioclastic wackestone to packstone. E, magnification of D; cross-section of *Dailyatia* sclerite with micritic infill. F, AJX-M/347.4, recrystallised bioclastic grainstone; light areas contain abundant archaeocyath fragments within a coarse crystalline spar, darker areas are iron-stained dolomite. G, I, AJX-M/374.3, AJX-M/415, recrystallised trilobitic packstone. H, AJX-M/392.3, bioclastic, glauconitic grainstone. J, AJX-M/429, poorly-sorted intraclastic grainstone; exoclasts contain predominantly highly-fragmented archaeocyath and shelly debris in a spar matrix. Detrital glauconitic grains are also present.

Fig. 19. Yalkalpo-2 drill core through the Parachilna Formation, Wilkawillina Limestone and Mernmerna Formation on the Benagerie Ridge, to the east of the Arrowie Basin (Fig. 1). New shelly fossil data demonstrate that the *Micrina etheridgei* Zone ranges from horizons previously interpreted to be Parachilna Formation (Zang et al., 2001), and lack of lithological textures typical of the Woodendinna Dolostone suggest that there is a cryptic unconformity in the lower parts of the Yalkalpo-2 drill core. The CARE occurs in the Mernmerna Formation, straddling the boundary between the *M. etheridgei* and *Dailyatia odyssei* zones. Brachs = brachiopods. Ecdys = ecdysozoans.

Fig. 20. Thin section photomicrographs of fabrics and textures in the Parachilna Formation, Wilkawillina Limestone and Mernmerna Formation from the Yalkalpo-2 drill core. A, YALK/798.85, poorly sorted submature sandstone. B–C, YALK/791.62, peloidal, quartz-rich grainstone. C, magnification of B; lithic fragments and quartz grains. D–E, YALK/780.55, laminated lime mudstone with abundant fine quartz sand. Glauconite is concentrated in bands. E, magnification of D; fine quartz sand component interspersed with glauconite. F, YALK/768.57, lime mudstone with porphyrotopic microspar and stylolites. G–H,

YALK/760.28, bioclastic wackestone containing fragmented archaeocyaths within a micritic matrix. H, magnification of G; haematite cement surrounding euhedral planar dolomite. I-J, YALK/734.46, bioclastic wackestone. J, magnification of I; archaeocyath debris infilled with microcrystalline spar, botryoidal microbial growths also present. K-L, YALK/714.34, wackestone with with porphyrotopic microspar. K, magnification of L; subhedral planar-s dolomite and calcite spar. M, YALK/628.69, contact between lime mudstone and well-sorted quartz sandstone.

Fig. 21. PIN stratigraphic section through the Mernmerna Formation in the Chambers Gorge region, eastern Flinders Ranges. Ranges of key shelly taxa through the *Dailyatia odyssei* Zone are shown. Taxa with occurrences below the section line are from a spot locality.  $\delta^{13}\text{C}$  data are around 0.0 to -1‰ and remain relatively stable, typical of post-CARE  $\delta^{13}\text{C}$  values worldwide. Brachs = brachiopods. Moll = molluscs.

Fig. 22. Thin section photomicrographs of fabrics and textures in carbonates from the Mernmerna Formation in the PIN section. A-C, PIN/0.0, wackestone. B-C, magnification of A. B, trilobite fragments with shelly fauna including hyoliths in cross-section with iron-stained infill and spar matrix. C, shelly fragments including archaeocyaths and trilobites. D-E, PIN/14.0, homogeneous fine lime mudstone with minor spar. E, magnification of D. F-G, PIN/73.5, dolomitised bioclastic packstone. G. Magnification of F; non-fabric destructive subhedral to nonplanar dolomite (fossils remain intact). Fossils. H-I, PIN, 99.0, bioclastic packstone with microbial laminations infilling V-shaped notch in sediment. I, magnification of H; shows fine microbial laminations and binding of micritic sediment.

Fig. 23. SCYW-791A drill core through the Andamooka Limestone on the Stuart Shelf.

Ranges of key shelly taxa through the *Dailyatia odyssei* Zone are shown.  $\delta^{13}\text{C}$  values are relatively stable throughout the lower and mid-parts of the sampled drill core, gradually becoming more positive in the upper levels. These  $\delta^{13}\text{C}$  values may be the MICE; however as shelly fauna were not recovered from these intervals, this remains to be determined. Brachs = brachiopods.

Fig. 24. Thin section photomicrographs of fabrics and textures in carbonates from the

Andamooka Limestone in the SCYW-791A drill core. A–C, SCYW-791A/16.0, clotted fenestral lime mudstone with spar-filled cavities. B–C, magnification of A; zoned euhedral planar dolomites in plain (B) and cross-polar (C) light. D–E, SCYW-791A/62.0, grainstone containing recrystallized intraclasts, ooids and shelly debris in a micrite and spar matrix.

Detrital glauconite is common (E). F–G, SCYW-791A/74.0, intraclastic packstone; endoclasts are elongate, and larger oncoids are irregular in outline and show signs of reworking. G, magnification of F; authigenic pyrite cements within calcite spar. H, SCYW-791A/81.0, clotted microbial lime mudstone with spar-lined cavities, archaeocyaths in low abundance. I, SCYW-791A/82.0, bioclastic grainstone with abundant archaeocyath fragments and sub-rounded intraclasts.

Fig. 25. Plot of  $^{206}\text{Pb}/^{238}\text{U}$  dates from single grains and fragments of zircon analyzed by CA-TIMS. Plotted with Isoplot 3.0 (Ludwig, 2003). Errors are at 2 sigma. A weighted mean date is shown and represented by the grey boxes behind the error bars. Error bars in black are included in weighted mean. Error bars in white are not included. One older date from BG Tuff is not shown. MSWD = mean square of weighted deviates; pof = probability of fit.

Fig. 26. Cross-plots of  $\delta^{18}\text{O}\text{‰}$  and  $\delta^{13}\text{C}\text{‰}$  data for each stratigraphic section and drill core. Omitted samples are shown in red.

Fig. 27. Global correlation of the lower Cambrian successions in the Arrowie and Stansbury basins of South Australia. Figure adapted from Devaere et al. (2013), Jacquet et al. (2017b), Kouchinsky et al. (2012), Landing et al. (2013), Landing and Kouchinsky (2016), Landing and Westrop (1998), Peng et al. (2012), Steiner et al. (2007). Global U/PB- $\delta^{13}\text{C}_{\text{CaCO}_3}$  age model in West Gondwana column from Maloof et al. (2010a), and dashed curve (including MICE) from Peng et al. (2012). Geochronological data are from Compston et al. (2008), Harvey et al. (2011), Maloof et al. (2010a) and Yang et al. (2018). Error bars have been included for SHRIMP dates. New geochronological data from South Australia are shown with red arrows; A = BG tuff (Mernmerna Formation),  $515.38 \pm 0.13$  Ma. B = Heatherdale Shale,  $514.98 \pm 0.22$  Ma. C = R1300538, Bunkers Range (Mernmerna Formation, Third Plain Creek Member),  $514.56 \pm 0.13$  Ma. D = 1830309 (Paralana core, Mernmerna Formation) =  $514.46 \pm 0.13$  Ma. Abbreviations: South Australia; BC = Billy Creek Formation, BS = Bunkers Sandstone, FTL = Fork Tree Limestone, KG = Kanmantoo Group, *K. r* Zone = *Kulparina rostrata* Zone, Orap Sh. = Oraparinna Shale, *P.h* = *Parabadiella huoi*, UM = Upper Mernmerna, WD = Woodendinna Dolostone, Wilka Lst = Wilkawillina Limestone, Wirra Lst = Wirrapowie Limestone, Wk. Fmn = Wangkonda Formation. South China (East Yunnan); Hong' Mb = Hongjingshao Member, MTS Sh. = Maotianshan Shale, Tsang' F = Tsanglangpu Formation. Northern and Central Siberia; *L. b* = *Lapworthella bella*, *L. t* = *Lapworthella tortuosa*, *P. jak* = *Profallotaspis janutensis*, *Rep* = *Repinaella*. Laurentia; *Fall* = *Fallotaspis*, *Fritz* = *Fritzaspis*. West Gondwana column' IF = Igoudine Formation. Dashed lines represent uncertain boundaries, particularly the base of Stage 4.

## Supplementary Files:

SL1. Table of raw  $\delta^{18}\text{O}\text{‰}$  and  $\delta^{13}\text{C}\text{‰}$  data from all sections and drill cores, and table of raw CA-TIMS data.

SL2. CL images of zircons from the BG tuff, Mernmerna Formation, Bunyeroo Gorge. Grains plucked for CA-TIMS analyses are indicated.

SL3. CL images of zircons from the Heatherdale Shale, Fleurieu Peninsula. Grains plucked for CA-TIMS analyses are indicated.

SL4. CL images of zircons from the Third Plain Creek Member of the Mernmerna Formation, Bunkers Range. Grains plucked for CA-TIMS analyses are indicated.

SL5. CL images of zircons from the Mernmerna Formation in the Paralana core. Grains plucked for CA-TIMS analyses are indicated.

SL6. CL images of zircons from the upper part of the Warragee Member, Billy Creek Formation, Angorichina, Flinders Ranges. Grains plucked for CA-TIMS analyses are indicated.

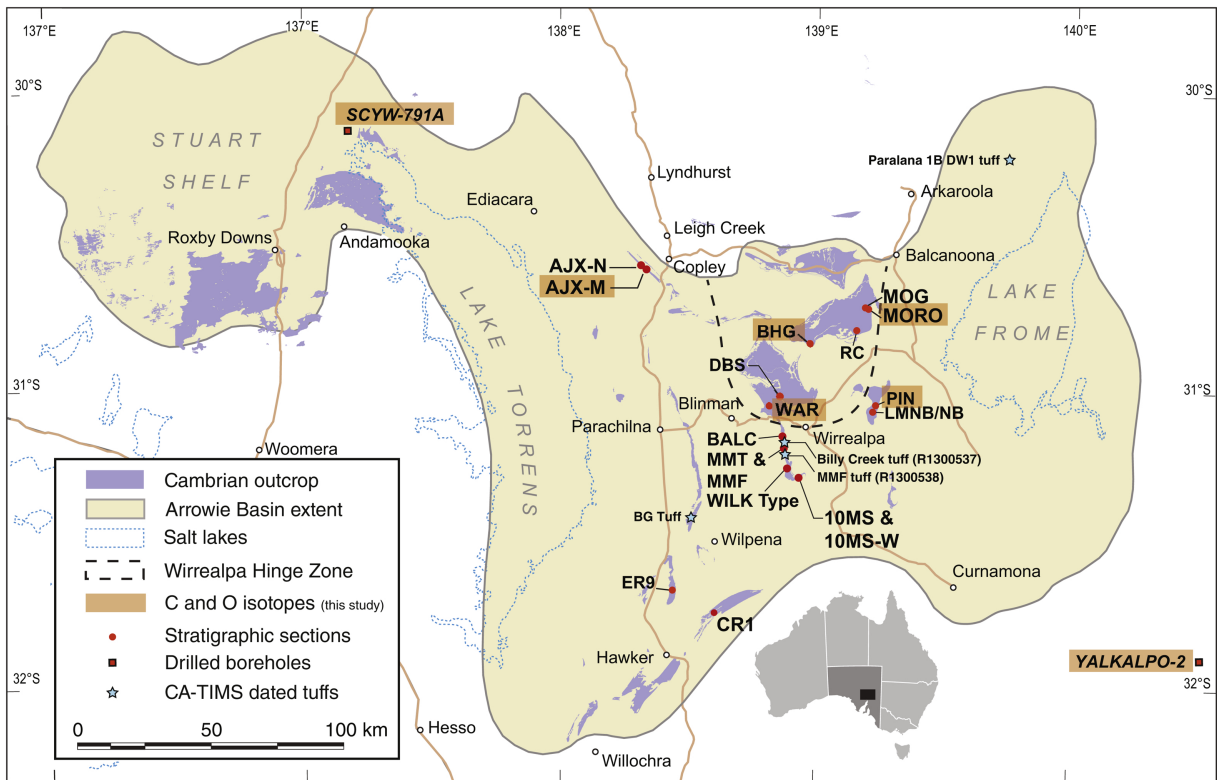


Figure 1



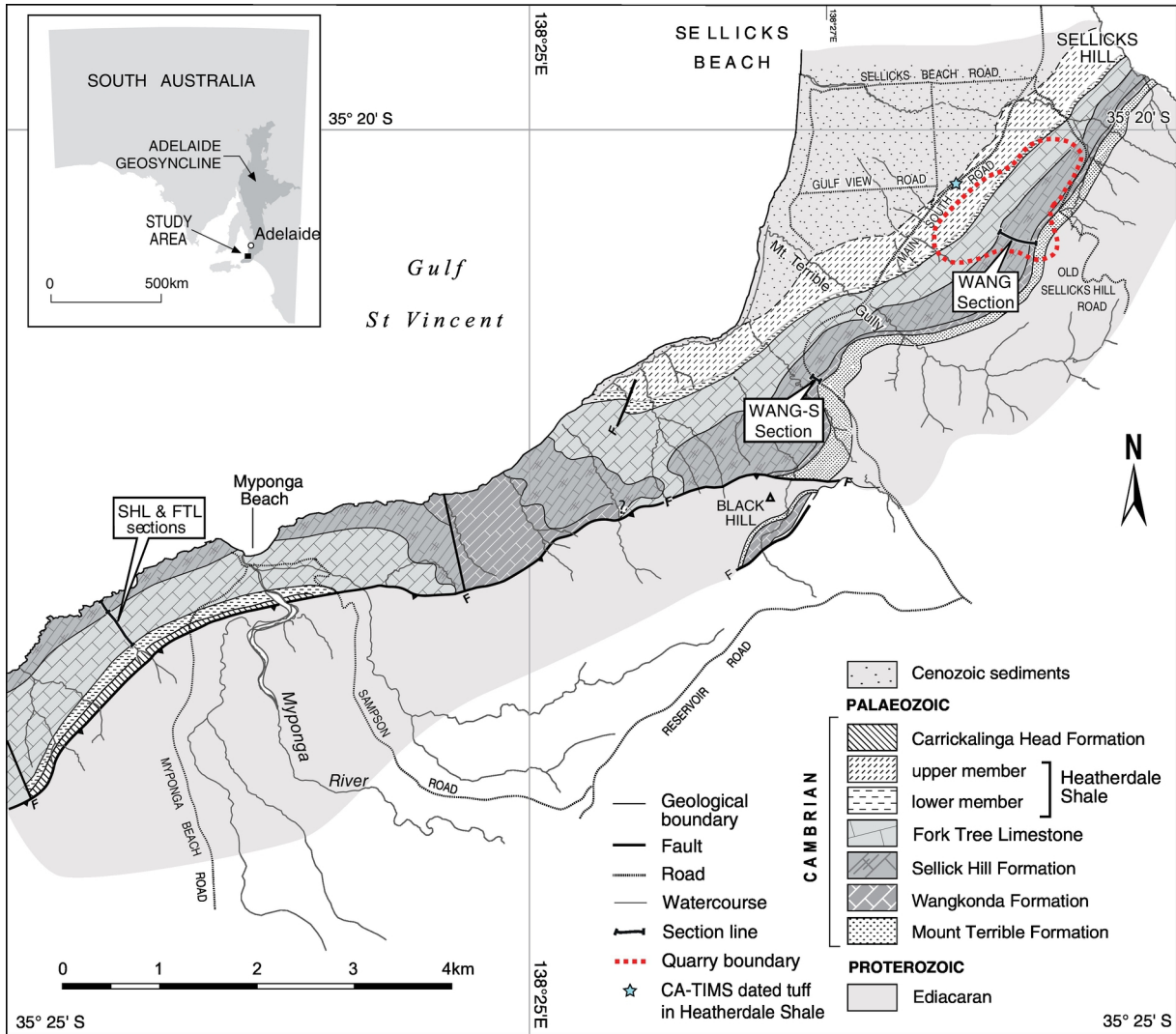


Figure 2

# WANG/WANG-S

(Wangkonda Formation and Sellick Hill Formation, Fleurieu Peninsula)

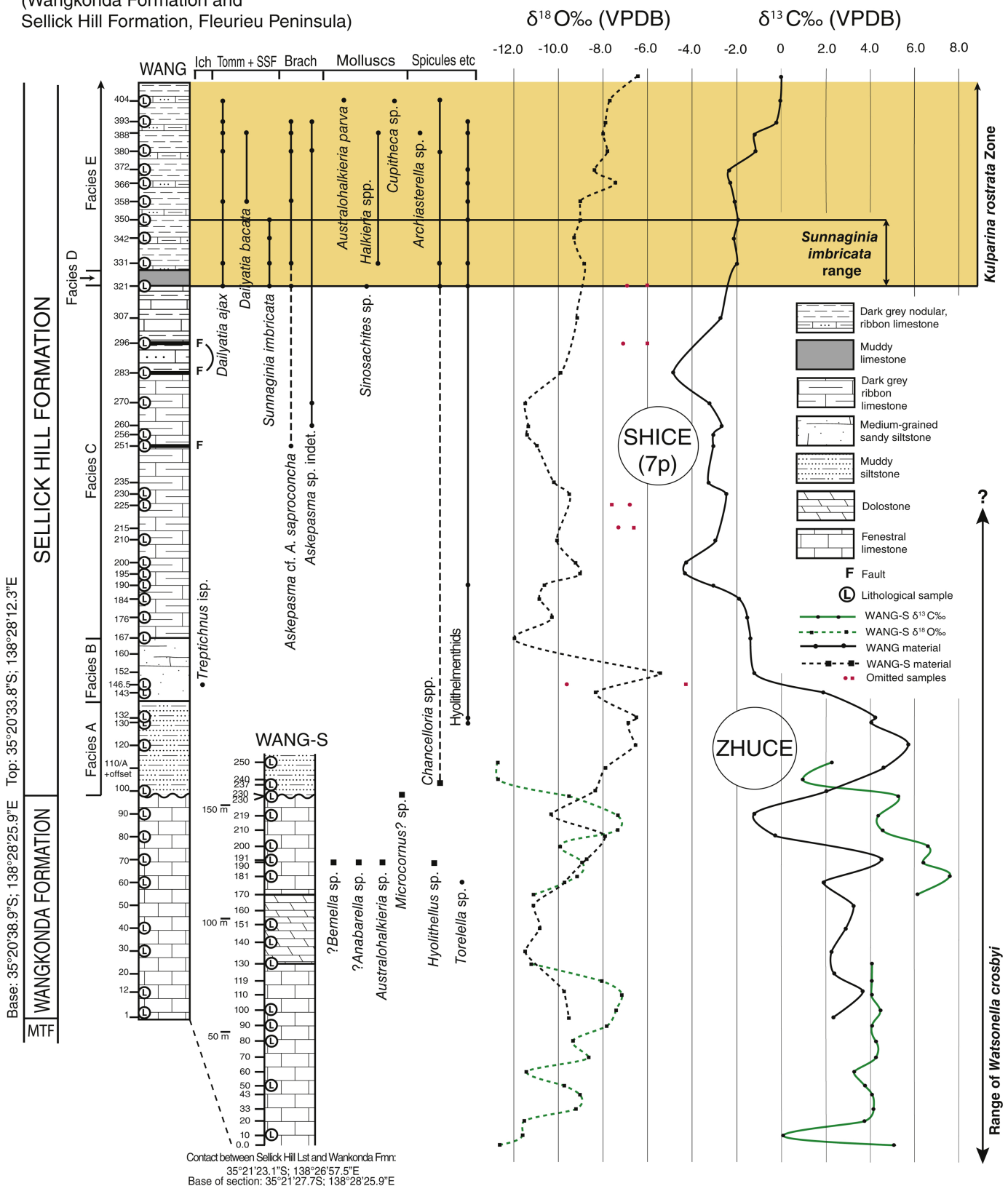
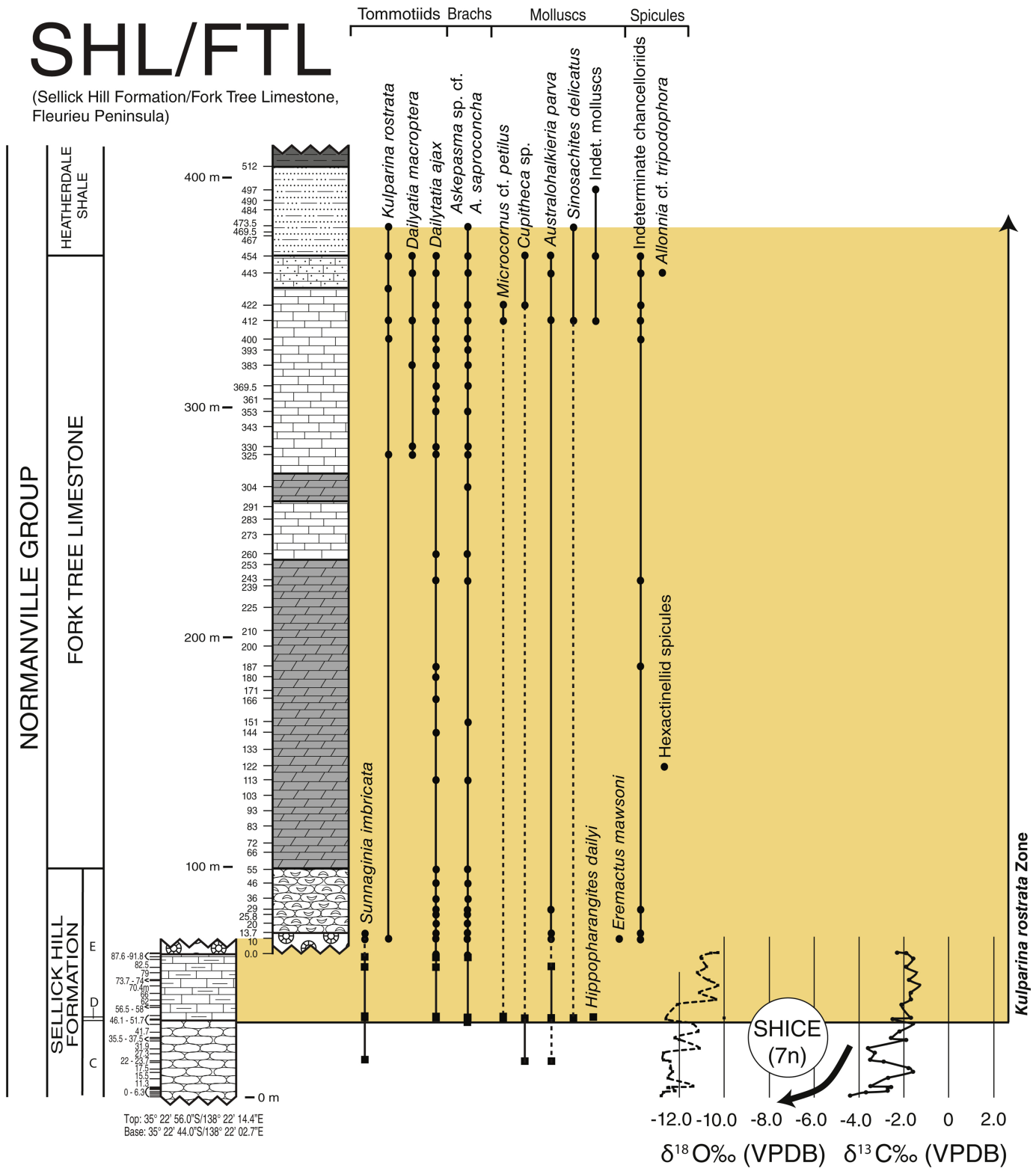


Figure 3

# SHL/FTL

(Sellick Hill Formation/Fork Tree Limestone, Fleurieu Peninsula)



Top: 35° 22' 56.0"S/138° 22' 14.4"E  
Base: 35° 22' 44.0"S/138° 22' 02.7"E

<ul style="list-style-type: none"> <li>⊙ Lithological sample (note, all horizons in SHL have a corresponding thin section)</li> <li>■ Material from SHL section</li> <li>● Material from FTL section</li> </ul>	<ul style="list-style-type: none"> <li> Archaeocyath bioherm. Bioclastic with micritic matrix.</li> <li> Finely laminated lime muds to sandy limestone. Bioclastic, peloidal with hardground surfaces.</li> <li> Flat-pebble conglomerate. Rounded sandy limestone clasts in fine quartz sand matrix.</li> </ul>	<ul style="list-style-type: none"> <li> Massive limestone</li> <li> Dolomitised limestone</li> <li> Ribbon limestone</li> </ul>	<ul style="list-style-type: none"> <li> Black, pyritic shale</li> <li> Calcareous shale</li> <li> Mottled limestone</li> </ul>
---	--	---	--

Figure 4

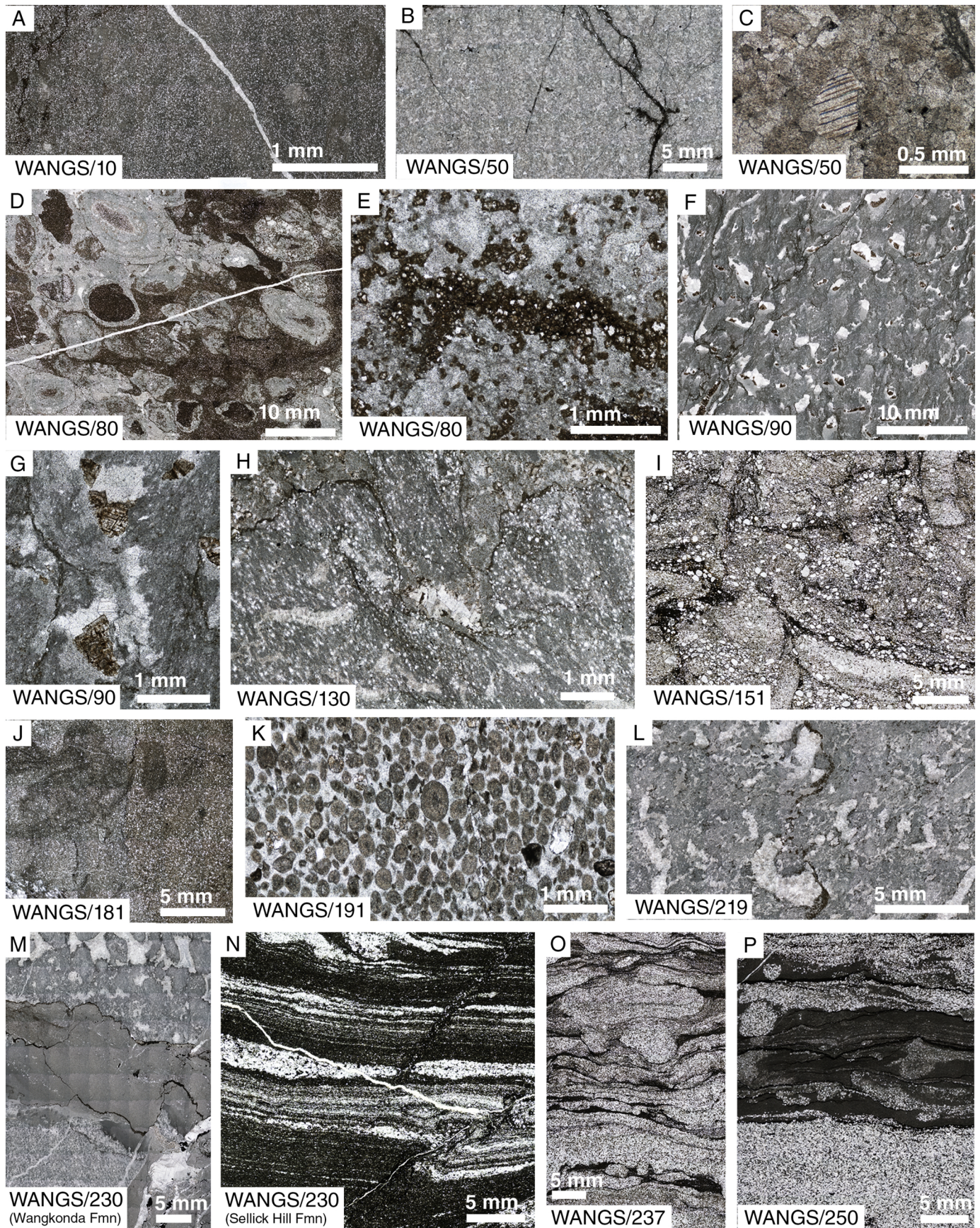


Figure 5

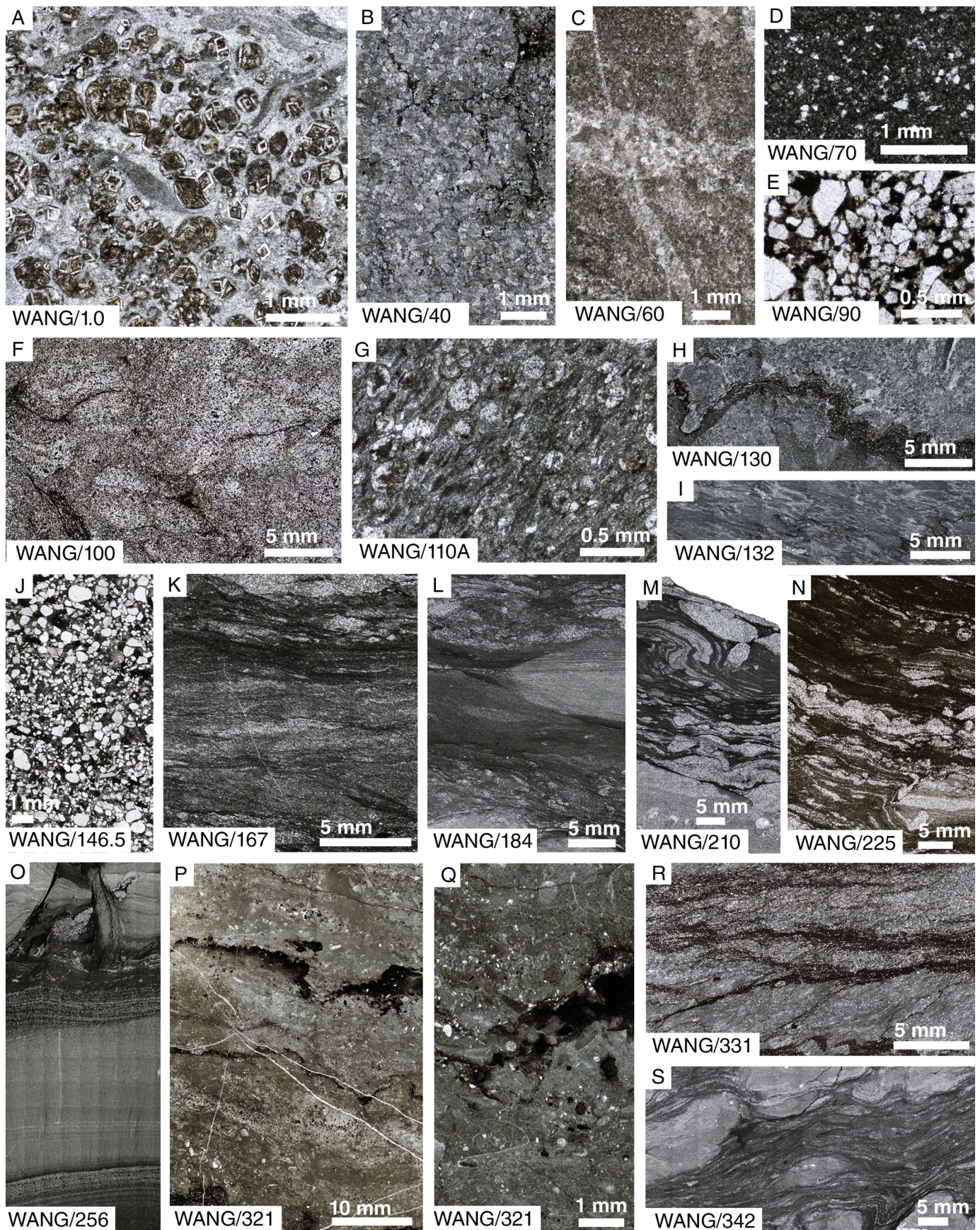


Figure 6

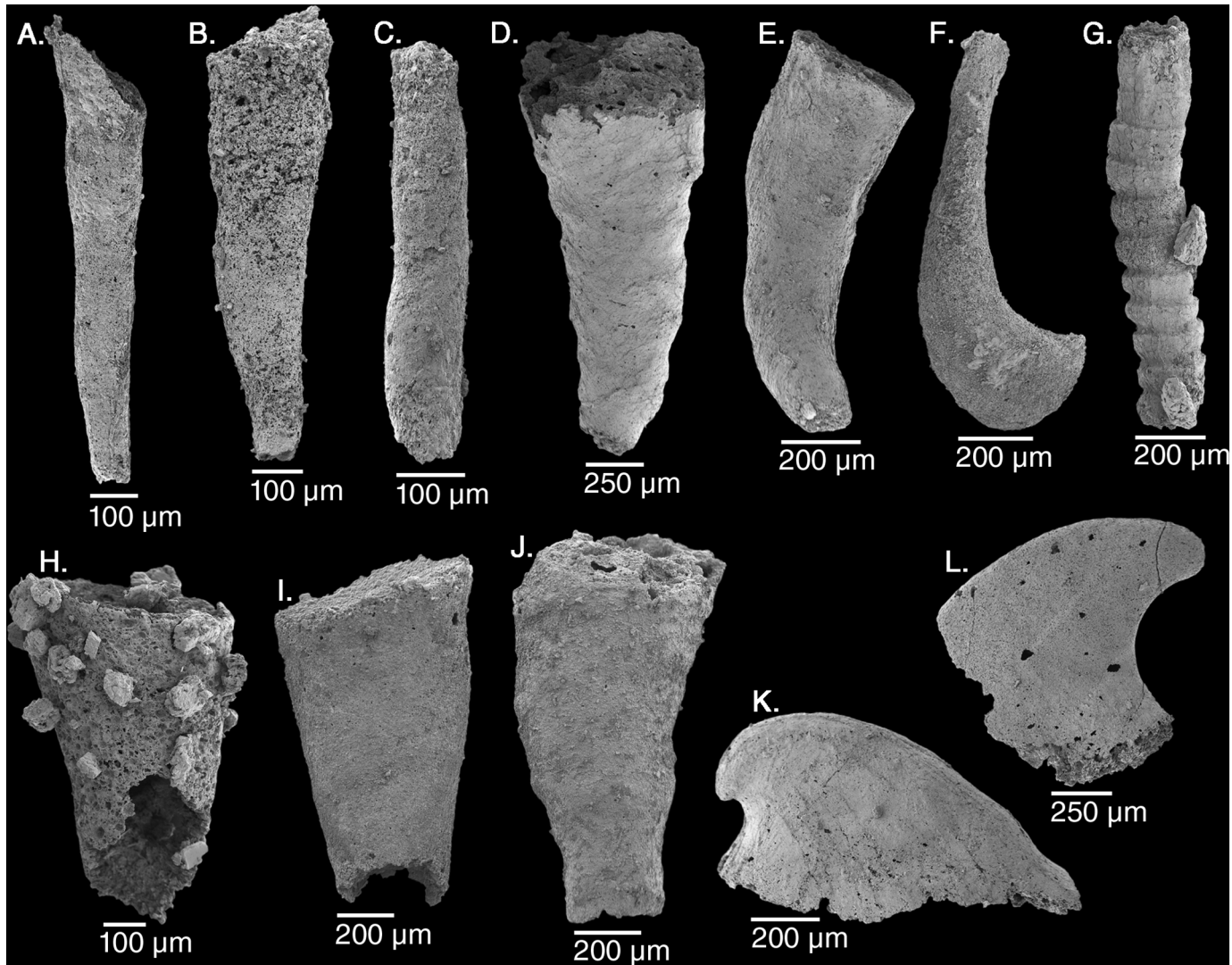


Figure 7

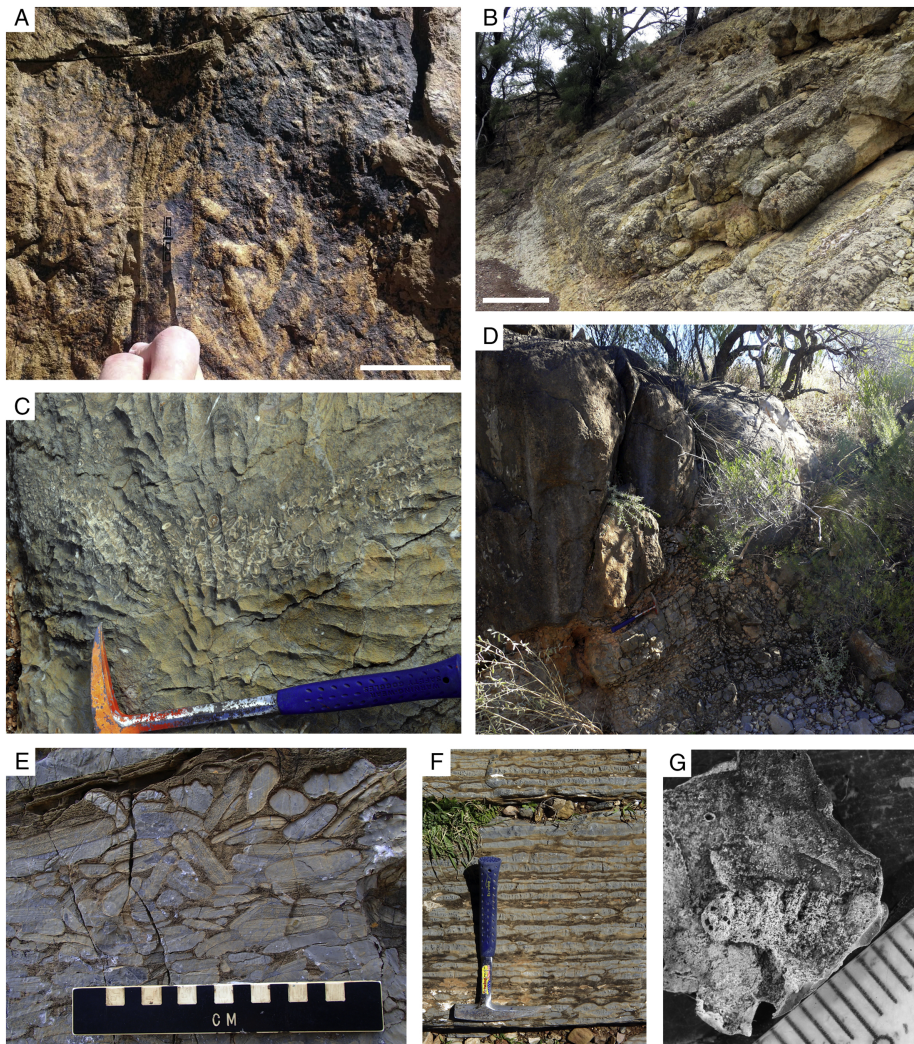


Figure 8

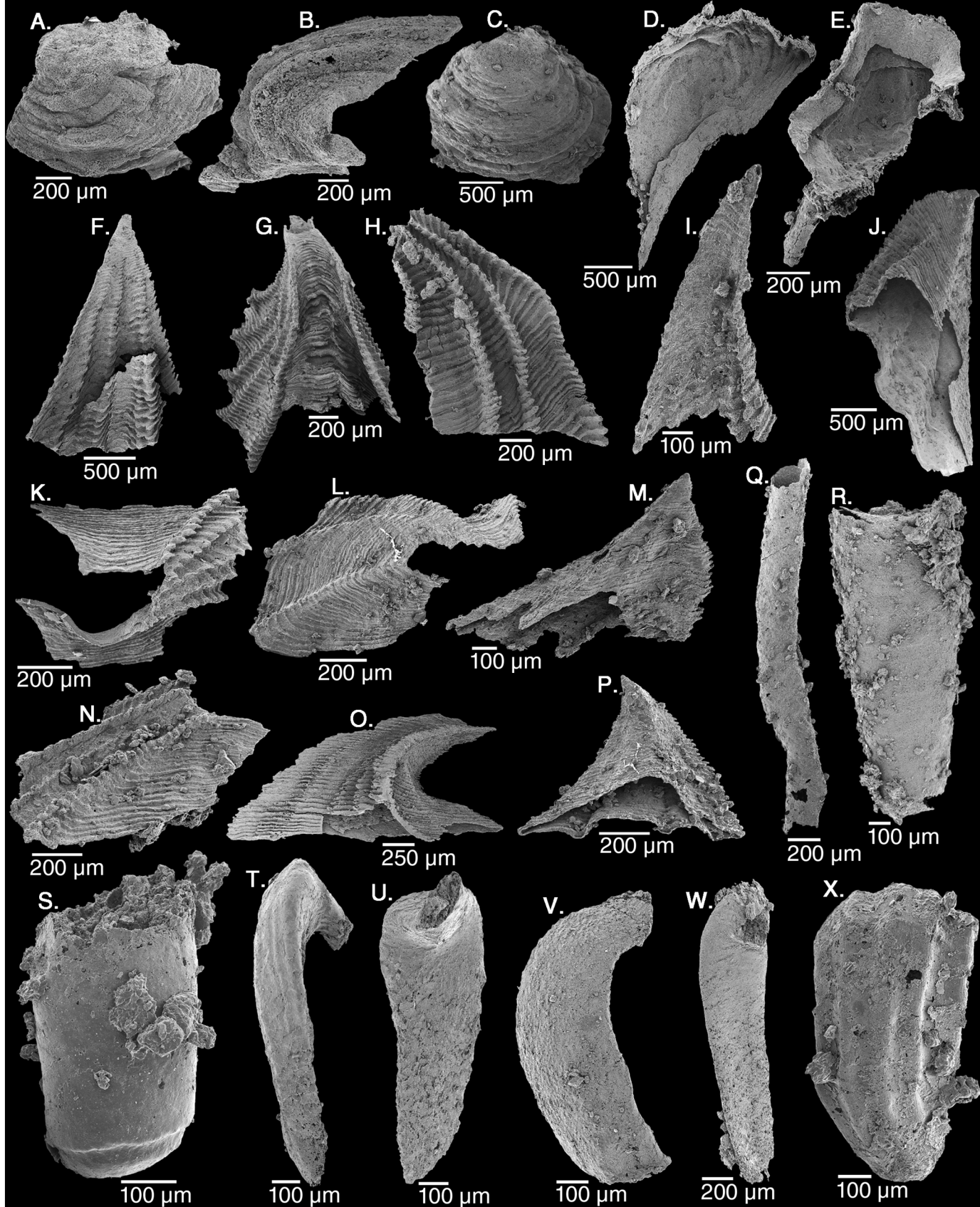


Figure 9



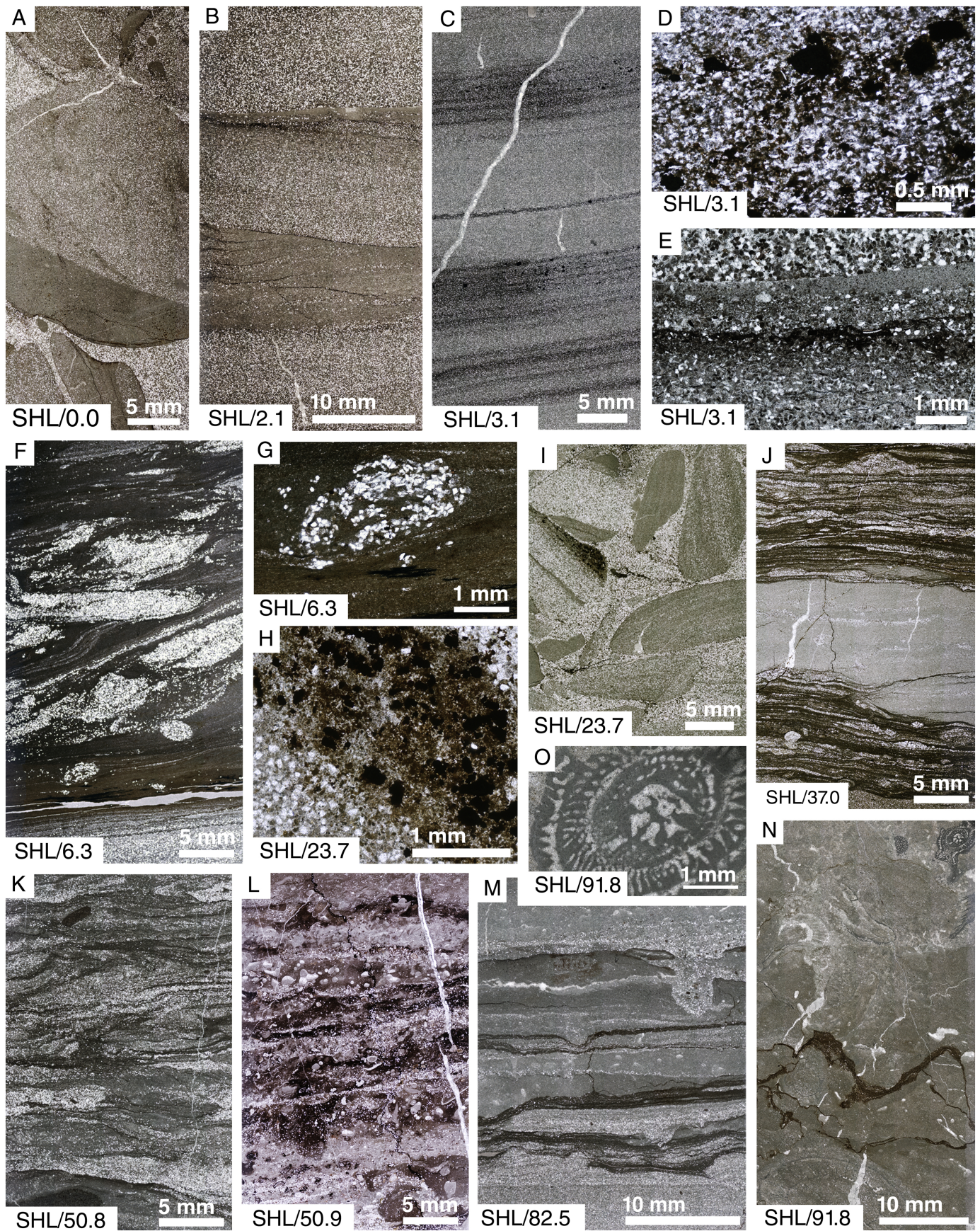


Figure 10

# WAR

(Warragee Bore, central Flinders Ranges)

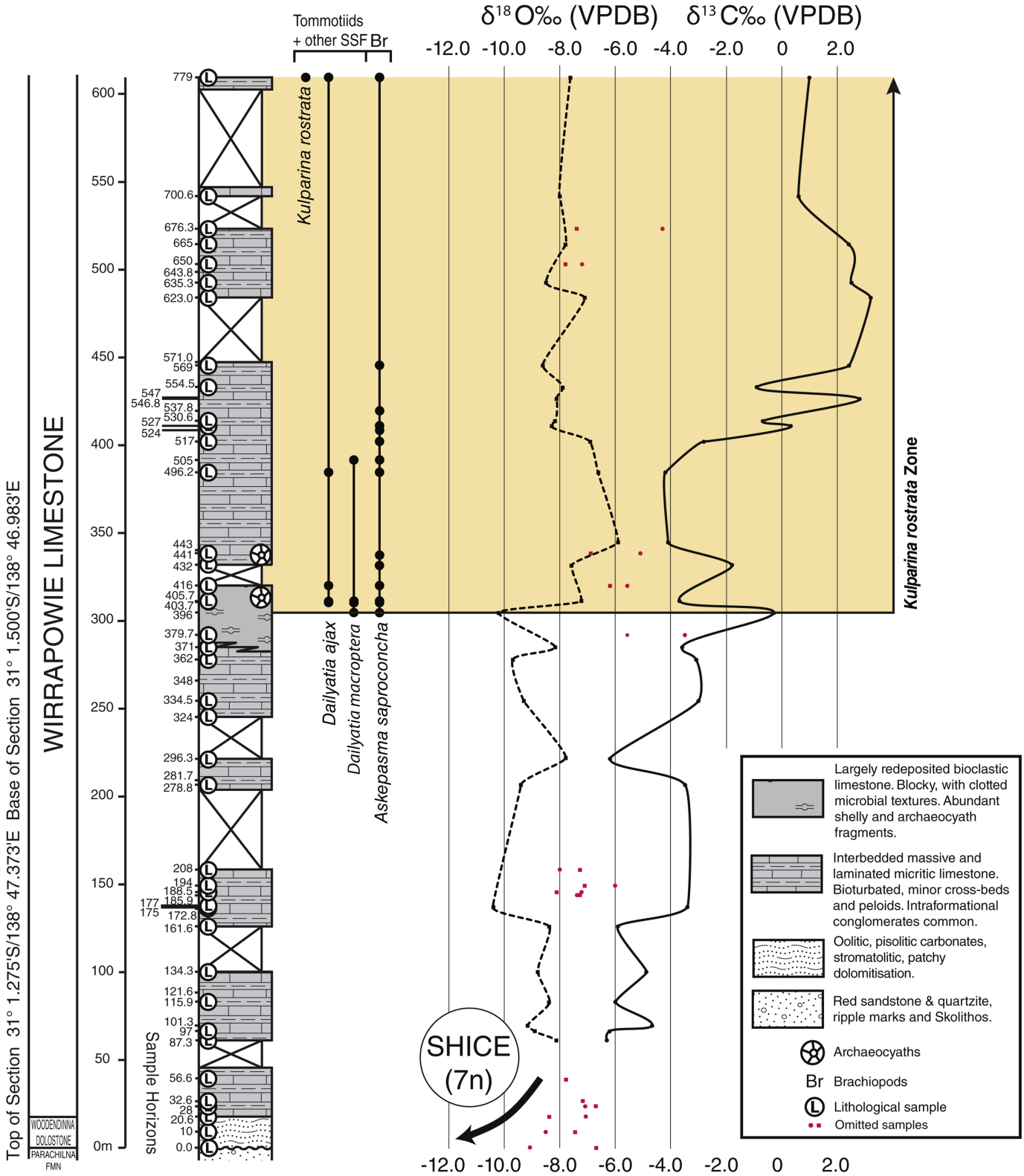


Figure 11

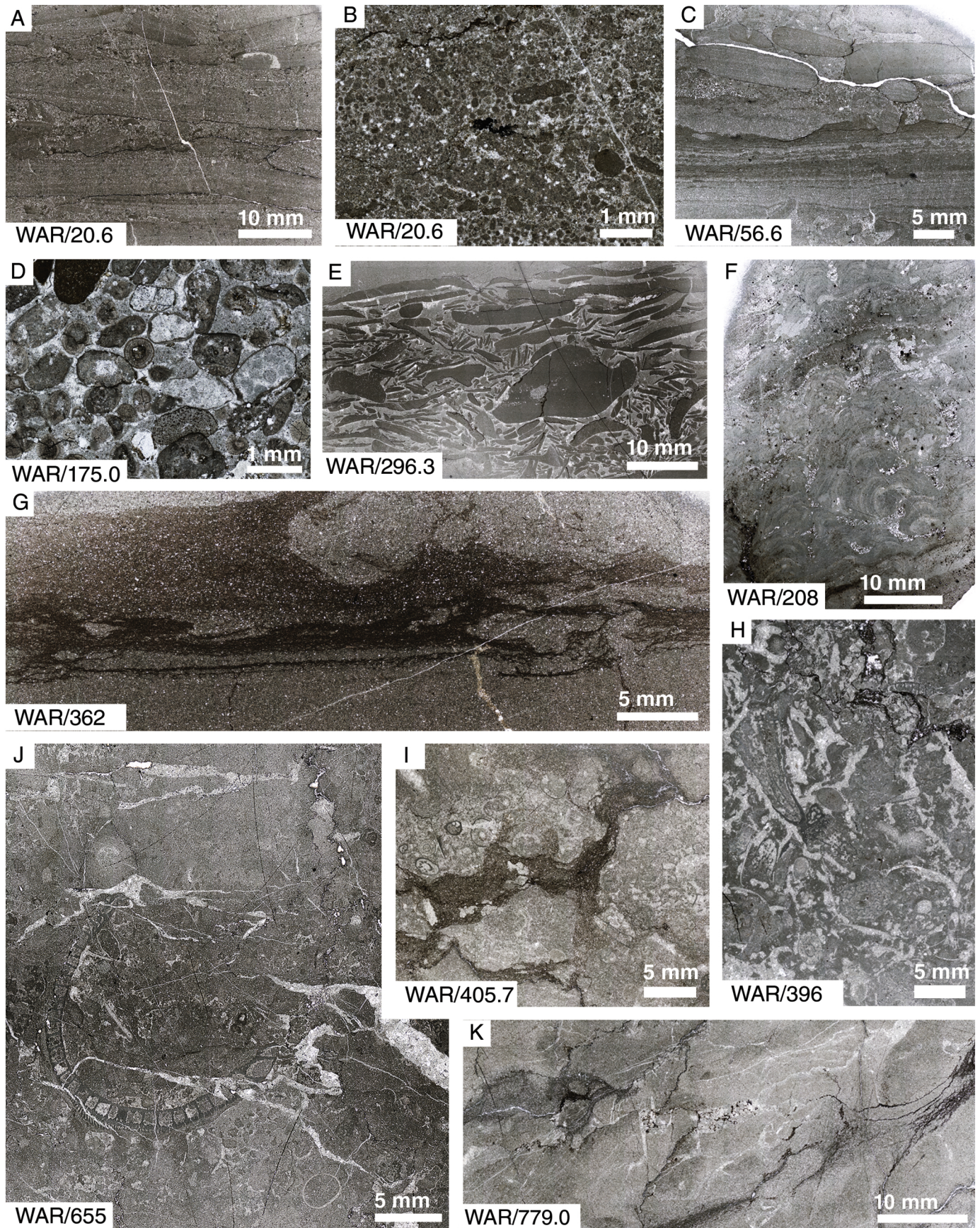


Figure 12

# MORO

(South of Moro Gorge, Arrowie Syncline, northern Flinders Ranges)

$\delta^{18}\text{O}\text{‰}$  (VPDB)  $\delta^{13}\text{C}\text{‰}$  (VPDB)

-12.0 -10.0 -8.0 -6.0 -4.0 -2.0 0 2.0

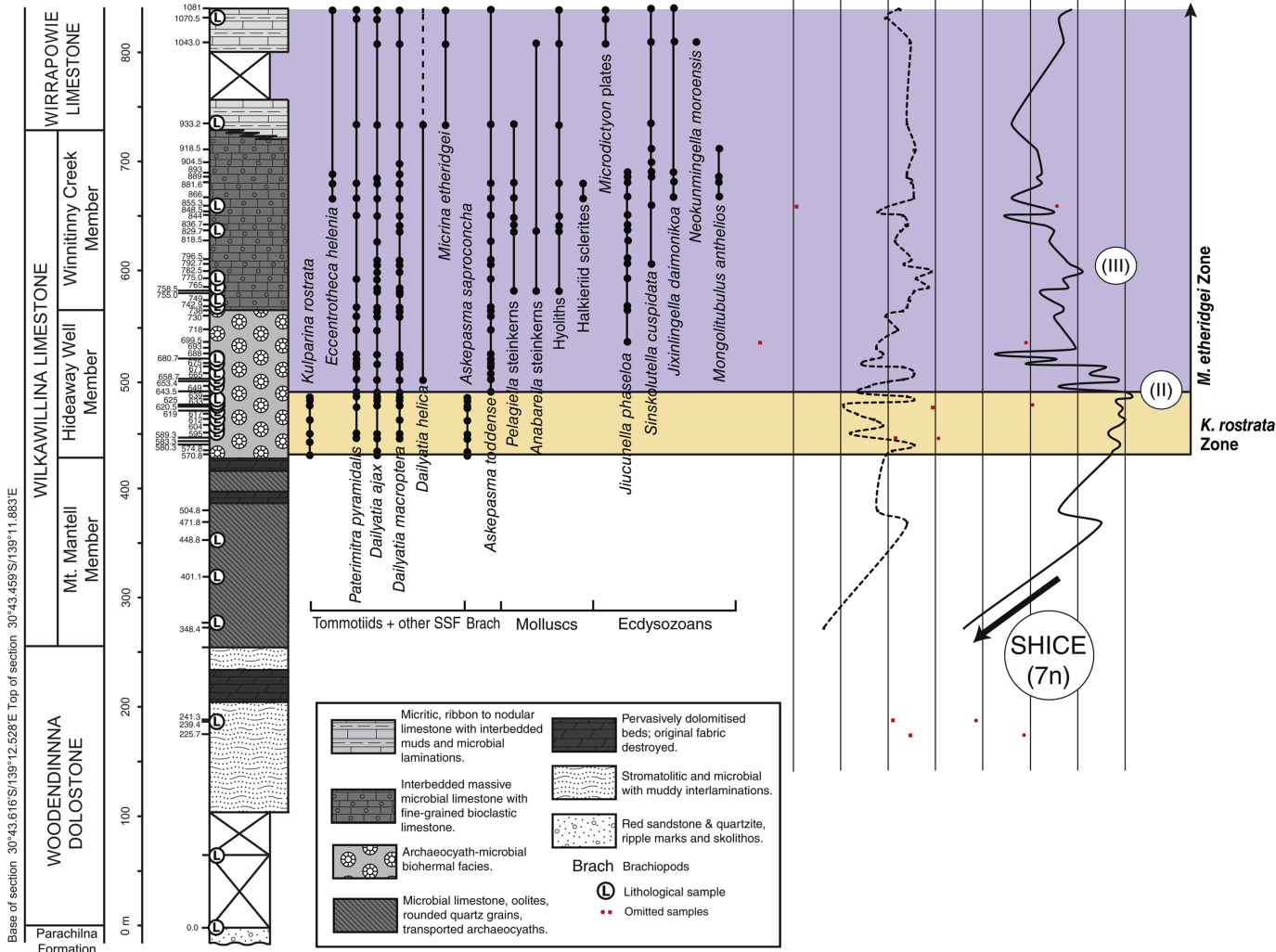


Figure 13

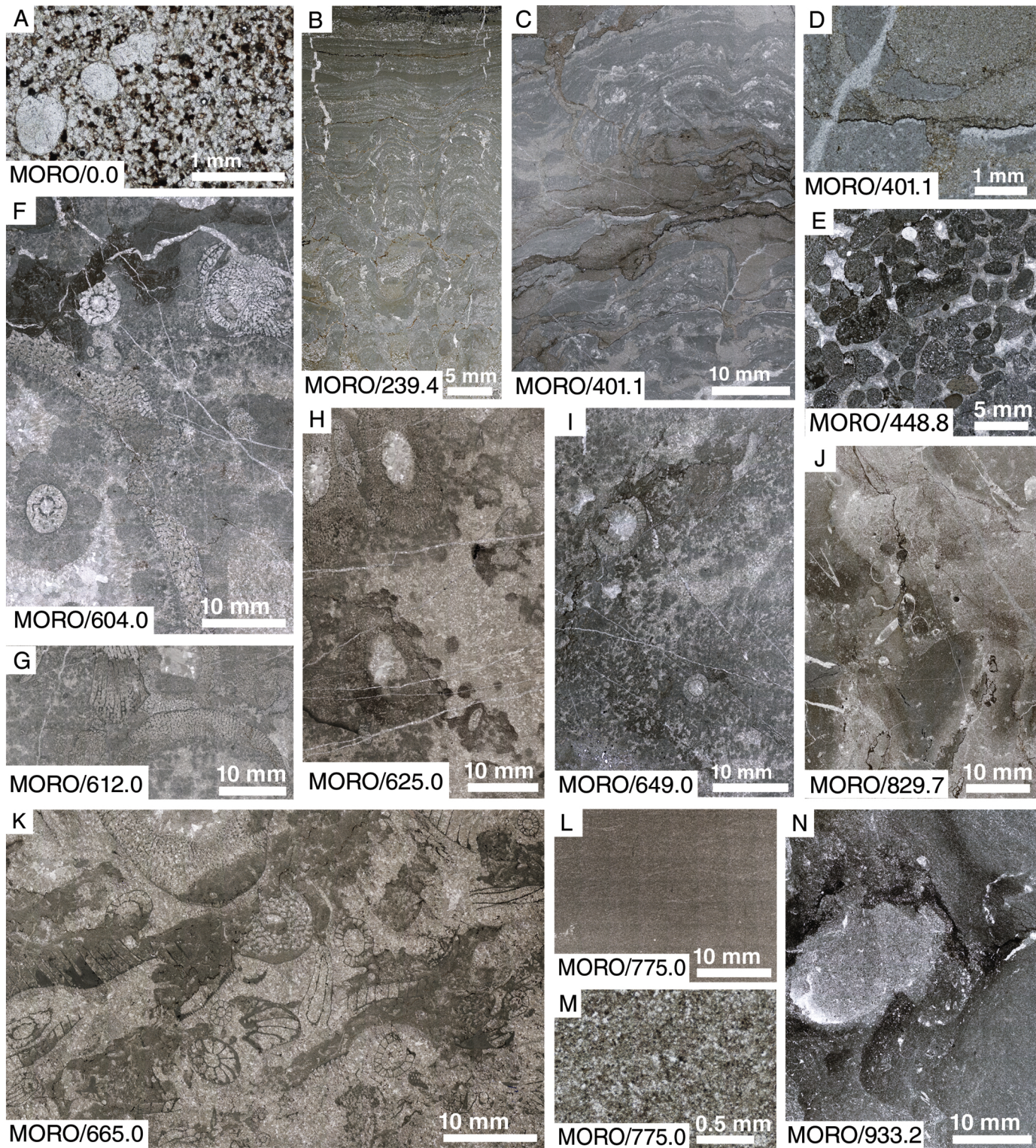


Figure 14

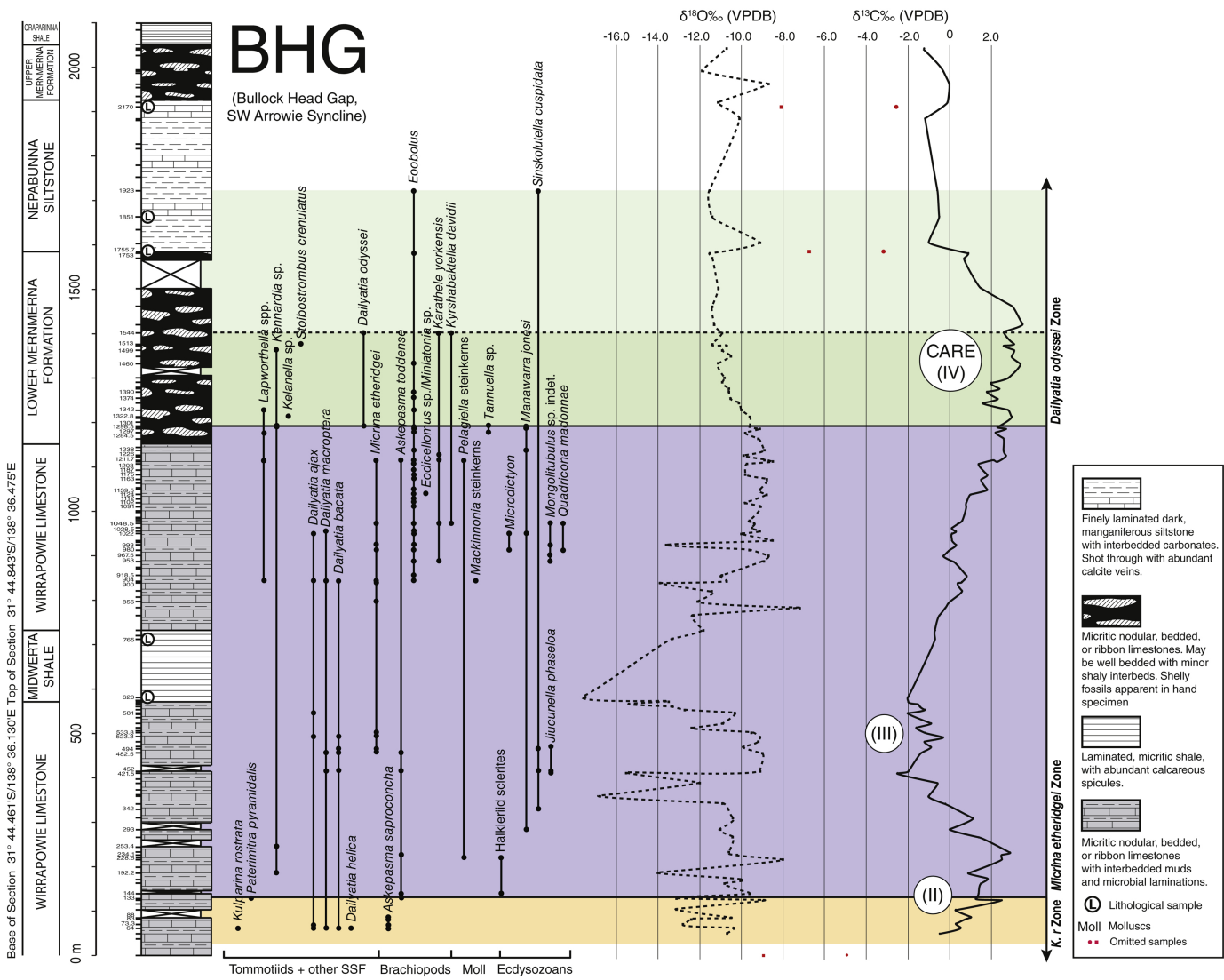


Figure 15

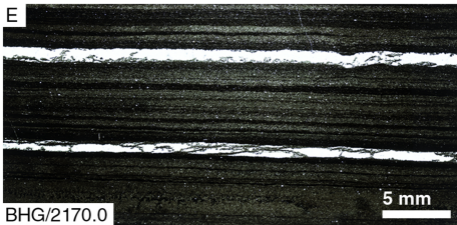
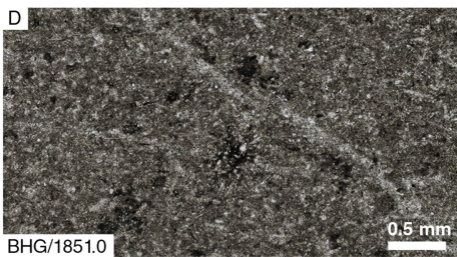
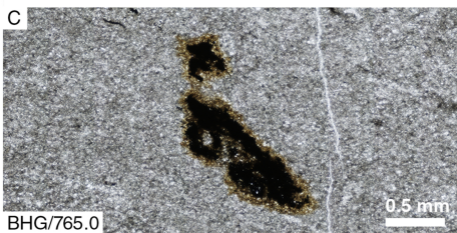
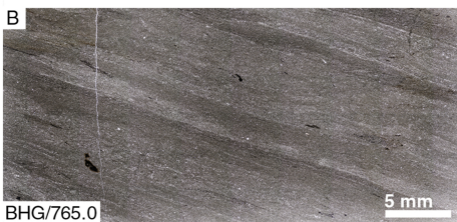
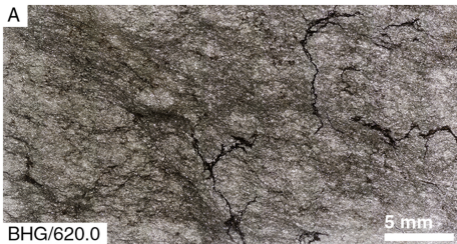


Figure 16

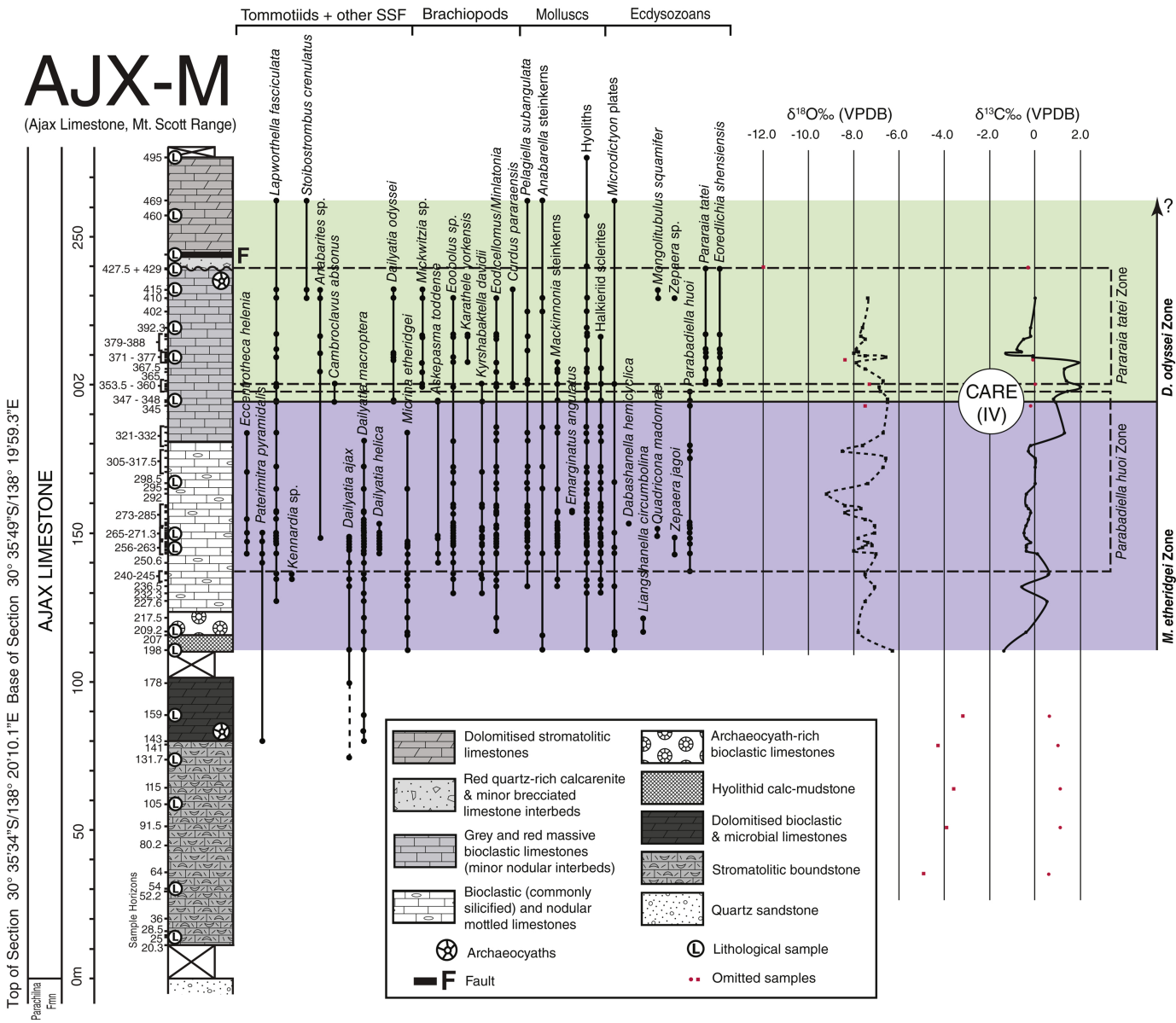


Figure 17



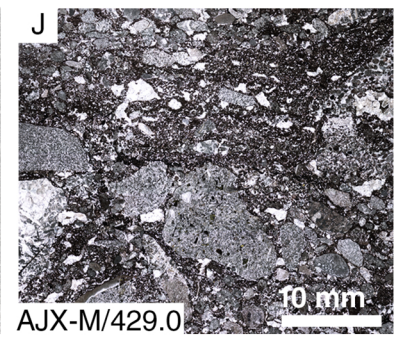
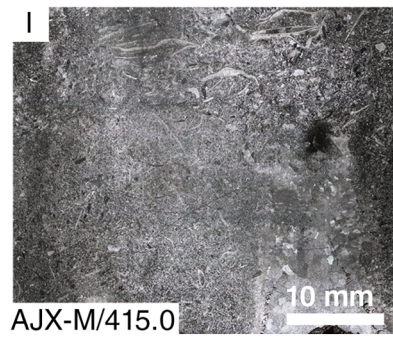
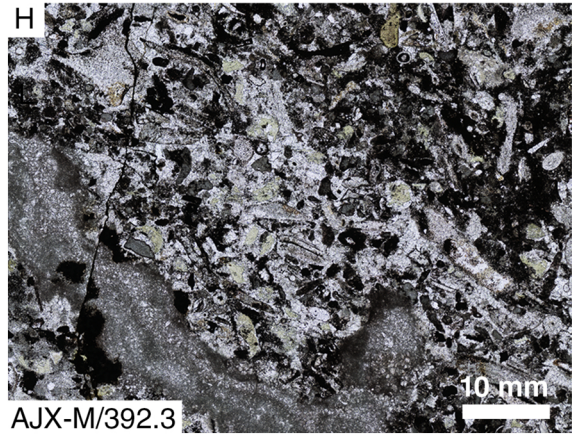
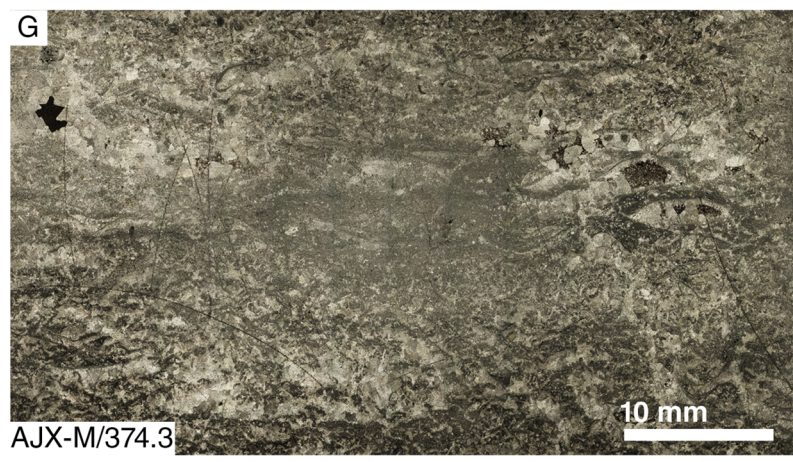
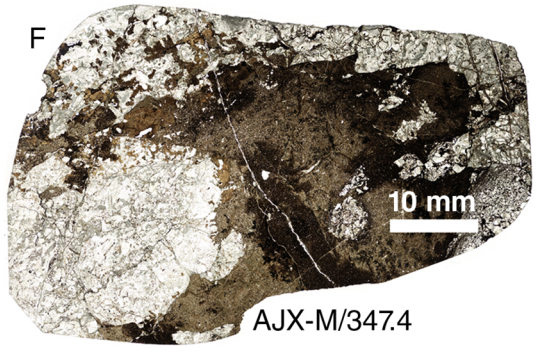
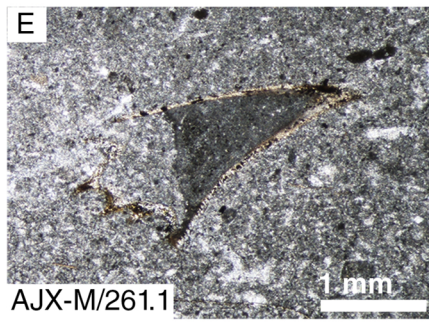
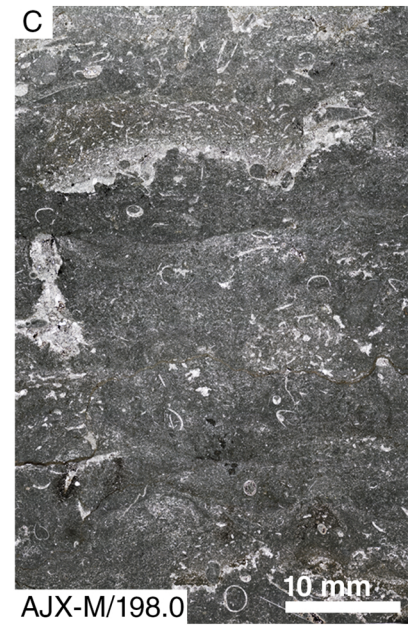
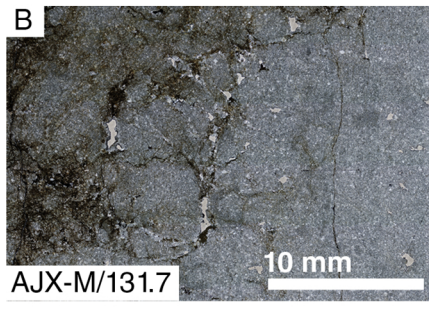
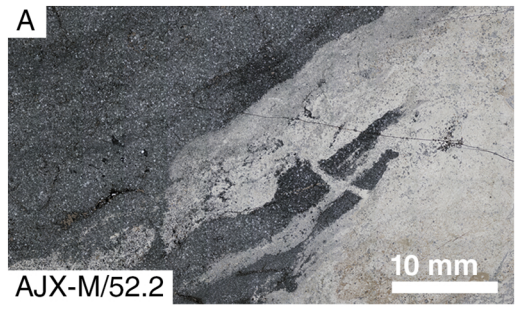


Figure 18

# YALKALPO-2

(Drill core, Benagerie Ridge 31°50'53.92"S/ 140°37'56.53"E)

$\delta^{18}\text{O}\text{‰}$  (VPDB)  $\delta^{13}\text{C}\text{‰}$  (VPDB)

-12.0 -10.0 -8.0 -6.0 -4.0 -2.0 0 2.0

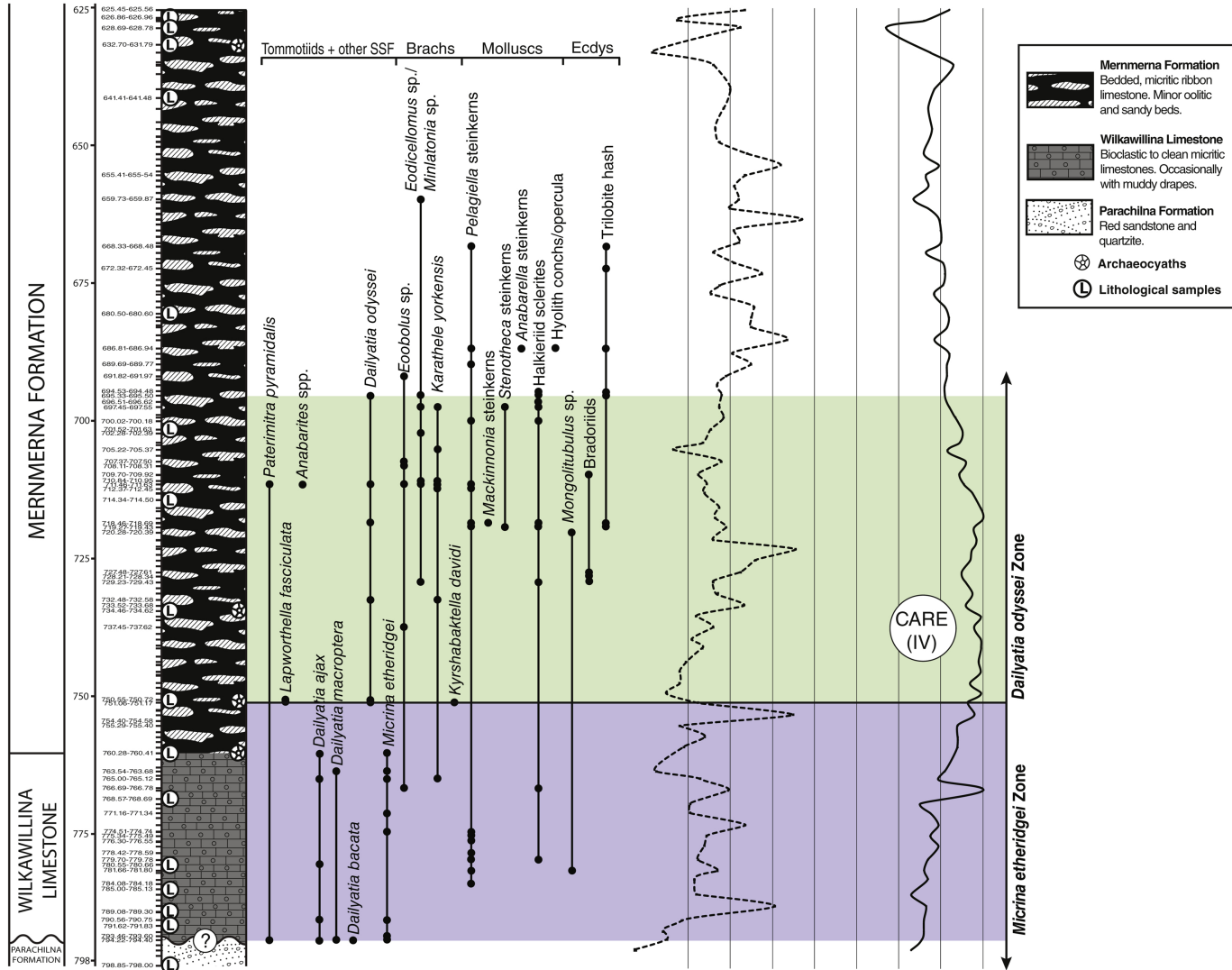


Figure 19

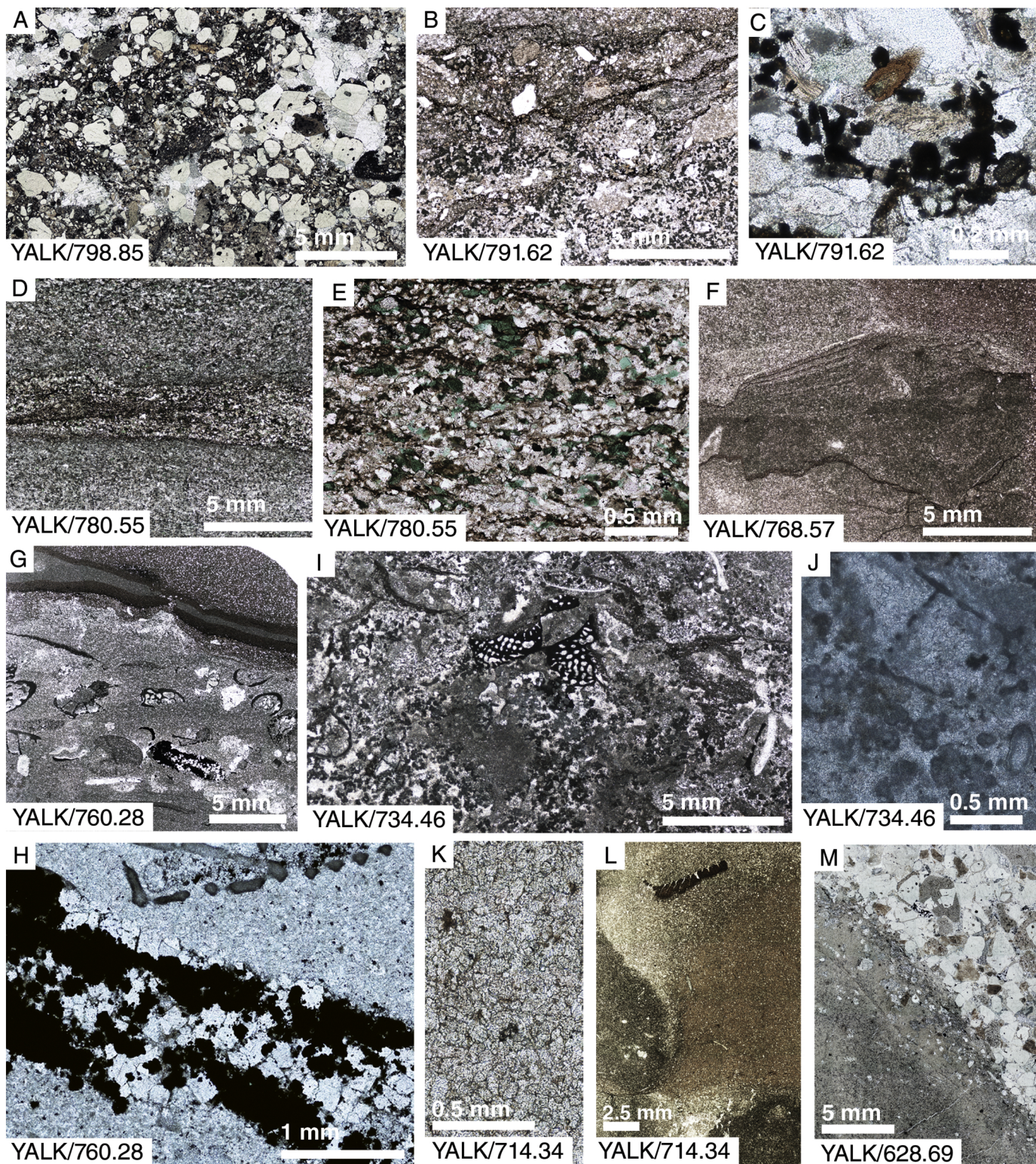


Figure 20

# PIN

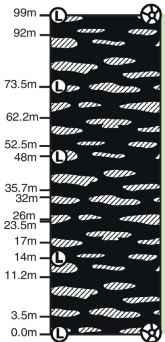
(Pinyatta Creek, Chambers Gorge)

Base of Section 31°00'04.1"S / 139°15'29.9"E  
 Top of Section 31°00'01.1"S / 139°15'30.9"E

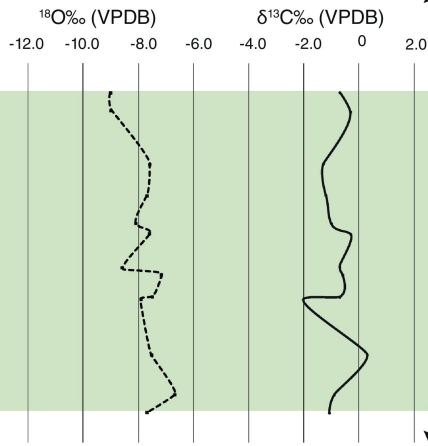
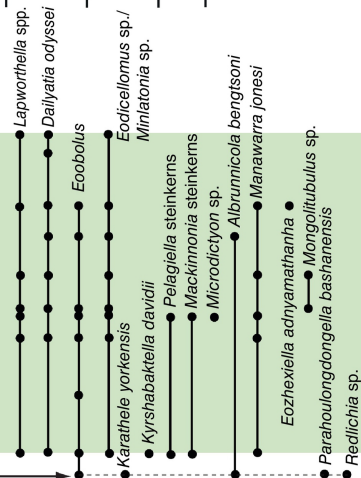
## MERNMERA FORMATION

50


0




Tom + SSF   Brachs   Moll   Ecdysozoans




↑ ?  
 Dailyatia odyssei Zone  
 ↓ ?



**Mernmera Formation**  
 Bedded, micritic ribbon limestone. Minor sandy beds.



Archaeocyaths



Lithological samples

Figure 21

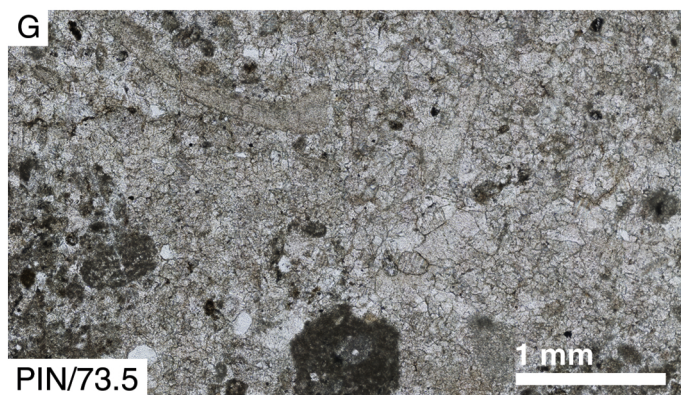
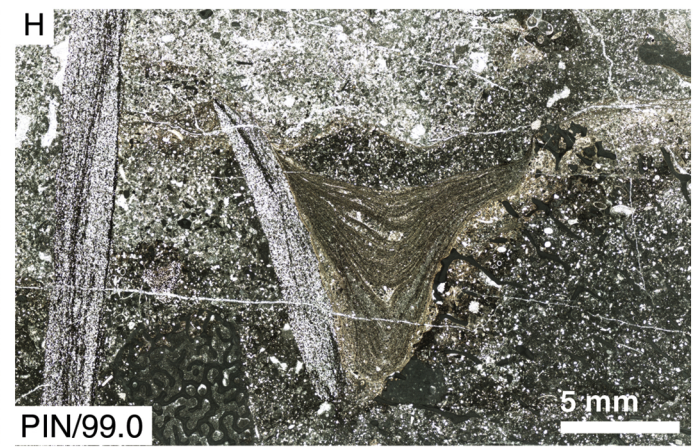
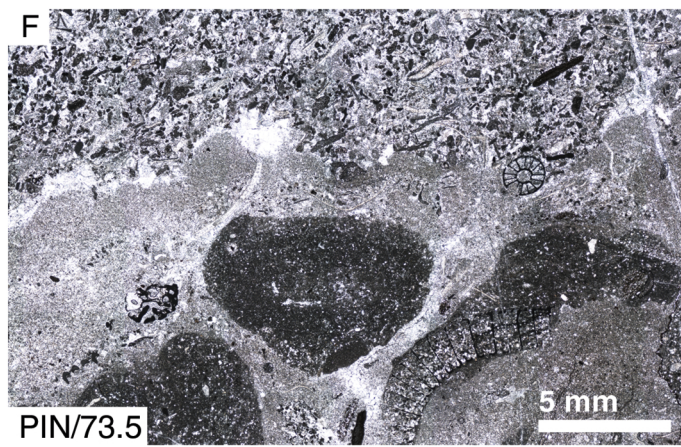
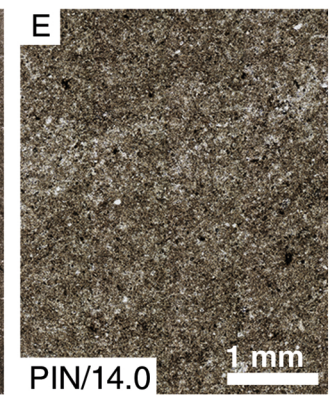
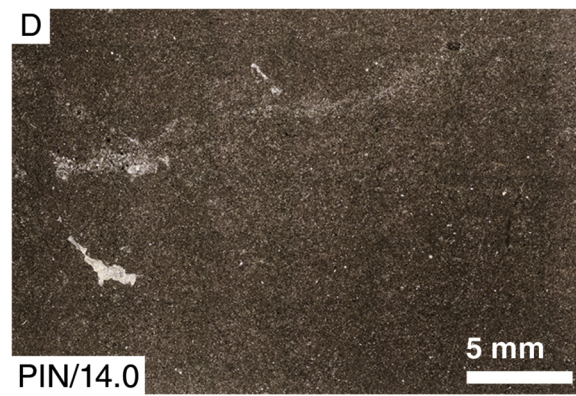
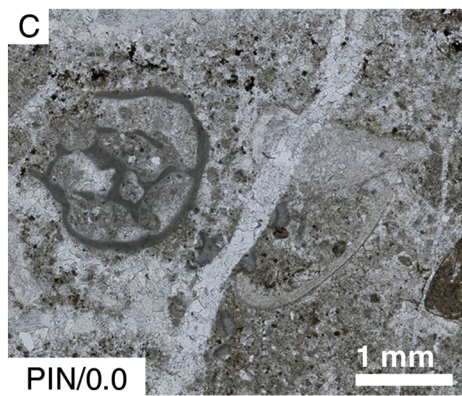
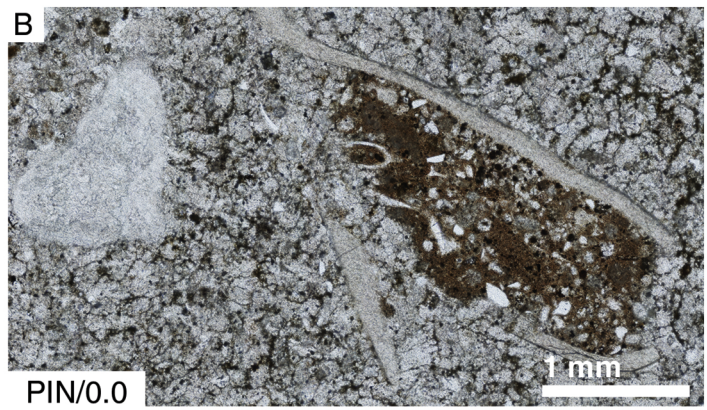
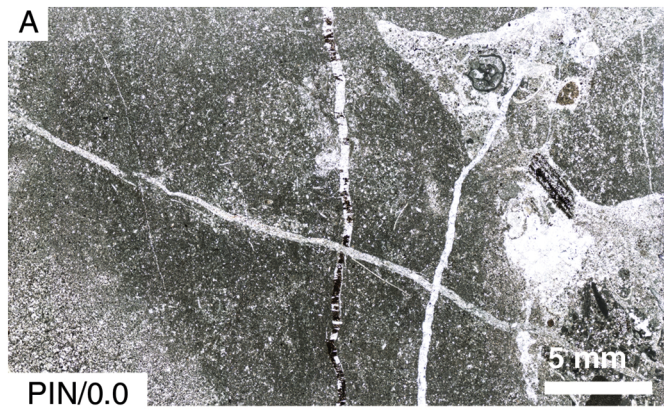


Figure 22

# SCYW-791A

(Drillcore, Stuart Shelf)

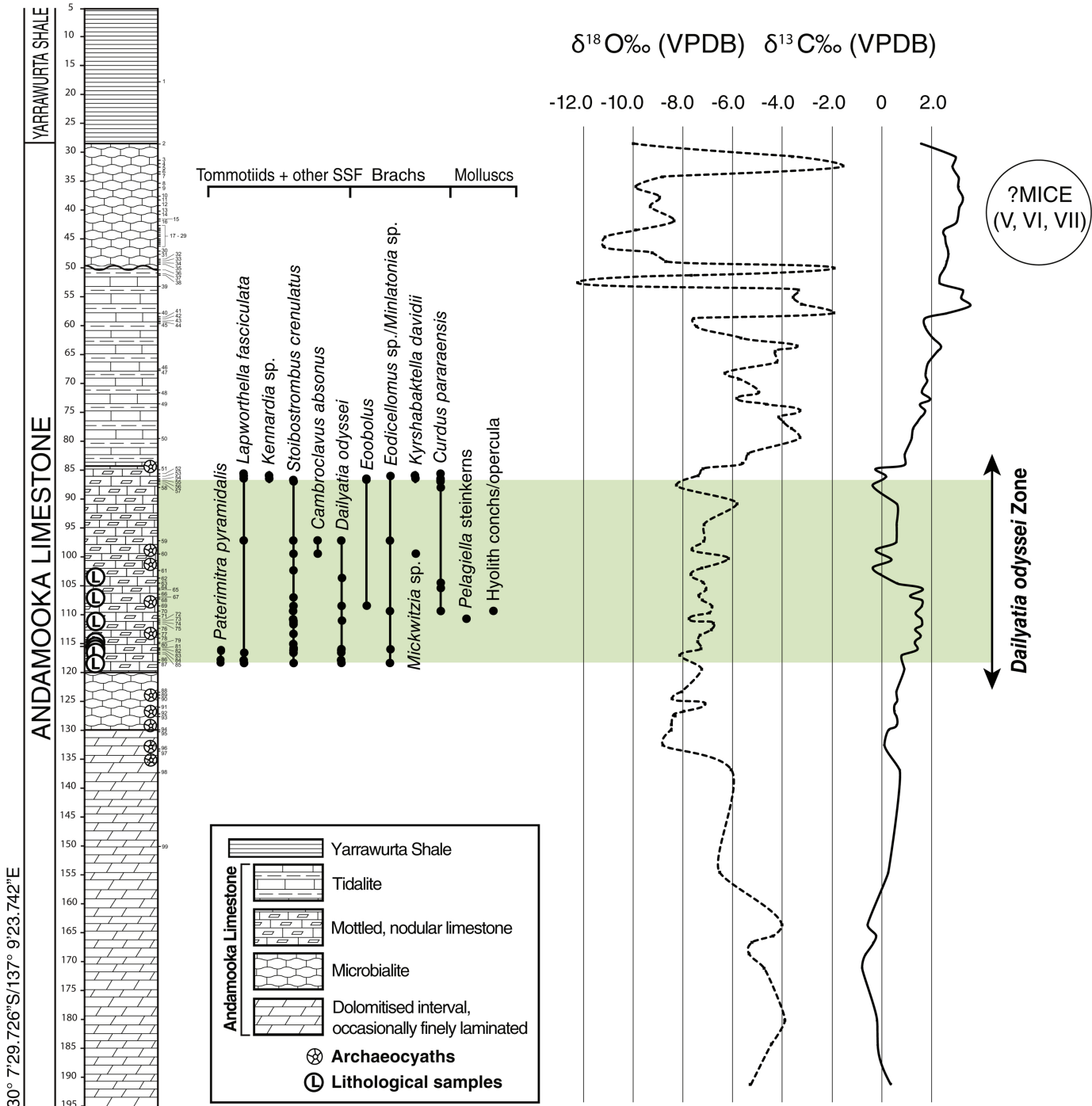


Figure 23

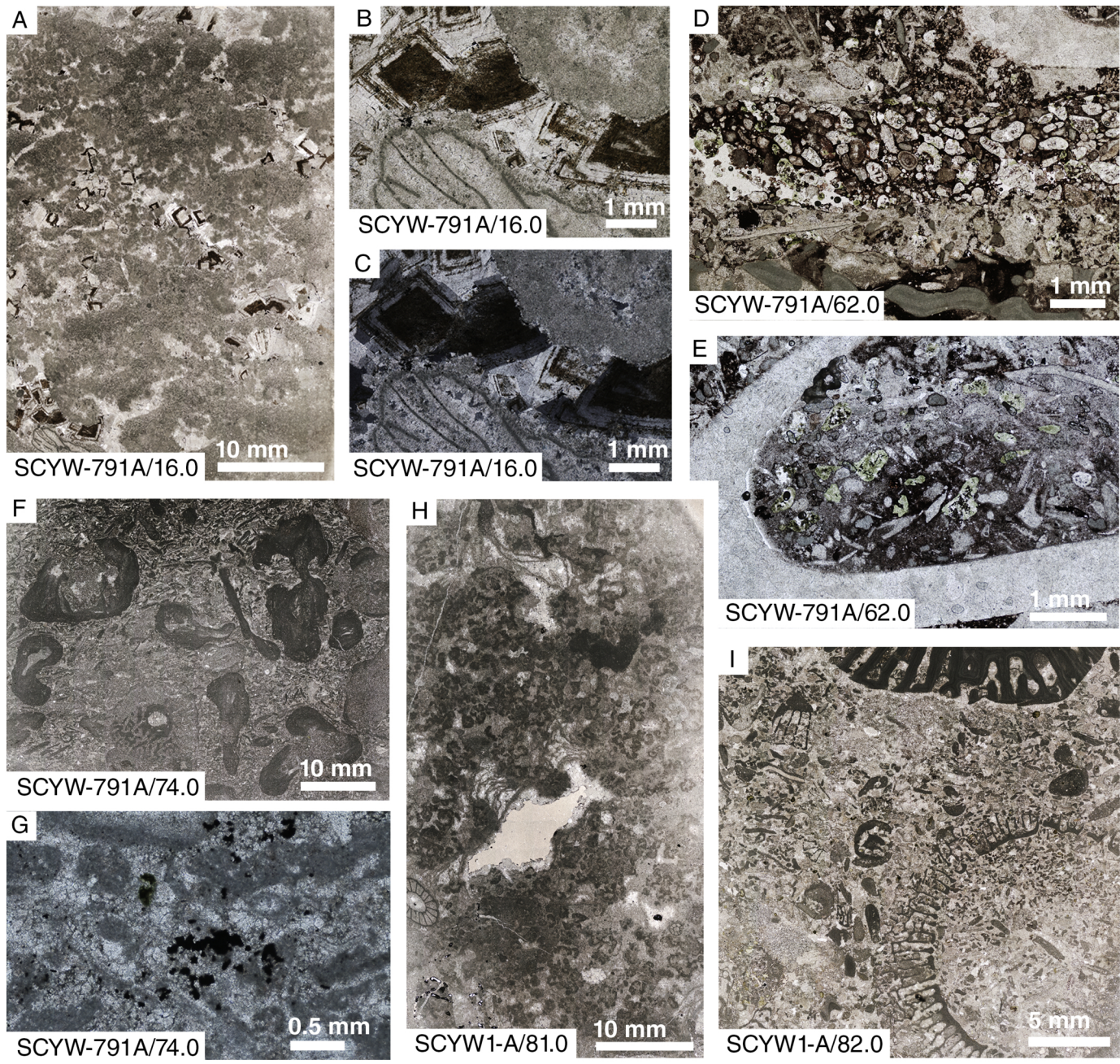


Figure 24

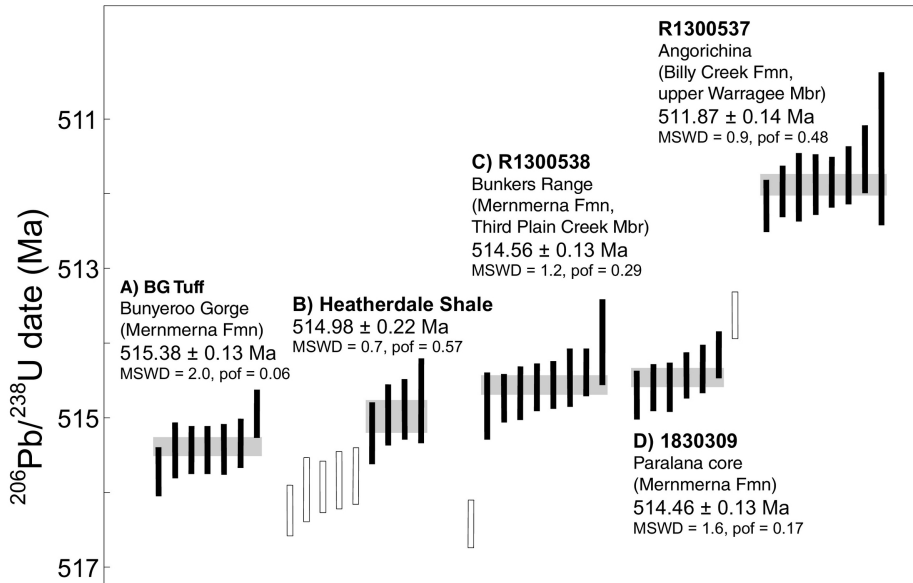


Figure 25



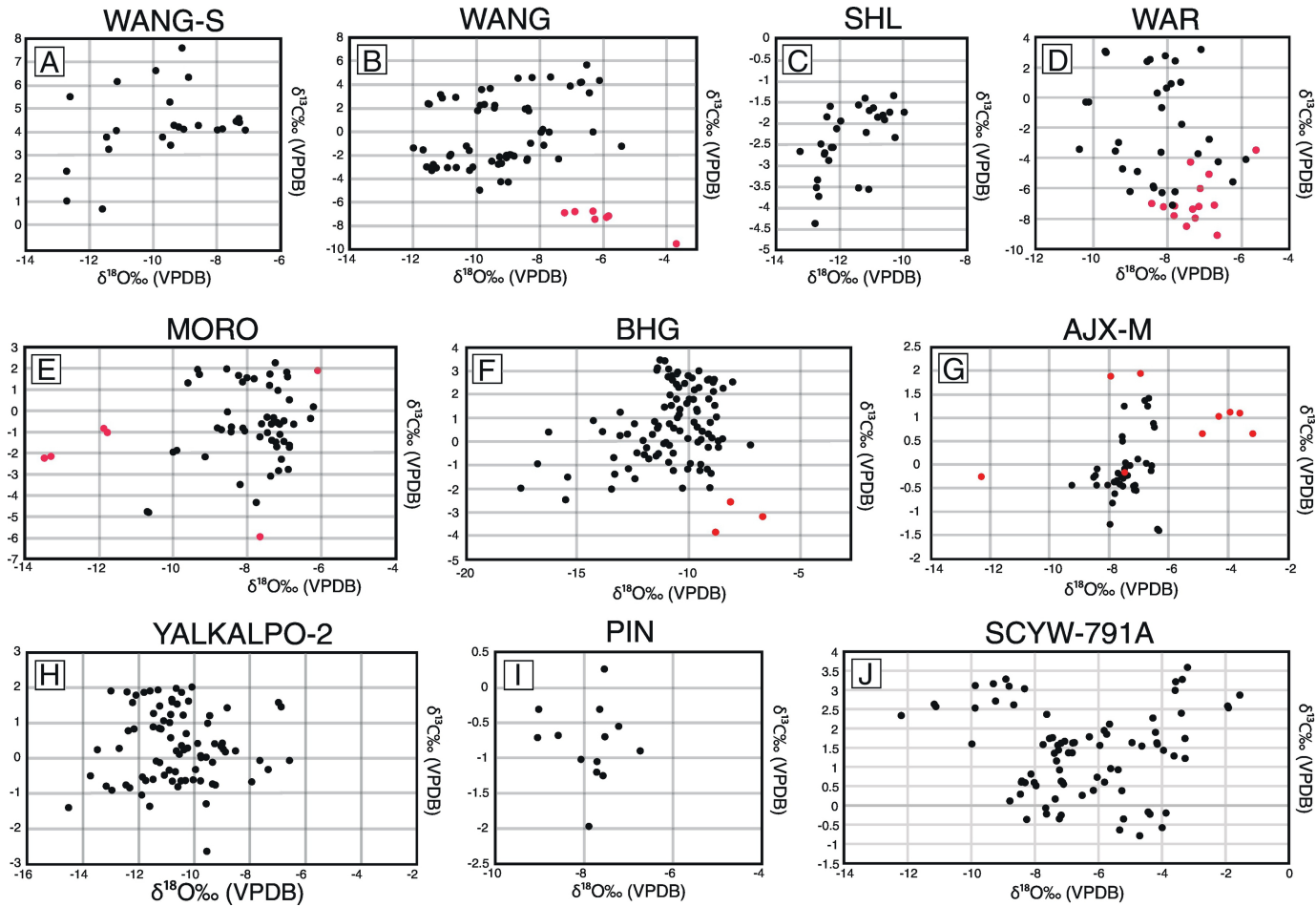


Figure 26

